

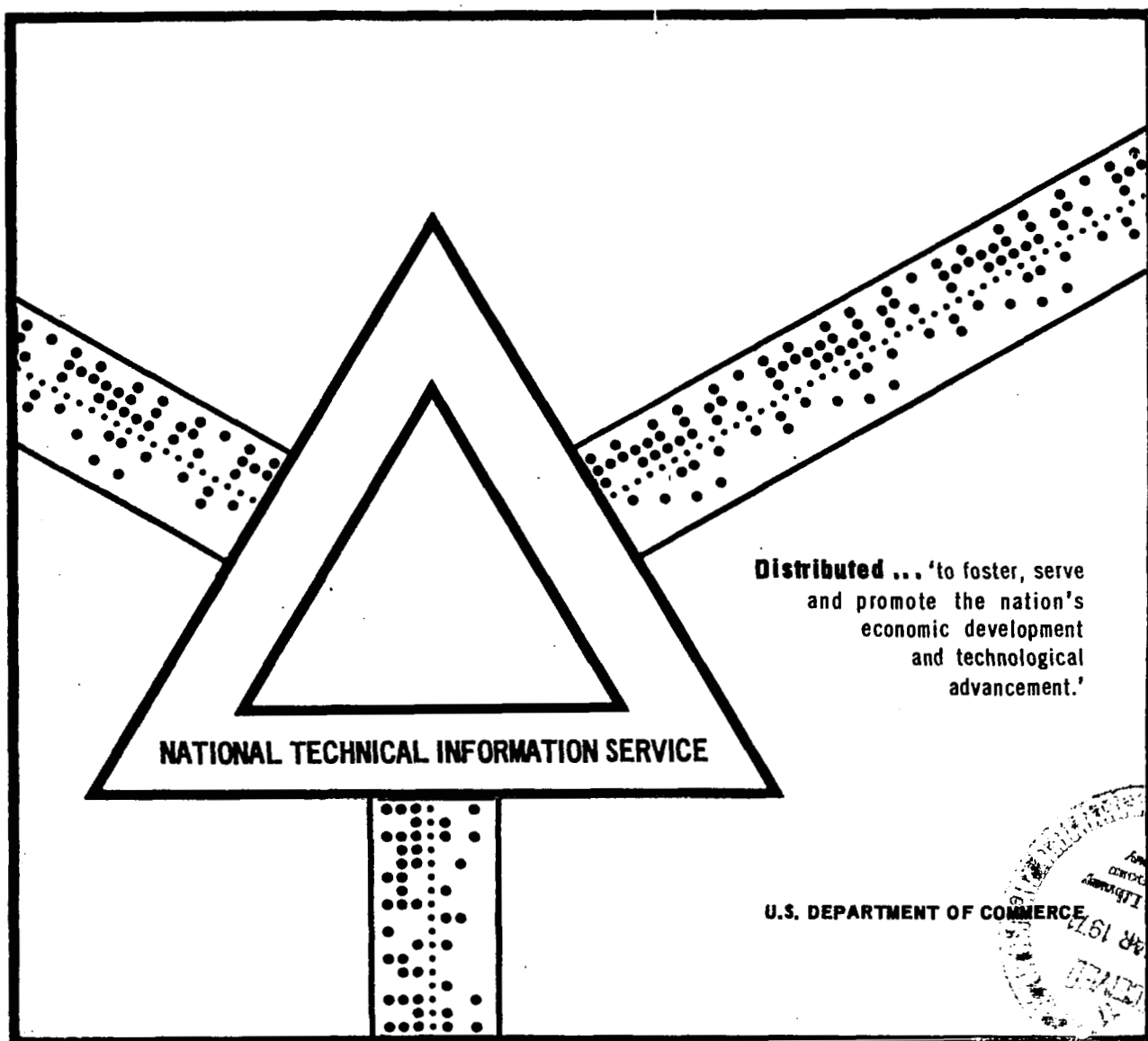
N70-41237

RAMAN BACKSCATTER OF LASER RADIATION IN
THE EARTH'S ATMOSPHERE

Samuel Harvey Melfi

1970

LOAN COPY: RE
AFWL (DO
KIRTLAND AF



This document has been approved for public release and sale.



0152427

RAMAN BACKSCATTER OF LASER RADIATION IN THE EARTH'S ATMOSPHERE

A dissertation

Presented to

The Faculty of the Department of Physics

The College of William and Mary in Virginia

In Partial Fulfillment

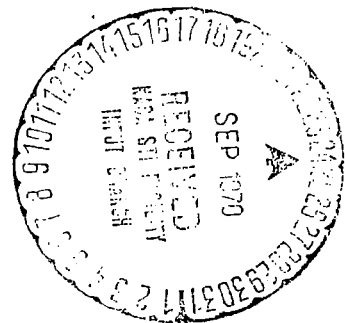
of the Requirements for the Degree of

Doctor of Philosophy

by

Samuel Harvey Melfi

1970



FACILITY FORM 602

N70-41237
(ACCESSION NUMBER)

163
(PAGES)

TMX-66388
(NASA CR OR TMX OR AD NUMBER)

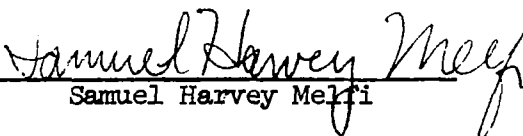
(THRU)

(CODE)

16
(CATEGORY)

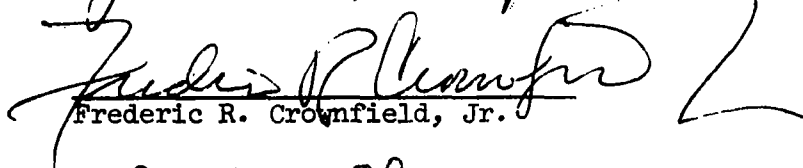
APPROVAL SHEET

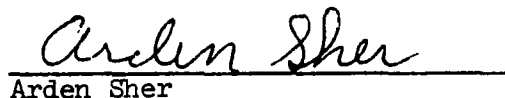
This dissertation is submitted in partial fulfillment of
the requirements for the degree of
Doctor of Philosophy


Samuel Harvey Melfi

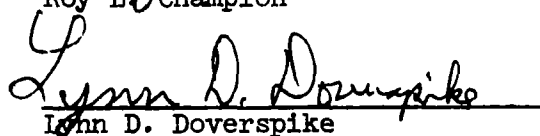
Approved, July 1970

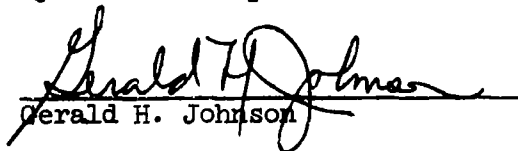

James D. Lawrence, Jr.


Frederic R. Crownfield, Jr.


Arden Sher


Roy L. Champion


Lynn D. Doverspike


Gerald H. Johnson

ACKNOWLEDGMENTS

The author wishes to express his appreciation to Dr. J. D. Lawrence under whose guidance this research was performed, and for his untiring advice throughout the preparation of this dissertation. He would also like to thank Stewart L. Ocheltree and Dr. M. P. McCormick of NASA for their many helpful discussions on this research program. Special appreciation is extended to W. H. Fuller, W. C. Hulten, C. E. Russ, and T. E. Wetterling for their help in obtaining the experimental results reported herein. Special thanks go to Barbara Pasternak for her computer programing, and Janette Fernandes for her assistance in reducing the data. The author would also like to thank the ESSA personnel at Wallops Island, Virginia, and Dr. J. M. Rosen of the University of Wyoming for providing balloon-borne meteorological support. Finally, the author would like to thank his wife, Nancy, for without her continuing moral support this dissertation could not have been possible.

TABLE OF CONTENTS

	PAGE
ACKNOWLEDGMENTS	iii
LIST OF FIGURES	vii
LIST OF TABLES	xii
ABSTRACT	xiv
CHAPTER	
I. INTRODUCTION	2
II. THEORY OF RAMAN AND RAYLEIGH SCATTERING BY A MOLECULE . .	5
A. Quantum Theory of Raman and Rayleigh Scattering . .	6
B. Rayleigh and Vibrational Raman Scattering	15
C. Rotational Raman Fine Structure of Rayleigh and Raman Vibrational Scattering	21
1. Pure Rotational Raman Fine Structure	22
2. Vibrational-Rotational Raman Fine Structure .	26
D. Cross Section Calculations for Raman Backscatter from N_2 and O_2	30
E. Calculation of the Raman Backscatter from the Atmosphere	35
F. Application of Raman Scattering to Measurements in the Atmosphere	44
III. MIXING IN THE EARTH'S LOWER ATMOSPHERE	49
IV. NOISE ANALYSIS	54

CHAPTER	PAGE
V. EQUIPMENT	59
A. Laser Transmitter	59
B. Receiver System	63
C. Alignment of the Receiver and Laser Transmitter . .	68
D. Supporting Equipment	71
VI. DATA ANALYSIS AND EXPERIMENTAL RESULTS	73
A. Data Analysis	73
B. Early Experimental Results Using a Monochromator to Select Spectral Bandpass	78
C. Experimental Results Using Interference Filters as Spectral Band Selectors	80
1. Examples of Average Analog Backscatter From the Atmosphere	82
2. Examples of Photon Counting Backscatter From the Atmosphere	87
3. Comparison of the Optical Radar Data With Meteorological Measurements	90
VII. CONCLUSIONS	97
VIII. APPENDICES	99

CHAPTER	PAGE
A. TRANSFORMATION OF THE POLARIZABILITY AND DIFFERENTIAL POLARIZABILITY TENSORS FROM A RANDOMLY ORIENTED MOLECULAR COORDINATE SYSTEM TO A LABORATORY COORDINATE SYSTEM	99
B. DERIVATION OF RAYLEIGH AND RAMAN VIBRATIONAL CROSS SECTIONS FOR ALL POLARIZATIONS AS A FUNCTION OF SCATTERING ANGLE	102
C. REDUCTION OF THE PURE ROTATIONAL RAMAN CROSS- SECTION EQUATION	106
D. SAMPLE CALCULATION OF ONE TERM IN THE ROTATIONAL RAMAN CROSS SECTION	108
E. A LISTING OF THE ROTATIONAL RAMAN FINE STRUCTURE BACKSCATTER CROSS SECTIONS OF N_2 AND O_2	110
F. AN ESTIMATE OF THE QUANTITY $(i_D + i_B)$	143
IX. REFERENCES	144
VITA	148

LIST OF FIGURES

FIGURE	PAGE
1. A plot of rotational fine structure for the nitrogen v = 0 → 1 vibrational Raman transition as a function of wavelength	34
2. Calculated Raman backscatter signal for nitrogen as a function of altitude using typical system parameters listed in table VI	45
3. Calculated Raman backscatter signal for oxygen as a function of altitude using typical system parameters listed in table VI	46
4. Calculated Raman backscatter signal for water vapor as a function of altitude using typical system parameters listed in table VI. Calculations are based on a constant mixing ratio of 1 gm/kg	47
5. A plot of receiver bandwidth and altitude resolution as a function of maximum altitude for nitrogen, oxygen, and water vapor with signal detection criterion S/N = 2	56
6. A plot of the product of counting time and number of laser transmissions as a function of maximum altitude for nitrogen, oxygen, and water vapor with signal detection criterion S/N = 2	58

FIGURE	PAGE
7. A photograph of the optical radar system installed in a mobile van	60
8. A sketch of the laser transmitter	61
9. A drawing of the telescope	64
10. The arrangement of the receiver system using a dual monochromator	65
11. A sketch of the modified receiver system using interference filters	69
12. Arrangement for aligning optical radar system	70
13. (a) Typical analog Raman return from atmospheric nitrogen	74
(b) A typical oscillogram taken for the purposes of photon counting	74
14. Initial computer plot of data from oscillogram given in figure 13(a)	75
15. Backscatter signal normalized to relative laser energy as a function of altitude (data from fig. 13(a))	76
16. The quantity Z^2V/E as a function of altitude (data from fig. 13(a))	77
17. Typical Raman backscatter returns from the atmosphere versus time after laser emission taken using the dual monochromator	79

18. A comparison of the ratio, $V_{H_2O}(Z)/V_{N_2}(Z)$, with water vapor mixing ratio w obtained from a radiosonde.
 \circ , $V_{H_2O}(Z)/V_{N_2}(Z)$ (left scale). \bullet , w (right scale) 81
19. Typical examples of average analog profiles for nitrogen and water vapor taken the night of December 4, 1969. The curves are the calculated nitrogen and water vapor signal returns normalized individually to the experimental data at the points indicated. The water vapor calculations were performed for a constant mixing ratio of 1 gm/kg 83
20. Typical examples of average analog profiles for nitrogen, oxygen, and water vapor taken the night of February 26, 1970. The curves represent calculated signal returns individually normalized to the experimental data at the points indicated. Water vapor calculations are for a constant mixing ratio of 1 gm/kg 84
21. Typical examples of analog average profiles for nitrogen, water vapor, and elastic backscatter taken the night of April 16, 1970. The curves represent calculated signal returns individually normalized to the experimental data at the points indicated. Water vapor calculations are for a constant mixing ratio of 1 gm/kg 85

22. Normalized comparison of nitrogen returns taken the nights of December 4, 1969, and June 11, 1970 86
23. Nitrogen and water vapor profiles using photon counting taken the night of April 16, 1970. The curve is the calculated photon count rate as a function of altitude for N_2 normalized to the experimental data at the point indicated 88
24. Nitrogen and elastic backscatter profiles using photon counting, taken the night of April 16, 1970. The curve is the calculated photon count rate as a function of altitude for N_2 normalized to the N_2 experimental data at the point indicated 89
25. The ratio of water vapor to nitrogen return signals normalized to the water vapor mixing ratio measured by a radiosonde at the point indicated. Both measurements made the night of February 26, 1970. Also shown is the radiosonde temperature profile and adiabatic temperature profiles 91
26. The ratio of normalized oxygen to nitrogen return signals as a function of altitude 93

27. The ratio of water vapor to nitrogen return signals normalized to the water vapor mixing ratio measured by a radiosonde. Both measurements made the night of April 16, 1970. Also shown is the radiosonde temperature profile and adiabatic temperature profiles 94
28. The ratio of the elastic scattered to nitrogen return signals normalized to the dust scattering cross section measured by a balloon-borne dust photometer. Both measurements made the night of April 16, 1970. Also shown is a radiosonde temperature profile taken the same night and adiabatic temperature profiles . . 96

LIST OF TABLES

TABLE	PAGE
I. Molecular Constants of N_2 and O_2	30
II. Backscatter cross sections of N_2 and O_2 for Rayleigh Backscatter, and the Sum of the Pure Rotational Raman Backscatter, with $\lambda_0 = 3471.5 \text{ \AA}$	30
III. Backscatter Cross Sections of N_2 and O_2 for $v = 0 \rightarrow 1$, $\Delta J = 0$ Vibrational Transition (Q Branch) and the Sum of the Vibration-Rotation Transitions (O Branch plus S Branch); $\lambda_{N_2} = 3777 \text{ \AA}$, $\lambda_{O_2} = 3669 \text{ \AA}$	31
IV. Differential Raman Backscatter Cross Sections for Rotational Fine Structure of the $v = 0 \rightarrow 1$ Vibrational Transition of N_2 . $\Delta J = +2$	32
V. Differential Raman Backscatter Cross Sections for Rotational Fine Structure of the $v = 0 \rightarrow 1$ Vibrational Transition of N_2 . $\Delta J = -2$	33
VI. Typical Parameters for the Raman Optical Radar	36
VII. Calculated Raman Backscatter Received Signal for the $v = 0 \rightarrow 1$ Vibrational Band of N_2 for Elterman's "Clear Atmosphere"	38
VIII. Calculated Raman Backscatter Received Signal for the $v = 0 \rightarrow 1$ Vibrational Band of N_2 for a Molecular Atmosphere	39

IX.	Calculated Raman Backscatter Received Signal for the $v = 0 \rightarrow 1$ Vibrational Band of O_2 for Elterman's "Clear Atmosphere".	40
X.	Calculated Raman Backscatter Received Signal for the $v = 0 \rightarrow 1$ Vibrational Band of O_2 for a Molecular Atmosphere	41
XI.	Calculated Raman Backscatter Received Signal for the ν_1 Symmetric Vibration Line of H_2O for Elterman's "Clear Atmosphere." (Assuming Constant Mixing Ratio of 1 gm/kg and Cross Section of the Order of the Nitrogen $v = 0 \rightarrow 1$ Transition)	42
XII.	Calculated Raman Backscatter Received Signal for the ν_1 Symmetric Vibration Line of H_2O for a Molecular Atmosphere. (Assuming Constant Mixing Ratio of 1 gm/kg and Cross Section of the Order of the Nitrogen $v = 0 \rightarrow 1$ Transition)	43

ABSTRACT

Laser optical radar techniques have been applied to the measurement of Raman backscatter in the atmosphere by nitrogen, oxygen, and water vapor. Ratios of the water vapor to nitrogen Raman return signals have been compared to independent radiosonde measurements of water vapor mixing ratio. Initial experiments performed using a dual monochromator indicated good agreement to altitudes above 1 km. In later experiments, using interference filters, agreement was good to altitudes above 3 km, with some disagreement evident below 1 km. The disagreement below 1 km may be due to relatively intense aerosol scattering not totally blocked by interference filters used to select the Raman band.

A concise treatment of Raman and Rayleigh scattering by molecules is presented for the geometry of the optical radar system and includes calculations of Rayleigh and vibrational Raman backscatter cross sections for nitrogen and oxygen, including rotational fine structure.

A detailed description of the optical radar system is given along with a noise analysis of Raman backscatter in the atmosphere.

In addition, the ratio of the elastic scattered return to the nitrogen return signal has been compared to the results of a balloon-borne dust photometer, with good agreement to above 3 km. Raman optical radar measurements of both water vapor and aerosol mixing agree with a qualitative analysis of turbulent mixing in the atmosphere.

RAMAN BACKSCATTER OF LASER RADIATION IN THE EARTH'S ATMOSPHERE

I. INTRODUCTION

Detailed measurements of molecular and aerosol constituents in the earth's atmosphere are necessary for the construction of atmospheric models and also to define the state of the atmosphere. Radiosonde measurements of temperature, wind velocity, and relative humidity as a function of pressure-altitude are routinely made in the lower atmosphere. The primary purpose of the radiosonde measurements is to indicate synoptic weather patterns and to make predictions, but they may also provide basic molecular information such as total number density and water vapor profiles. Such measurements are made with instruments attached to slow rising balloons (1,000 ft/min) whose lateral position is determined by the horizontal wind velocity and, in consequence, such measurements represent neither an instantaneous nor a true vertical profile.

Remote light scattering techniques have provided a measure of the aerosol distribution in the earth's atmosphere. In 1930, Synge⁽¹⁾ suggested a searchlight technique to measure atmospheric properties by observing light scattering by the atmosphere. Subsequently, other investigators⁽²⁻⁵⁾ have studied the atmosphere using this technique.

With the development of the high-powered pulsed laser, providing an intense source of light, new emphasis was placed on light scattering as a remote technique for sensing atmospheric constituents. Fiocco and Smullin⁽⁶⁾ first reported observations of backscattered radiation from the atmosphere using a ruby laser optical radar system. Other investigators using the optical radar technique to study the atmosphere include

Bain and Sanford,⁽⁷⁾ Collis and Ligda,⁽⁸⁾ and Kent, Clemesha and Wright.⁽⁹⁾ These research programs have primarily been concerned with the observation of high-altitude aerosol layers, including mesospheric layers and the 20 km dust layer.

In a detailed study of the state of the atmosphere, individual molecular profiles should be measured. The molecular species in the lower atmosphere include water vapor and other trace constituents including pollutants, and nitrogen and oxygen for altitudes above 80 km. Schotland⁽¹⁰⁾ has examined absorption techniques using an optical radar system to infer water vapor profiles. Bowman, Gibson and Sandford⁽¹¹⁾ have reported the observation of resonance scattering from sodium at an altitude of 90 km. The observation of Raman backscatter by a particular molecular species, using an optical radar system, provides a basic technique to quantitatively measure individual molecular constituent profiles.

The observation of Raman backscatter from atmospheric nitrogen and oxygen was first reported by Leonard⁽¹²⁾ in 1967, using a pulsed nitrogen laser. Later Cooney⁽¹³⁾ observed nitrogen Raman backscatter to an altitude of 2 km. In 1969, Melfi, Lawrence and McCormick⁽¹⁴⁾ reported the first observation of Raman scattering in the atmosphere by water vapor molecules, using a frequency doubled ruby laser. Early in 1970, Cooney⁽¹⁵⁾ also reported the observation of Raman scattering by water vapor. Very recently, Kobayasi and Inaba⁽¹⁶⁾ have observed an indication of Raman backscatter by SO₂, CO, and CO₂ in a smoke stack plume located 20 m from their optical radar system.

This dissertation presents the results of a research program initiated to study, in detail, Raman scattering as a means to obtain quantitative remote profiles of individual atmospheric molecular species as a necessary first step in obtaining a better understanding of the earth's lower atmosphere. To this end:

(1) A concise treatment of Raman and Rayleigh molecular scattering is presented.

(2) A qualitative analysis of mixing of constituents in the earth's atmosphere due to turbulent diffusion is discussed.

(3) A noise analysis of Raman scattering by nitrogen, oxygen, and water vapor observed by an optical radar system is performed.

(4) Finally, a comparison of the results of the initial Raman optical radar experiments with independent meteorological measurements is presented.

The only molecular profile in the atmosphere being measured routinely is water vapor. In view of the limitations of radiosonde measurements, the Raman optical radar technique offers the possibility of performing instantaneous vertical measurements of the profiles of not only water vapor but also other trace constituents in the atmosphere. Although the measurements reported here were made only on the vertical, the technique offers the potential of quantitatively measuring two- and three-dimensional distributions of individual atmospheric constituents. These distribution measurements should provide a means of studying, on a local basis, turbulent diffusion, pollution dissipation, and cloud formation.

II. THEORY OF RAMAN AND RAYLEIGH SCATTERING BY A MOLECULE

General

In 1928, Raman⁽¹⁷⁾ observed that when various molecules are irradiated with light of frequency ν the scattered radiation consisted not only of frequency ν (Rayleigh scattering) but other frequencies such as $\nu - \nu_1$, $\nu - \nu_2$, . . . (Raman scattering). These Raman lines are now termed Stokes lines; other Raman lines $\nu + \nu_1$, $\nu + \nu_2$, . . . are referred to as anti-Stokes lines.

This effect was predicted qualitatively as early as 1923⁽¹⁸⁾ using classical theory. The classical argument was based on the realization that changes in polarizability of molecules due to their rotation or vibration give rise to scattering at other frequencies.

The quantum mechanical treatment first performed by Kramers and Heisenberg⁽¹⁹⁾ and later by Dirac⁽²⁰⁾ treats the problem as a two-photon process. A photon incident on a molecule is annihilated and the molecule is excited to a "virtual" state. The molecule de-excites and another photon is created. If after the scattering process the molecule is in the same internal state as before, the process is called Rayleigh scattering. If, however, after scattering the molecule is in a different state, then Raman scattering has occurred.

In this chapter, an attempt is made to present a concise treatment of Raman and Rayleigh scattering in the atmosphere. To this end the chapter has been divided into six sections. In section IIA, a general quantum mechanical discussion of Raman and Rayleigh scattering,

based on Heitler's⁽²¹⁾ treatment, is presented. Building on this quantum mechanical base, section IIB presents Placzek's⁽²²⁾ polarizability treatment, which assumes that the vibrations of molecules can be treated as normal modes of simple harmonic motion. Further assumptions are made in section IIC concerning the rotational structure of the Rayleigh and Raman vibrational bands. This rotational analysis is limited to rigid diatomic molecules such as O_2 and N_2 . The last three sections are devoted to relating the theory of Raman and Rayleigh scattering to the geometry of the laser experiment in the atmosphere.

IIA. Quantum Theory of Raman and Rayleigh Scattering

The quantum mechanical behavior of any system can be described by the wavefunction, Ψ , of the system satisfying the wave equation:

$$i\hbar\dot{\Psi} = H\Psi \quad (1)$$

where $\dot{\Psi} = \frac{\partial\Psi}{\partial t}$, Ψ is the total wavefunction, and H is the total Hamiltonian operator. H may be divided into the following parts:

$$H = H_r + H_m + H_{int} \quad (2)$$

where H_r is the Hamiltonian of the radiation field, H_m is the Hamiltonian of the molecule, and H_{int} is the interaction Hamiltonian.

Let

$$H_0 \equiv H_r + H_m \quad (3)$$

with the eigenfunctions of H_0 denoted by

$$\Psi_n = \Psi_{n_1, n_2, \dots, n_\lambda, \dots} \psi_m \quad (4)$$

where $n_1, n_2, \dots, n_\lambda, \dots$ are the occupation numbers of the photons and ψ_m is the wavefunction of the molecule.

The total differential transition probability from an initial state denoted by 0 to all states denoted by n is: ⁽²¹⁾

$$d\omega_{no} = \frac{2\pi}{\hbar} \left[|H_{no} + K_{no}|^2 \right] d\rho \epsilon_n \quad (5)$$

where H_{no} is from first-order perturbation considerations given by:

$$H_{no} = \langle \Psi_n | H_{int} | \Psi_0 \rangle, \quad (6)$$

K_{no} is the second-order perturbation matrix element of the form:

$$K_{no} = \sum_{n'} \frac{H_{nn'} H_{n'o}}{\epsilon_o - \epsilon_{n'}} \quad (7)$$

with n' denoting intermediate states of the molecule, $d\rho \epsilon_n$ the density of final states and ϵ the total energy of the system.

To calculate H_{no} and K_{no} in equations (6) and (7), the interaction Hamiltonian has to be defined. It can be shown that the interaction Hamiltonian is given by⁽²¹⁾

$$H_{int} = H^{(1)} + H^{(2)}$$

where

$$H^{(1)} = - \sum_k \frac{e_k}{m_k c^2} \left[\vec{p}_k \cdot \vec{A}(k) \right] \quad (8)$$

and

$$H^{(2)} = \sum_k \frac{e_k^2}{2m_k c^2} \vec{A}^2(k) \quad (9)$$

where k denotes the various electrons in the molecule, m is the mass of each electron, and \vec{A} , the vector potential, can be expressed as

$$\vec{A} = \sum_{\lambda} \left(a_{\lambda} \vec{A}_{\lambda} + a_{\lambda}^{\dagger} \vec{A}_{\lambda}^* \right) \quad (10)$$

where λ denotes the set of photon states with wave vector \vec{k}_{λ} and polarization \vec{e}_{λ} ,

$$\vec{A}_{\lambda} = \sqrt{4\pi c^2} \vec{e}_{\lambda} e^{i\vec{k} \cdot \vec{r}} \quad (11)$$

and \vec{r} is the position vector of the electron with a_{λ}^{\dagger} , a_{λ} creation and annihilation operators, respectively.

In a two-photon scattering process, an incident photon of wave vector \vec{k}_0 will be considered absorbed and a scattered photon of wave vector \vec{k} emitted.

The states of the molecule will be denoted by m_i and, in particular, the initial state by m_0 , and final state by m with respective energies E_i , E_0 , and E . Conservation of energy requires that

$$E_0 + \hbar\omega_0 = E + \hbar\omega$$

That is, the initial energy of the system before the scattering process equals the final energy afterwards. If $\hbar\omega_0 = \hbar\omega$, then the scattering is considered Rayleigh, since no net transfer of energy to the molecule has taken place. If, however, $\hbar\omega_0 \neq \hbar\omega$ or $E_0 \neq E$, then a net transfer of energy has taken place between the photon field and the molecule, and the process is termed Raman scattering.

To calculate the transition probability for scattering, it is necessary to consider only those processes which contain the annihilation of photon \vec{k}_0 and the creation of photon \vec{k} . For simplicity, a single electron molecule will be considered initially and the results will then be generalized to a multielectron molecule. For a single electron molecule, the components of the interaction Hamiltonian become

$$H^{(1)} = - \frac{e}{mc^2} (\vec{p} \cdot \vec{A}) \quad (12)$$

and

$$H^{(2)} = \frac{e^2}{2mc^2} \vec{A}^2 \quad (13)$$

Equation (10) indicates that the second part of the interaction Hamiltonian, $H^{(2)}$, connects states differing by two photons using

first-order perturbation theory. The square of the vector potential from equation (10) can be written

$$\begin{aligned} \vec{A}^2 = \sum_{\lambda \zeta} \left[a_{\lambda} a_{\zeta} (\vec{A}_{\lambda} \cdot \vec{A}_{\zeta}) + a_{\lambda} a_{\zeta}^{\dagger} (\vec{A}_{\lambda} \cdot \vec{A}_{\zeta}^{*}) + a_{\lambda}^{\dagger} a_{\zeta} (\vec{A}_{\lambda}^{*} \cdot \vec{A}_{\zeta}) \right. \\ \left. + a_{\lambda}^{\dagger} a_{\zeta}^{\dagger} (\vec{A}_{\lambda}^{*} \cdot \vec{A}_{\zeta}^{*}) \right] \end{aligned} \quad (14)$$

If it is assumed that a photon described by ζ is annihilated and a photon described by λ is created, then the third term is the only term that is effective in this coupling. For this process,

$$H_{no}^{(2)} = \frac{e^2}{2mc^2} \langle \psi_{0\dots l_k, 0\dots}^* | \vec{A}^2 | \psi_{0\dots l_{k_0}, 0\dots} \psi_{m_0} \rangle \quad (15)$$

Substituting equations (14) and (11) into equation (15) and letting $\zeta \rightarrow \vec{k}$, \vec{e}_{k_0} , and $\lambda \rightarrow \vec{k}$, $\vec{e}_{\vec{k}}$ gives

$$\begin{aligned} H_{no}^{(2)} &= \frac{e^2}{2m} 4\pi \langle \psi_{l_k}^* \psi_m^* | a_{\vec{k}}^{\dagger} a_{k_0} \vec{e}_{\vec{k}} \cdot \vec{e}_{k_0} e^{i(\vec{k}_0 - \vec{k}) \cdot \vec{r}} | \psi_{l_{k_0}} \psi_{m_0} \rangle \\ &= \vec{e}_{\vec{k}} \cdot \vec{e}_{k_0} \frac{e^2}{2m} 4\pi \langle \psi_{l_k}^* | a_{\vec{k}}^{\dagger} a_{k_0} | \psi_{l_{k_0}} \rangle \langle \psi_m^* | e^{i(\vec{k}_0 - \vec{k}) \cdot \vec{r}} | \psi_{m_0} \rangle \end{aligned} \quad (16)$$

Using the relationships

$$a_{\vec{k}} \psi_{n_k} = \sqrt{\frac{n_k}{2\omega_k}} \psi_{n_k-1}$$

and

$$a_k^+ \psi_{n_k} = \sqrt{\frac{n(n_k+1)}{2\omega_k}} \psi_{n_k+1}$$

equation (16) becomes

$$H_{no}^{(2)} \approx \vec{e}_k \cdot \vec{e}_{k_0} \frac{e^2}{m} \frac{2\pi n}{\sqrt{\omega_0 \omega}} e^{i(\vec{k}-\vec{k}_0) \cdot \vec{x}} \delta_{nm_0} \quad (17)$$

where \vec{x} represents the position of the molecule.

To complete the analysis of the two-photon scattering problem, it is necessary to consider the first part of the Hamiltonian, $H^{(1)}$, given in equation (12), under second-order perturbation theory. This will require considering two possible intermediate states of the system:

I. A \vec{k}_0 photon is absorbed; in this intermediate state of the system no photons are present, then a \vec{k} photon is emitted.

II. A \vec{k} photon is emitted; in this intermediate state there are two photons present, then a \vec{k}_0 photon is absorbed.

The two intermediate states can be written as

$$\bar{\Psi}_I = \bar{\Psi}_0 \psi_{m_1}$$

and

$$\bar{\Psi}_{II} = \bar{\Psi}_{1_{k_0}, 1_k} \psi_{m_1}$$

and the initial (o) and final (n) states can be written as

$$\Psi_0 = \Psi_{l_{k_0}} \Psi_{m_0}$$

and

$$\Psi_n = \Psi_{l_k} \Psi_m$$

Combining equations (10), (11), and (12) gives

$$H_{I0}^{(1)} = -\frac{e}{mc^2} \sqrt{4\pi c^2} \langle \Psi_0^* \Psi_{m_1}^* | \vec{p} \cdot \vec{e}_{k_0} a_{k_0} e^{i\vec{k}_0 \cdot \vec{r}} | \Psi_{l_{k_0}} \Psi_{m_0} \rangle$$

or

$$H_{I0}^{(1)} = -\frac{e}{mc^2} \sqrt{\frac{2\pi mc^2}{\omega_0}} e^{i\vec{k}_0 \cdot \vec{x}} (p_\mu)_{m_1 m_0} \quad (18)$$

where p_μ is the component of momentum of the electron in the direction of the polarization of the incident photon.

In a similar fashion

$$\left. \begin{array}{l} H_{II0}^{(1)} \\ H_{nI}^{(1)} \\ H_{nII}^{(1)} \end{array} \right\} = -\frac{e}{mc^2} \sqrt{2\pi mc^2} \left\{ \begin{array}{l} \frac{1}{\sqrt{\omega}} e^{-i\vec{k} \cdot \vec{x}} (p_\nu)_{m_1 m_0} \\ \frac{1}{\sqrt{\omega}} e^{-i\vec{k} \cdot \vec{x}} (p_\nu)_{mm_i} \\ \frac{1}{\sqrt{\omega_0}} e^{i\vec{k}_0 \cdot \vec{x}} (p_\mu)_{mm_i} \end{array} \right. \quad (19)$$

where p_ν is the component of the momentum of the electron in the direction of the emitted photon.

From equation (7),

$$K_{no}^{(1)} = \sum_I \frac{H_{nI}^{(1)} H_{I0}^{(1)}}{\mathcal{E}_0 - \mathcal{E}_I} + \sum_{II} \frac{H_{nII}^{(1)} H_{II0}^{(1)}}{\mathcal{E}_0 - \mathcal{E}_{II}} \quad (20)$$

Substituting equations (18) and (19) into equation (20) and noting that

$$\mathcal{E}_0 - \mathcal{E}_I = E_0 - E_1 + \hbar\omega_0$$

$$\mathcal{E}_0 - \mathcal{E}_{II} = E_0 - E_1 - \hbar\omega$$

$K_{no}^{(1)}$ becomes

$$K_{no}^{(1)} = \frac{e^2}{m} \frac{2\pi\hbar}{\sqrt{\omega_0\omega}} e^{i(\vec{k}_0 - \vec{k}) \cdot \vec{x}} \left[\frac{1}{mc^2} \sum_i \left(\frac{(p_\nu)_{mm_1} (p_\mu)_{m_1 m_0}}{E_0 - E_1 + \hbar\omega_0} + \frac{(p_\mu)_{mm_1} (p_\nu)_{m_1 m_0}}{E_0 - E_1 - \hbar\omega} \right) \right] \quad (21)$$

The total differential transition probability is, from equation (5)

$$d\omega_{no} = \frac{2\pi}{\hbar} \left[|H_{no}^{(2)} + K_{no}^{(1)}|^2 \right] d\rho \mathcal{E}_n \quad (5)$$

Substituting equations (17) and (21) for $H_{no}^{(2)}$ and $K_{no}^{(1)}$, respectively, into equation (5) gives for $d\omega_{no}$

$$d\omega_{no} = \frac{(2\pi)^3 \hbar e^4}{m\omega_0\omega} \left[\frac{1}{mc^2} \sum_i \left(\frac{(p_\nu)_{mm_1} (p_\mu)_{m_1 m_0}}{E_0 - E_1 + \hbar\omega_0} + \frac{(p_\mu)_{mm_1} (p_\nu)_{m_1 m_0}}{E_0 - E_1 - \hbar\omega} \right) + \delta_{mm_0} \cos \theta \right]^2 d\rho \mathcal{E}_n \quad (22)$$

where θ is the angle between the polarizations of the incident and scattered photons.

Using for the density of final states

$$d\rho_{\mathcal{E}_n} = \frac{\hbar^2 \omega^2 d\Omega}{(2\pi\hbar c)^3}$$

where Ω is the solid angle, and considering a unit volume normalization with stationary molecules, the differential scattering cross section can be written as

$$\begin{aligned} \frac{d\varphi_{no}}{d\Omega} = & \left(\frac{e^2}{mc^2} \right)^2 \frac{\omega}{\omega_0} \left\{ \frac{1}{mc^2} \sum_i \left[\frac{\left(\sum_k p_{\nu k} \right)_{mm_1} \left(\sum_j p_{\mu j} \right)_{m_1 m_0}}{E_0 - E_i + \hbar\omega_0} \right. \right. \\ & \left. \left. + \frac{\left(\sum_k p_{\mu k} \right)_{mm_1} \left(\sum_j p_{\nu j} \right)_{m_1 m_0}}{E_0 - E_i - \hbar\omega} \right] + \delta_{mm_0} \cos \theta \right\}^2 \end{aligned} \quad (23)$$

where the sums over j and k are taken over all electrons in the molecule.

Equation (23) can be written in a more concise form as

$$\frac{d\varphi_{no}}{d\Omega} = \frac{\omega^3 \omega_0}{c^4} \left| (\alpha_{\mu\nu})_{mm_0} \right|^2 \quad (24)$$

where $(\alpha_{\mu\nu})_{mm_0}$ is the μ, ν element of the polarizability tensor defined as

$$\begin{aligned} (\alpha_{\mu\nu})_{mm_0} = & \frac{e^2}{m^2 \omega_0 \omega} \left\{ \frac{1}{mc^2} \sum_i \left[\frac{\left(\sum_k p_{\nu k} \right)_{mm_1} \left(\sum_j p_{\mu j} \right)_{m_1 m_0}}{E_0 - E_i + \hbar\omega_0} \right. \right. \\ & \left. \left. + \frac{\left(\sum_k p_{\mu k} \right)_{mm_1} \left(\sum_j p_{\nu j} \right)_{m_1 m_0}}{E_0 - E_i - \hbar\omega} \right] + \delta_{mm_0} \cos \theta \right\} \end{aligned}$$

The more familiar form of the differential scattering cross section for the intensity of light is obtained by multiplying the right side of equation (25) by the ratio of photon energies (ω/ω_0) to give

$$\frac{d\sigma}{d\Omega}(\mu, \nu, \text{mm}_0) = \frac{\omega^4}{c^4} \left| (\alpha_{\mu\nu})_{\text{mm}_0} \right|^2 \quad (26)$$

Equation (26) indicates that both Raman and Rayleigh scattering intensities vary inversely as the fourth power of the wavelength of the scattered light, since $\left| (\alpha_{\mu\nu})_{\text{mm}_0} \right|^2$ is approximately independent of wavelength when the wavelength of the incident light is not near a resonance of the molecule. Calculations of the polarizability tensor for complicated molecules have only had limited success.⁽²³⁾ Placzek's polarizability theory,⁽²²⁾ which is discussed in the following sections of this chapter, provide a basis for calculating Raman and Rayleigh scattering cross sections.

II B. Rayleigh and Vibrational Raman Scattering

Neglecting rotation of the molecule, the wavefunction of the molecule, ψ_m , can be expressed approximately as

$$\psi_m = \psi_e \prod_j \psi_{v_j}(q_j) \quad (27)$$

where ψ_e is the electronic part of the wavefunction, the q_j 's are the normal coordinates for vibration of the molecule, and the ψ_v 's are the wavefunctions for the normal vibrations (Harmonic oscillator wavefunctions).

The polarizability tensor operator, $\alpha_{\mu\nu}$, may be expanded in a Taylor's expansion about the equilibrium positions of the normal vibrations to give to first order in the q_j 's

$$\alpha_{\mu\nu} = \alpha_{\mu\nu}^0 + \sum_j \left(\frac{d\alpha_{\mu\nu}}{dq_j} \right)_0 q_j \quad (28)$$

Utilizing equation (28), the matrix elements of the polarizability tensor can be written as

$$\begin{aligned} (\alpha_{\mu\nu})_{mm_0} &= \langle \psi_m^* | \alpha_{\mu\nu}^0 | \psi_{m_0} \rangle + \sum_j \langle \psi_m^* \left(\frac{d\alpha_{\mu\nu}}{dq_j} \right)_0 q_j | \psi_{m_0} \rangle \\ &= \alpha_{\mu\nu}^0 \delta_{mm_0} + \sum_j \alpha'_{\mu\nu} \left|_0 \langle \psi_m^* | q_j | \psi_{m_0} \rangle \right. \end{aligned} \quad (29)$$

since $\alpha_{\mu\nu}^0$ and $\alpha'_{\mu\nu} = \frac{d\alpha_{\mu\nu}}{dq_j}$ are constant. The term $\alpha'_{\mu\nu}$ is commonly referred to as the differential polarizability tensor.

The first term on the right side of equation (29) gives rise to Rayleigh and pure rotational Raman scattering, since the initial and final vibrational states of the molecule remain unchanged. The second term on the right side of equation (29) gives rise to Raman vibrational scattering.

Combining equation (27) with the second term on the right side of equation (29) gives for the matrix elements of the polarizability tensor for Raman vibrational scattering:

$$\alpha'_{\mu\nu} \langle \psi_m | q_j | \psi_{m_0} \rangle = \alpha'_{\mu\nu} \delta_{ee'} \langle \psi_{v_j}^* (q_j) | q_j | \psi_{v_j'} (q_j) \rangle \quad (30)$$

$$= \alpha'_{\mu\nu} \delta_{ee'} \begin{cases} \left[\frac{\hbar}{2m\omega_j} (v_j + 1) \right]^{1/2} & \text{for } v_j' = v_j + 1 \\ \left[\frac{\hbar}{2m\omega_j} v_j \right]^{1/2} & \text{for } v_j' = v_j - 1 \\ 0 & \text{otherwise} \end{cases} \quad (31)$$

which are well known solutions for the harmonic oscillator wavefunction. Equation (31) indicates the selection rules for Raman vibrational scattering as

$$\Delta v = \pm 1$$

From equations (26) and (28) the cross section for Rayleigh scattering is

$$\frac{d\sigma}{d\Omega}(\mu, \nu, \omega_0) = \frac{\omega_0^4}{c^4} |\alpha'_{\mu\nu}|^2 \quad (32)$$

For the Raman vibrational cross section, the relative number of molecules occupying vibrational excited states must be considered. Weighting the states by the Maxwell-Boltzmann distribution law and using equations (26) and (31), the cross section per molecule is

$$\frac{d\phi}{d\Omega}(\mu, \nu, \text{mm}_0)_\omega = \frac{\omega^4}{c^4} \frac{\sum_{\nu_j} e^{-E_{\nu_j}/KT} \left\{ \alpha'_{\mu\nu} \left[\frac{\hbar}{2m\omega_j} (\nu_j + 1) \right]^{1/2} \right\}^2}{\sum_{\nu_j} e^{-E_{\nu_j}/KT}} \quad (33)$$

for $\Delta\nu = +1$ and $\omega = (\omega_0 - \omega_j)$ or

$$\frac{d\phi}{d\Omega}(\mu, \nu, \omega, j) = \frac{\omega^4}{c^4} \frac{\hbar}{2m\omega_j} \frac{|\alpha'_{\mu\nu}|^2}{1 - e^{-\hbar\omega_j/KT}} \quad (34)$$

The anti-Stokes band $\Delta\nu = -1$ will not be considered since the effect is not observed for most gases at room temperature.

Equations (32) and (34) give the differential cross section per molecule for Rayleigh and Stokes vibrational Raman scattering, respectively, for light polarized in a coordinate system fixed in the molecule. In a practical experiment, where the gas molecules are randomly oriented, an average must be taken over all possible orientations of the molecule and related to a laboratory coordinate system. That is, $|\alpha_{\mu,\nu}|^2$ will be transformed to an orientation averaged $\langle |\alpha_{\Omega,\Sigma}|^2 \rangle$, where $\mu, \nu = x_i$, $i = 1, 2$, or 3 , are the molecular coordinates and $\Omega, \Sigma = x_i$, $i = 1, 2$, or 3 , are the laboratory coordinates. This transformation and averaging is treated in detail in appendix A with the results for the polarizability tensor

$$\underbrace{\langle |\alpha_{\Omega, \Sigma}^0|^2 \rangle} = \frac{1}{45} \begin{bmatrix} 45\alpha^2 + 4\beta^2 & 3\beta^2 & 3\beta^2 \\ 3\beta^2 & 45\alpha^2 + 4\beta^2 & 3\beta^2 \\ 3\beta^2 & 3\beta^2 & 45\alpha^2 + 4\beta^2 \end{bmatrix} \quad (35)$$

where the symbol $\underbrace{\quad}$ indicates a tensor quantity.

$$\alpha = \frac{1}{3}(\alpha_1 + \alpha_2 + \alpha_3)$$

and

$$\beta^2 = \frac{1}{2} \left[(\alpha_1 - \alpha_2)^2 + (\alpha_2 - \alpha_3)^2 + (\alpha_1 - \alpha_3)^2 \right]$$

with α_1 , α_2 , and α_3 the principal values of the $\alpha_{\mu\nu}$ matrix.

The term α is referred to as the isotropic part of the polarizability and β as the anisotropic part.

The results of the transformation and averaging of the differential polarizability tensor from appendix A is

$$\underbrace{\langle |\alpha'_{\Omega, \Sigma}|^2 \rangle} = \frac{1}{45} \begin{bmatrix} 45\alpha'^2 + 4\beta'^2 & 3\beta'^2 & 3\beta'^2 \\ 3\beta'^2 & 45\alpha'^2 + 4\beta'^2 & 3\beta'^2 \\ 3\beta'^2 & 3\beta'^2 & 45\alpha'^2 + 4\beta'^2 \end{bmatrix} \quad (36)$$

Therefore, in the laboratory coordinate system, equations (32) and (34) become:

For Rayleigh scattering,

$$\frac{d\Phi}{d\Omega}(\Omega, \Sigma, \omega_0) = \frac{\omega_0^4}{c^4} \langle |\alpha_{\Omega \Sigma}|^2 \rangle \quad (37)$$

and for Raman vibrational scattering,

$$\frac{d\varphi}{d\Omega}(\Omega, \Sigma, \omega, j) = \frac{\omega^4}{c^4} \frac{\hbar}{2m\omega_j} \frac{\langle |\alpha'_{\Omega\Sigma}|^2 \rangle}{1 - e^{-\hbar\omega_j/KT}} \quad (38)$$

for $\Delta v = +1$ and $\omega = (\omega_0 - \omega_j)$.

A complete analysis of equations (37) and (38) with respect to polarizations of the incident and scattered light as a function of scattering angle is given in appendix B. In the optical radar experiment, only backscatter is of interest. For backscatter polarized parallel to the laser's polarization, $\Omega = \Sigma$ in equations (37) and (38). Therefore, for Rayleigh backscatter,

$$\frac{d\varphi}{d\Omega}(\omega_0)_{\parallel} = \frac{\omega_0^4}{c^4} \left(\alpha^2 + \frac{4}{45} \beta^2 \right) \quad (39)$$

and for Raman vibrational backscatter,

$$\frac{d\varphi}{d\Omega}(\omega)_{\parallel} = \frac{\omega^4}{c^4} \frac{\hbar}{2m\omega_j} \frac{\left(\alpha'^2 + \frac{4}{45} \beta'^2 \right)}{1 - e^{-\hbar\omega_j/KT}} \quad (40)$$

for $\Delta v = +1$ and $\omega = (\omega_0 - \omega_j)$.

For backscatter polarized perpendicular to the laser's polarization, $\Omega \neq \Sigma$. Therefore, for Rayleigh backscatter,

$$\frac{d\varphi}{d\Omega}(\omega_0)_{\perp} = \frac{\omega_0^4}{c^4} \left(\frac{3}{45} \beta^2 \right) \quad (41)$$

and for Raman vibrational backscatter,

$$\frac{d\sigma}{d\Omega}(\omega)_1 = \frac{\omega^4}{c^4} \frac{\pi}{2m\omega_j} \frac{\left(\frac{3}{45} \beta'^2\right)}{1 - e^{-h\omega_j/KT}} \quad (42)$$

for $\Delta v = +1$ and $\omega = (\omega_0 - \omega_j)$.

The cross sections given in equations (39) and (41) include, in addition to the true Rayleigh line, pure rotational Raman fine structure. This fine structure is also present in the vibrational Raman effect whose cross sections are given in equations (40) and (42).

An analysis of rotational fine structure for diatomic molecules such as nitrogen and oxygen is presented in the next section.

IIC. Rotational Raman Fine Structure of Rayleigh and Raman Vibrational Scattering

If rotation of the molecule is included, the wavefunction ψ_m can be approximately expressed as

$$\psi_m = \psi_e \prod_j \psi_{vj}(q_j) \psi_r \quad (43)$$

where ψ_r is the rotational part of the molecular wavefunction.

To determine the distribution of the rotational fine structure, equation (29) will be rewritten to include rotation as

$$\begin{aligned} (\alpha_{\mu\nu})_{mm_0} &= \langle \psi_r^* | \alpha_{\mu\nu}^0 | \psi_r \rangle \delta_{ee'} \delta_{vv'} \\ &+ \sum_j \langle \psi_r^* | \alpha_{\mu\nu}' | \psi_r \rangle \langle \psi_{vj}^* | q_j | \psi_{vj} \rangle \end{aligned} \quad (44)$$

Although $\alpha_{\mu\nu}^0$ and $\alpha_{\mu\nu}^1$ are constant in the molecular frame of reference, when the polarizability tensor is transformed to laboratory coordinates, as outlined in appendix A, the direction cosine functions cause the rotational matrix elements to be non-zero. This is illustrated by substituting equation (A-3) into equation (44):

$$\begin{aligned}
 (\alpha_{\Omega\Sigma})_{mm_0} = & \sum_i \alpha_i \langle \psi_r^* | \cos(i,\Sigma) \cos(i,\Omega) | \psi_r \rangle \\
 & + \sum_{ij} \alpha_i' \langle \psi_r^* | \cos(i,\Sigma) \cos(i,\Omega) | \psi_r \rangle \langle \psi_{v_j}^* | q_j | \psi_{v_j} \rangle \quad (45)
 \end{aligned}$$

The first term on the right side of equation (45) gives rise to the rotational Raman fine structure on the Rayleigh scattering line. The second term gives rise to the Raman rotational fine structure of the vibrational Raman effect.

II C1. Pure Rotational Raman Fine Structure

Considering first the rotational Raman fine structure on the Rayleigh line and limiting the analysis to a rigid rotating molecule (a good approximation for nitrogen and oxygen), the rotational part of the molecular wavefunction can be written as

$$\psi_r = Y_J^m(\theta, \varphi) = \sqrt{\frac{2J+1}{4\pi} \frac{(J-m)!}{(J+m)!}} P_J^m(\cos \theta) e^{im\varphi} \quad (46)$$

where the $Y_J^m(\theta, \varphi)$'s are normalized spherical harmonics.

The energy levels of the rigid rotator are

$$E_J^0 = \frac{h^2 J(J+1)}{2I_0} \quad (47)$$

where I_0 is the molecular moment of inertia.

If

$$B_0 \equiv \frac{h}{8\pi^2 c I_0}$$

then equation (47) becomes

$$E_J^0 = chB_0 J(J+1) \quad (48)$$

where B_0 is referred to as the molecular rotation constant.

In analogy to equation (33), the cross section for the pure rotational Raman scattering can be written as

$$\begin{aligned} \frac{d\sigma}{d\Omega}(\Omega, \Sigma, \omega, J) &= \frac{\omega^4 g_J (2J+1) e^{-B_0 J(J+1)hc/KT}}{c^4 \sum_J g_J (2J+1) e^{-B_0 J(J+1)hc/KT}} \\ &\times \left[\sum_i \alpha_i \langle \psi_r^* | \cos(i, \Sigma) \cos(i, \Omega) | \psi_r \rangle \right]^2 \quad (49) \end{aligned}$$

with $\omega = \omega_0 \pm \omega_r$ where

$$\omega_r = \frac{E_{J'} - E_J}{h} = 2\pi c B_0 [J'(J'+1) - J(J+1)]$$

and g_J is the nuclear degeneracy.

Approximating the summation by integration, as shown in appendix C, equation (49) becomes

$$\frac{d\varphi}{d\Omega}(\Omega, \Sigma, \omega, J) = \frac{\omega^4}{c^4} \frac{2B_0 hc}{KT} \frac{g_J(2J+1)e^{-B_0 J(J+1)hc/KT}}{g_J^+ + g_J^-} \times \left[\sum_i \alpha_i \langle \psi_r^* | \cos(i, \Sigma) \cos(i, \Omega) | \psi_r \rangle \right]^2 \quad (50)$$

where g_J^+ and g_J^- are the nuclear degeneracies for J even and odd, respectively.

Substituting the rotational wavefunction given in equation (46) into equation (50) results in the complete equation for pure rotational Raman scattering:

$$\frac{d\varphi}{d\Omega}(\Omega, \Sigma, \omega, J) = \frac{\omega^4}{c^4} \frac{2B_0 hc}{KT} \frac{g_J(2J+1)e^{-B_0 J(J+1)hc/KT}}{g_J^+ + g_J^-} \times \left[\sum_i \alpha_i \langle Y_J^{*m}(\theta, \varphi) | \cos(i, \Sigma) \cos(i, \Omega) | Y_J^{m'}(\theta, \varphi) \rangle \right]^2 \quad (51)$$

A sample calculation of part of one of the terms in the rotational matrix elements is given in appendix D, which indicates that the selection rules for the rotational Raman effect are $\Delta J = 0, \pm 2$. Placzek⁽²²⁾ performed the complete analysis using cylindrical coordinates and determined the J dependence of the cross sections to be

$$\frac{3(J+1)(J+2)}{2(2J+3)} \quad \text{for } \Delta J = +2$$

and

$$\frac{3(J-1)J}{2(2J-1)} \quad \text{for } \Delta J = -2$$

(52)

Using the J dependence given in equation (52), the relative distribution of the cross sections for pure rotational Raman scattering is

$$\frac{d\sigma}{d\Omega}(\Omega, \Sigma, \omega, J) \propto \frac{\omega^4}{c^4} \frac{2B_0 hc}{KT} \frac{g_J}{g_J^+ + g_J^-} \frac{3(J+1)(J+2)}{2(2J+3)} e^{-B_0 J(J+1)hc/KT} \quad (53)$$

for $\Delta J = +2$, $J = 0, 1, 2, \dots$

$$\omega = \omega_0 - \omega_r$$

and

$$\omega_r = 8\pi c B_0 \left(J + \frac{3}{2} \right),$$

and

$$\frac{d\sigma}{d\Omega}(\Omega, \Sigma, \omega, J) \propto \frac{\omega^4}{c^4} \frac{2B_0 hc}{KT} \frac{g_J}{g_J^+ + g_J^-} \frac{3(J-1)J}{2(2J-1)} e^{-B_0 J(J+1)hc/KT} \quad (54)$$

for $\Delta J = -2$, $J = 2, 3, 4, \dots$

$$\omega = \omega_0 - \omega_r$$

and

$$\omega_r = 8\pi c B_0 \left(J - \frac{1}{2} \right)$$

Placzek⁽²²⁾ has shown that only the β^2 component in the total cross section contributes to transitions involving $\Delta J = \pm 2$, and that for a rotor 25 percent of the β^2 component contributes to the $\Delta J = 0$ transitions.

Equations (39) and (41) for the backscatter cross sections may, therefore, be divided as follows:

$$\frac{d\varphi}{d\Omega}(\omega_o)_{||} = \frac{\omega_o^4}{c^4} \left(\alpha^2 + \frac{1}{45} \beta^2 \right) \quad \text{for } \Delta J = 0 \quad (55)$$

$$\frac{d\varphi}{d\Omega}(\omega_o)_{||} = \frac{\omega_o^4}{c^4} \frac{3}{45} \beta^2 \quad \text{for all transitions } \Delta J = \pm 2 \quad (56)$$

$$\frac{d\varphi}{d\Omega}(\omega_o)_{\perp} = \frac{\omega_o^4}{c^4} \left(\frac{3}{180} \beta^2 \right) \quad \text{for } \Delta J = 0 \quad (57)$$

and

$$\frac{d\varphi}{d\Omega}(\omega_o)_{\perp} = \frac{\omega_o^4}{c^4} \left(\frac{9}{180} \beta^2 \right) \quad \text{for all transitions } \Delta J = \pm 2 \quad (58)$$

Thus by calculating the relative distribution of cross sections for the rotational Raman fine structure, utilizing equations (53) and (54) and relating their sum to equations (56) and (58), an approximate value for the individual rotational cross sections can be obtained. This calculation is performed for nitrogen and oxygen in section IID.

IIC2. Vibrational-Rotational Raman Fine Structure

In a vibrating rotating molecule the rotational energy levels will be affected by the molecule's vibrational state. The higher the vibrational state, the larger the average separation of atoms in the molecule, thus giving rise to an increased moment of inertia. The energy levels of the rotational states in the ground vibrational level given in equation (47) could have been expressed in terms of average molecular separation as:

$$E_J^0 = \frac{\hbar^2 J(J+1)}{2M} \left(\frac{1}{r_0^2} \right) \quad (59)$$

where M is the molecular reduced mass and $\left(\frac{1}{r_0^2} \right)$ is a measure of atomic separation. In similar fashion the rotational energy levels for a molecule in the v th vibrational excited state can be written as

$$\begin{aligned} E_J^v &\approx \frac{\hbar^2 J(J+1)}{2M} \left(\frac{1}{r_v^2} \right) \\ &= chB_v J(J+1) \end{aligned} \quad (60)$$

where the v th rotational constant is

$$B_v = \frac{h}{8\pi^2 cM} \left(\frac{1}{r_v^2} \right) = \frac{h}{8\pi^2 cI_v} \quad (61)$$

Pauling and Wilson⁽²⁴⁾ show that B_v can be written as

$$B_v = B_e - \alpha_e \left(v + \frac{1}{2} \right) + \dots \quad (62)$$

where B_e and α_e are molecular constants. If the treatment is restricted to vibrating rotors, the selection rules remain

$$\Delta J = 0, \pm 2$$

The relative distribution of cross sections for the rotational fine structure of the vibrational Raman scattering is the same as the pure rotational case except, of course, the frequencies are different.

This relative distribution is

$$\frac{d\varphi}{d\Omega}(\Omega, \Sigma, \omega, J) \propto \frac{\omega^4}{c^4} \frac{2B_0 hc}{KT} \frac{g_J}{g_J^+ + g_J^-} \frac{3(J+1)(J+2)}{2(2J+3)} e^{-B_0 J(J+1)hc/KT} \quad (63)$$

for $\Delta J = +2$, $J = 0, 1, 2, \dots$, $\Delta v = +1$ and $0 - 1$ transition

where

$$\omega = (\omega_0 - \omega_{rj})$$

with

$$\begin{aligned} \omega_{rj} &= \frac{E_{J'v'} - E_{Jv}}{h} \\ &= \omega_j + 2\pi c \left[6B_1 + (5B_1 - B_0)J + (B_1 - B_0)J^2 \right] \end{aligned}$$

and

$$\frac{d\varphi}{d\Omega}(\Omega, \Sigma, \omega, J) \propto \frac{\omega^4}{c^4} \frac{2B_0 hc}{KT} \frac{g_J}{g_J^+ + g_J^-} \frac{3(J-1)J}{2(2J-1)} e^{-B_0 J(J+1)hc/KT} \quad (64)$$

for $\Delta J = -2$, $J = 2, 3, 4, \dots$, $\Delta v = +1$ and $0 - 1$ transition

where

$$\omega = (\omega_0 - \omega_{rj})$$

with

$$\omega_{rj} = \omega_j + 2\pi c \left[2B_1 - (3B_1 + B_0)J + (B_1 - B_0)J^2 \right]$$

As in the case of pure rotational fine structure, Placzek's analysis showed that only the β'^2 component in the total vibrational

cross section contributes to transitions involving $\Delta J = \pm 2$, and that for a vibrating rotor 25 percent of the β'^2 component contributes to $\Delta J = 0$ transitions. As was indicated above, equations (40) and (42) may be divided as follows:

$$\frac{d\varphi(\omega)}{d\Omega}_{\parallel} = \frac{\omega^4}{c^4} \frac{h}{2m\omega_j} \frac{\left(\alpha'^2 + \frac{1}{45} \beta'^2\right)}{1 - e^{-h\omega_j/KT}} \quad \text{for } \begin{matrix} \Delta J = 0 \\ \Delta V = +1 \end{matrix} \quad (65)$$

$$\frac{d\varphi(\omega)}{d\Omega}_{\parallel} = \frac{\omega^4}{c^4} \frac{h}{2m\omega_j} \frac{\frac{3}{45} \beta'^2}{1 - e^{-h\omega_j/KT}} \quad \text{for all transitions } \begin{matrix} \Delta J = \pm 2 \\ \Delta V = +1 \end{matrix} \quad (66)$$

$$\frac{d\varphi(\omega)}{d\Omega}_{\perp} = \frac{\omega^4}{c^4} \frac{h}{2m\omega_j} \frac{\frac{3}{180} \beta'^2}{1 - e^{-h\omega_j/KT}} \quad \text{for } \begin{matrix} \Delta J = 0 \\ \Delta V = +1 \end{matrix} \quad (67)$$

and

$$\frac{d\varphi(\omega)}{d\Omega}_{\perp} = \frac{\omega^4}{c^4} \frac{h}{2m\omega_j} \frac{\frac{9}{180} \beta'^2}{1 - e^{-h\omega_j/KT}} \quad \text{for all transitions } \begin{matrix} \Delta J = \pm 2 \\ \Delta V = +1 \end{matrix} \quad (68)$$

Again calculating the relative distribution of cross sections for the vibration-rotation lines, utilizing equations (63) and (64) and relating their sum to equations (66) and (68), an approximate value of the cross section for each individual line can be obtained. This calculation will also be performed for N_2 and O_2 in section IID.

IID. Cross-Section Calculations for Raman Backscatter From N₂ and O₂

The molecular constants for the calculation of scattering cross sections of N₂ and O₂ are summarized in table I.

TABLE I.- MOLECULAR CONSTANTS OF N₂ AND O₂

	$\alpha \times 10^{24}$ (cm ³)	$\beta \times 10^{24}$ (cm ³)	$\alpha' \times 10^{16}$ (cm ²)	$\beta' \times 10^{16}$ (cm ²)	ν_j $v = 0 \rightarrow 1$	B_e (cm ⁻¹)	α_e
N ₂	1.79	0.95	1.6	2.2	2330.7	2.010	0.0187
O ₂	1.63	1.2	1.4	2.3	1554.7	1.44566	0.01579

The values for α , β , α' , and β' were determined from data published in reference 25. The remaining constants in table I are listed by Herzberg.⁽²⁶⁾ The results of substituting the appropriate values from table I into the backscatter cross sections given in equations (55) through (58) and (65) through (68) are summarized in tables II and III.

TABLE II.- CROSS SECTIONS OF N₂ AND O₂ FOR RAYLEIGH BACKSCATTER

AND THE SUM OF THE PURE ROTATIONAL RAMAN BACKSCATTER

WITH $\lambda_0 = 3471.5 \text{ \AA}$

	$\frac{d\sigma}{d\Omega}(\omega_0)_{\parallel}$ $\Delta J = 0$ (cm ² ster ⁻¹)	$\frac{d\sigma}{d\Omega}(\omega_0)_{\parallel}$ All transitions $\Delta J = \pm 2$ (cm ² ster ⁻¹)	$\frac{d\sigma}{d\Omega}(\omega_0)_{\perp}$ $\Delta J = 0$ (cm ² ster ⁻¹)	$\frac{d\sigma}{d\Omega}(\omega_0)_{\perp}$ All transitions $\Delta J = \pm 2$ (cm ² ster ⁻¹)
N ₂	3.5×10^{-27}	6.5×10^{-29}	1.6×10^{-29}	3.2×10^{-29}
O ₂	2.9×10^{-27}	1.0×10^{-28}	2.6×10^{-29}	5.1×10^{-29}

TABLE III.- BACKSCATTER CROSS SECTIONS OF N_2 AND O_2 FOR $v = 0 \rightarrow 1$,
 $\Delta J = 0$ VIBRATIONAL TRANSITION (Q-BRANCH), AND THE SUM OF
 THE VIBRATION-ROTATION TRANSITIONS (O-BRANCH PLUS S-
 BRANCH); $\lambda_{N_2} = 3777 \text{ \AA}$, $\lambda_{O_2} = 3669 \text{ \AA}$

	$\frac{d\phi}{d\Omega}(\omega)_{\parallel}$ $\Delta J = 0$ ($\text{cm}^2\text{ster}^{-1}$)	$\frac{d\phi}{d\Omega}(\omega)_{\parallel}$ All transitions $\Delta J = \pm 2$ ($\text{cm}^2\text{ster}^{-1}$)	$\frac{d\phi}{d\Omega}(\omega)_{\perp}$ $\Delta J = 0$ ($\text{cm}^2\text{ster}^{-1}$)	$\frac{d\phi}{d\Omega}(\omega)_{\perp}$ All transitions $\Delta J = \pm 2$ ($\text{cm}^2\text{ster}^{-1}$)
N_2	2.1×10^{-30}	2.5×10^{-31}	6.4×10^{-32}	1.3×10^{-31}
O_2	2.4×10^{-30}	4.1×10^{-31}	1.0×10^{-31}	2.0×10^{-31}

The relative cross sections of N_2 and O_2 for the rotational fine structure has been calculated using equations (53), (54), (63), and (64), and the results are given in Appendix E. Also given in Appendix E are the normalized cross sections determined by dividing each relative cross section by the sum of the relative cross sections for $\Delta J = \pm 2$. An approximate value for the true cross sections are obtained by multiplying each normalized cross section by the appropriate value from tables II and III. An abbreviated listing of these results for the rotational fine structure of the nitrogen $v = 0 \rightarrow 1$ vibrational transition are given in tables IV and V and are plotted in figure 1. A complete listing of the fine structure cross sections of N_2 and O_2 is given in Appendix E.

TABLE IV.- DIFFERENTIAL BACKSCATTER CROSS SECTIONS FOR ROTATIONAL
FINE STRUCTURE OF THE $v = 0 \rightarrow 1$ RAMAN VIBRATIONAL
TRANSITION OF N_2 . $\Delta J = +2$

J	$\lambda, (\mu)$	Normalized cross section $\Delta J = -2$	$\frac{d\sigma}{d\Omega}(\omega)_\perp$	$\frac{d\sigma}{d\Omega}(\omega)_\parallel$
0	3.77880E-01	1.71574E-C2	2.18070E-33	4.36140E-33
1	3.77993E-01	1.51296E-02	1.92297E-33	3.84593E-33
2	3.78105E-01	4.15475E-02	5.28069E-33	1.05614E-32
3	3.78217E-01	2.53898E-02	3.22705E-33	6.45409E-33
4	3.78328E-01	5.76401E-02	7.32606E-33	1.46521E-32
5	3.78439E-01	3.09756E-C2	3.93700E-33	7.87400E-33
6	3.78550E-01	6.37150E-C2	8.09818E-33	1.61964E-32
7	3.78659E-01	3.15539E-02	4.01050E-33	8.02101E-33
8	3.78769E-01	6.04501E-C2	7.68321E-33	1.53664E-32
9	3.78878E-01	2.80811E-C2	3.56910E-33	7.13820E-33
10	3.78986E-01	5.07144E-02	6.44581E-33	1.28916E-32
11	3.79094E-01	2.22900E-02	2.83305E-33	5.66611E-33
12	3.79202E-01	3.81931E-02	4.85435E-33	9.70869E-33
13	3.79309E-01	1.59605E-02	2.02857E-33	4.05715E-33
14	3.79415E-01	2.60455E-02	3.31039E-33	6.62078E-33
15	3.79521E-01	1.03799E-02	1.31928E-33	2.63857E-33
16	3.79627E-01	1.61718E-02	2.05543E-33	4.11087E-33
17	3.79732E-01	6.15871E-03	7.82772E-34	1.56554E-33
18	3.79837E-01	9.17611E-03	1.16628E-33	2.33257E-33
19	3.79941E-01	3.34405E-03	4.25029E-34	8.50059E-34
20	3.80045E-01	4.77049E-03	6.06329E-34	1.21266E-33
21	3.80148E-01	1.66534E-03	2.11665E-34	4.23329E-34
22	3.80251E-01	2.27664E-03	2.89361E-34	5.78723E-34
23	3.80353E-01	7.61889E-04	9.68360E-35	1.93672E-34
24	3.80454E-01	9.98793E-04	1.26947E-34	2.53893E-34
25	3.80556E-01	3.20615E-04	4.07501E-35	8.15003E-35

TABLE V.- DIFFERENTIAL BACKSCATTER CROSS SECTIONS FOR ROTATIONAL
FINE STRUCTURE OF THE $v = 0 \rightarrow 1$ RAMAN VIBRATIONAL
TRANSITION OF N_2 . $\Delta J = -2$

J	$\lambda, (\mu)$	Normalized cross section $\Delta J = +2$	$\frac{d\sigma}{d\Omega}(\omega)_\perp$	$\frac{d\sigma}{d\Omega}(\omega)_\parallel$
2	3.77539E-01	1.62544E-02	2.06594E-33	4.13188E-33
3	3.77425E-01	1.38260E-02	1.75728E-33	3.51456E-33
4	3.77310E-01	3.66237E-02	4.65487E-33	9.30975E-33
5	3.77194E-01	2.15886E-02	2.74391E-33	5.48783E-33
6	3.77078E-01	4.72757E-02	6.00874E-33	1.20175E-32
7	3.76962E-01	2.45064E-02	3.11477E-33	6.22954E-33
8	3.76845E-01	4.86239E-02	6.18010E-33	1.23602E-32
9	3.76728E-01	2.32279E-02	2.95226E-33	5.90452E-33
10	3.76610E-01	4.29241E-02	5.45565E-33	1.09113E-32
11	3.76492E-01	1.92338E-02	2.44461E-33	4.88923E-33
12	3.76373E-01	3.35066E-02	4.25869E-33	8.51738E-33
13	3.76254E-01	1.42055E-02	1.80552E-33	3.61103E-33
14	3.76134E-01	2.34790E-02	2.98418E-33	5.96836E-33
15	3.76014E-01	9.46426E-03	1.20291E-33	2.40581E-33
16	3.75894E-01	1.48978E-02	1.89351E-33	3.78702E-33
17	3.75773E-01	5.72702E-03	7.27904E-34	1.45581E-33
18	3.75651E-01	8.60679E-03	1.09392E-33	2.18785E-33
19	3.75530E-01	3.16170E-03	4.01852E-34	8.03703E-34
20	3.75407E-01	4.54398E-03	5.77540E-34	1.15508E-33
21	3.75284E-01	1.59734E-03	2.03022E-34	4.06044E-34
22	3.75161E-01	2.19803E-03	2.79370E-34	5.58740E-34
23	3.75038E-01	7.40152E-04	9.40734E-35	1.88147E-34
24	3.74914E-01	9.76023E-04	1.24052E-34	2.48105E-34
25	3.74789E-01	3.15067E-04	4.00450E-35	8.00900E-35
26	3.74664E-01	3.98413E-04	5.06383E-35	1.01277E-34
27	3.74539E-01	1.23364E-04	1.56795E-35	3.13591E-35

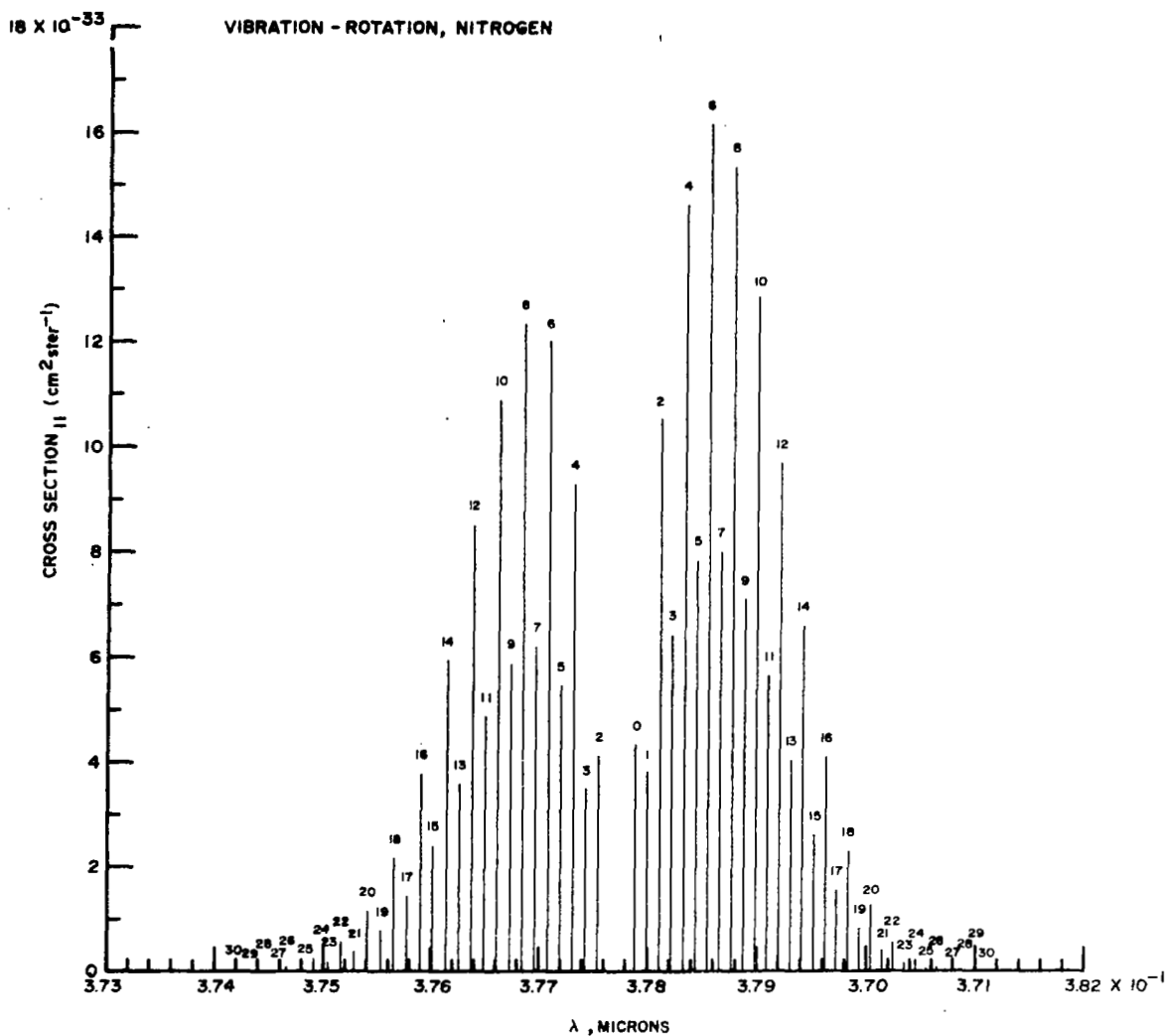


Figure 1.- A plot of rotational fine structure for the nitrogen $v = 0 \rightarrow 1$ vibrational Raman transition as a function of wavelength.

IIE. Calculation of the Raman Backscatter From the Atmosphere

For a system pointing on the vertical, the optical radar equation for Raman backscatter from the atmosphere is: ⁽¹⁴⁾

$$i_S(Z) = \frac{\gamma(\lambda_R) \eta(\lambda_R) cEA}{2Z^2} \frac{d\phi}{d\Omega_{\lambda_R}} n(Z) q(\lambda_0, Z) q(\lambda_R, Z) \quad (69)$$

where

i_S is the photomultiplier cathode current

$Z = \frac{ct}{2}$ is the altitude

t is the elapsed time after laser emission

γ is the system optical efficiency

η is the cathode spectral sensitivity

E is the total laser energy at λ_0

A is the area of the receiver telescope

n is the number density of Raman scattering molecules

q is the atmospheric transmissivity

λ_0 is the wavelength of the incident light

and

λ_R is the Raman wavelength

Characteristic values of the constant terms in equation (69) for the optical radar system used in this investigation are listed in table VI. No attempt was made to absolutely calibrate the optical radar system, therefore the values in table VI, with the exception of A , must be considered approximate.

TABLE VI.- TYPICAL PARAMETERS FOR
THE RAMAN OPTICAL RADAR

$\gamma_{3669} \text{ \AA}$	≈ 0.02
$\gamma_{3777} \text{ \AA}$	≈ 0.08
$\gamma_{3976} \text{ \AA}$	≈ 0.30
η	$\approx 0.04 \text{ amperes watt}^{-1}$
E	$\approx 0.04 \text{ joules}$
A	0.13 m^2

Since the optical receiver system is assumed not to be polarization sensitive and the interference filter passband included rotational fine structure, the total effective backscatter cross section can be written

$$\begin{aligned} \frac{d\sigma}{d\Omega}(\omega) &= \frac{d\sigma}{d\Omega}(\omega)_{\parallel, \Delta J=0} + \frac{d\sigma}{d\Omega}_{\perp, \Delta J=0} \\ &+ \sum_J \left[\frac{d\sigma}{d\Omega}(\omega)_{\parallel, \Delta J=\pm 2} + \frac{d\sigma}{d\Omega}(\omega)_{\perp, \Delta J=\pm 2} \right] W(\omega_J) \end{aligned} \quad (70)$$

where $W(\omega_J)$ is the relative transmission of the interference filter, normalized to 1 at the peak transmission. $W(\lambda_J)$ is assumed for the purpose of these calculations to be Gaussian with a full width at half maximum transmission equal to 35 \AA . The measured transmission curves of the interference filters indicate that this is a good assumption.

Using the cross section values given in table III and Appendix E, the total effective backscatter cross section for N_2 and O_2 are:

$$\frac{d\sigma}{d\Omega}(3777 \text{ \AA})_{N_2}^0 = 2.5 \times 10^{-30} \text{ cm}^2 \text{ ster}^{-1} \quad (71)$$

and

$$\frac{d\sigma}{d\Omega}(3669 \text{ Å})_{\text{O}_2} = 3.0 \times 10^{-30} \text{ cm}^2 \text{ster}^{-1} \quad (72)$$

The water vapor molecule is in the class of molecules called an asymmetric top. The ν_1 symmetric vibration (3569 cm^{-1}) cross section will, for purposes of calculation, be assumed to be of the same order as the nitrogen cross section. Therefore,

$$\frac{d\sigma}{d\Omega}(3976 \text{ Å})_{\text{H}_2\text{O}} \simeq 10^{-30} \text{ cm}^2 \text{ster}^{-1} \quad (73)$$

Using these cross sections in equation (69), an estimate of the backscatter return from the atmosphere may be made. These estimates are listed in tables VII through XII. The values q_M and q_T were obtained from Elterman⁽²⁷⁾ and denote transmissivity for a pure molecular atmosphere and a "clear atmosphere," respectively. The pure molecular atmospheric model is based on the U.S. Standard Atmosphere, 1962⁽²⁸⁾ and includes only the attenuation of light due to the gaseous atmosphere. The "clear atmosphere," developed by Elterman, includes, in addition, the attenuation effects attributed to the presence of aerosols. The number density of N_2 and O_2 was derived from the U.S. Standard Atmosphere, 1962.⁽²⁸⁾ Water vapor number densities are based on a constant mixing ratio of 1 gm/kg. The other signal terms in these tables were calculated using

$$V = i_s R G$$

where R is the effective load resistance (25Ω) and G is the phototube gain (10^8) and

TABLE VII.- CALCULATED RAMAN BACKSCATTER RECEIVED SIGNAL FOR THE
 $\nu = 0 \rightarrow 1$ VIBRATIONAL BAND OF N_2 FOR
 ELTERMAN'S "CLEAR ATMOSPHERE."

Z (km)	$q(3400 \text{ \AA})_{T*}$	$q(3800 \text{ \AA})_{T*}$	n_{N_2} (meter ⁻³)	i_s (amperes)	V (volts)	n_s (ct/sec)
0.20	.9505	.9577	1.9514	2.726760×10^{-10}	6.816900×10^{-1}	1.704225×10^9
0.40	.9034	.9172	1.9140	6.086000×10^{-11}	15.215000×10^{-2}	3.803750×10^8
0.60	.8586	.8784	1.8772	2.406160	6.015400	1.503850
0.80	.8161	.8413	1.8409	1.212640	3.031600	.757900
1.00	.7757	.8057	1.8052	6.927200×10^{-12}	17.318000×10^{-3}	4.329500×10^7
1.20	.7529	.7868	1.7700	4.470800	11.177000	2.794250
1.40	.7308	.7683	1.7354	3.052080	7.630200	1.907550
1.60	.7093	.7502	1.7012	2.171200	5.428000	1.357000
1.80	.6885	.7326	1.6676	1.594040	3.985100	.996275
2.00	.6683	.7153	1.6345	1.199400	2.998500	.749625
2.20	.6552	.7050	1.6019	9.387200×10^{-13}	23.468000×10^{-4}	5.867000×10^6
2.40	.6424	.6948	1.5698	7.468000	18.670000	4.667500
2.60	.6298	.6847	1.5382	6.024800	15.062000	3.765500
2.80	.6174	.6748	1.5071	4.917600	12.294000	3.073500
3.00	.6053	.6650	1.4765	4.054800	10.137000	2.534250
3.20	.5964	.6582	1.4464	3.404400	8.511000	2.127750
3.40	.5877	.6516	1.4167	2.881600	7.204000	1.801000
3.60	.5790	.6449	1.3876	2.454800	6.137000	1.534250
3.80	.5705	.6384	1.3588	2.104400	5.261000	1.315250
4.00	.5621	.6319	1.3305	1.813600	4.534000	1.133500
4.20	.5553	.6270	1.3027	1.578800	3.947000	.986750
4.40	.5486	.6221	1.2753	1.380400	3.451000	.862750
4.60	.5419	.6173	1.2484	1.211600	3.029000	.757250
4.80	.5354	.6125	1.2219	1.068000	2.670000	.667500
5.00	.5289	.6077	1.1959	9.440000×10^{-14}	23.600000×10^{-5}	5.900000×10^5
6.00	.5026	.5987	1.0720	5.500000	13.750000	3.437500
7.00	.4853	.5718	.9581	3.331600	8.329000	2.082250
8.00	.4626	.5577	.8539	2.113600	5.284000	1.321000
9.00	.4466	.5460	.7585	1.402000	3.505000	.876250
10.00	.4330	.5353	.6715	9.556000×10^{-15}	23.890000×10^{-6}	5.972500×10^4
11.00	.4215	.5262	.5924	6.668000	16.670000	4.167500
12.00	.4115	.5189	.5066	4.612000	11.530000	2.882500
13.00	.4033	.5122	.4329	3.248800	8.122000	2.030500
14.00	.3961	.5066	.3700	2.326000	5.815000	1.453750

*Elterman, L; AFCL Environmental Research Paper No. 20, 1964

TABLE VIII.- CALCULATED RAMAN BACKSCATTER RECEIVED SIGNAL FOR THE
 $\nu = 0 \rightarrow 1$ VIBRATIONAL BAND OF N_2 FOR A MOLECULAR ATMOSPHERE

Z (km)	$q(3400 \text{ \AA})_{M*}$	$q(3800 \text{ \AA})_{M*}$	n_{N_2} (meter ⁻³)	i_s (amperes)	V (volts)	n_s (ct/sec)
0.20	.9839	.9899	1.9514	2.917480×10^{-10}	7.293700×10^{-1}	1.823425×10^9
0.40	.9681	.9799	1.9140	6.967920×10^{-11}	17.419800×10^{-2}	4.354950×10^8
0.60	.9526	.9700	1.8772	2.958480	7.396200	1.849050
0.80	.9373	.9602	1.8409	1.589520	3.973800	.993450
1.00	.9222	.9505	1.8052	9.715880×10^{-12}	24.289700×10^{-3}	6.072425×10^7
1.20	.9088	.9417	1.7700	6.459080	16.147700	4.036925
1.40	.8955	.9331	1.7354	4.542720	11.356800	2.839200
1.60	.8825	.9245	1.7012	3.329020	8.322550	2.080637
1.80	.8696	.9161	1.6676	2.517612	6.294030	1.573507
2.00	.8569	.9076	1.6345	1.951320	4.878300	1.219575
2.20	.8456	.9001	1.6016	1.546480	3.866200	.966550
2.40	.8344	.8927	1.5698	1.246468	3.116170	.779042
2.60	.8234	.8853	1.5382	1.018464	2.546160	.636540
2.80	.8125	.8779	1.5071	8.419240×10^{-13}	21.048100×10^{-4}	5.262025×10^6
3.00	.8018	.8707	1.4765	7.032400	17.581000	4.395250
3.20	.7922	.8641	1.4464	5.936960	14.842400	3.710600
3.40	.7828	.8577	1.4167	5.052240	12.630600	3.157650
3.60	.7735	.8512	1.3876	4.328400	10.821000	2.705250
3.80	.7643	.8449	1.3588	3.731080	9.327700	2.331925
4.00	.7552	.8385	1.3305	3.233240	8.083100	2.020775
4.20	.7471	.8329	1.3027	2.821600	7.054000	1.763500
4.40	.7391	.8273	1.2753	2.473160	6.182900	1.545725
4.60	.7311	.8217	1.2484	2.176240	5.440600	1.360150
4.80	.7233	.8162	1.2219	1.922400	4.806000	1.201500
5.00	.7156	.8107	1.1959	1.703960	4.259900	1.064975
6.00	.6817	.7864	1.0720	9.801600×10^{-14}	24.504000×10^{-5}	6.126000
7.00	.6528	.7653	.9581	5.997600	14.994000	3.748500
8.00	.6281	.7470	.8539	3.843600	9.609000	2.402250
9.00	.6068	.7310	.7585	2.550400	6.376000	1.594000
10.00	.5885	.7171	.6715	1.740000	4.350000	1.087500
11.00	.5729	.7051	.5924	1.214000	3.035000	.758750
12.00	.5596	.6948	.5066	8.396000×10^{-15}	20.990000×10^{-6}	5.247500×10^5
13.00	.5485	.6861	.4329	5.916000	14.790000	3.697500
14.00	.5392	.6788	.3700	4.240000	10.600000	2.650000

*Elterman, L; AFCL Environmental Research Paper No. 20, 1964

TABLE IX.- CALCULATED RAMAN BACKSCATTER RECEIVED SIGNAL FOR THE
 $v = 0 \rightarrow 1$ VIBRATIONAL BAND OF O_2 FOR ELTERMAN'S
 "CLEAR ATMOSPHERE."

Z (km)	$q(3400 \text{ \AA})_{T^*}$	$q(3600 \text{ \AA})_{T^*}$	n_{O_2} (meter ⁻³)	i_S (amperes)	V (volts)	n_S (ct/sec)
0.20	.9050	.9537	.5022	2.144720×10^{-11}	5.361800×10^{-7}	1.340450×10^8
0.40	.9034	.9096	.4926	4.767600×10^{-12}	11.919000×10^{-3}	2.979750×10^7
0.60	.8586	.8674	.4831	1.883520	4.708800	1.177200
0.80	.8161	.8273	.4737	9.417200×10^{-13}	23.543000×10^{-4}	5.885750×10^6
1.00	.7757	.7890	.4646	5.358400	13.396000	3.349000
1.20	.7529	.7683	.4555	3.448160	8.620400	2.155100
1.40	.7308	.7481	.4466	2.347520	5.868800	1.467200
1.60	.7093	.7285	.4378	1.665280	4.163200	1.040800
1.80	.6885	.7094	.4291	1.218960	3.047400	.761850
2.00	.6683	.6907	.4206	9.146400×10^{-14}	22.866000×10^{-5}	5.716500×10^5
2.20	.6552	.6791	.4122	7.141200	17.853000	4.463250
2.40	.6424	.6676	.4040	5.668400	14.171000	3.542750
2.60	.6298	.6564	.3958	4.561200	11.403000	2.850750
2.80	.6174	.6453	.3878	3.713680	9.284200	2.321050
3.00	.6053	.6344	.3800	3.055360	7.638400	1.909600
3.20	.5964	.6268	.3722	2.560080	6.400200	1.600050
3.40	.5877	.6192	.3646	2.162880	5.407200	1.351800
3.60	.5790	.6116	.3571	1.838720	4.596800	1.149200
3.80	.5705	.6042	.3497	1.573040	3.932600	.983150
4.00	.5621	.5969	.3424	1.353040	3.382600	.845650
4.20	.5553	.5912	.3352	1.175520	2.938800	.734700
4.40	.5486	.5856	.3282	1.026240	2.565600	.641400
4.60	.5419	.5800	.3212	8.990400×10^{-15}	22.476000×10^{-6}	5.619000×10^4
4.80	.5354	.5744	.3144	7.908000	19.770000	4.942500
5.00	.5289	.5689	.3077	6.978400	17.446000	4.361500
6.00	.5026	.5461	.2759	3.964000	9.910000	2.477500
7.00	.4853	.5273	.2466	2.426920	6.067300	1.516825
8.00	.4626	.5112	.2198	1.530520	3.826300	.956575
9.00	.4466	.4976	.1952	1.009200	2.523000	.630750
10.00	.4330	.4858	.1728	6.850000×10^{-16}	17.125000×10^{-7}	4.281250×10^3
11.00	.4215	.4757	.1524	4.759200	11.898000	2.974500
12.00	.4115	.4667	.1304	3.277200	8.193000	2.048250
13.00	.4033	.4598	.1114	2.303600	5.759000	1.439750
14.00	.3961	.4534	.0952	1.644000	4.110000	1.027500

*Elterman, L; AFCRL Environmental Research Paper No. 20, 1964

TABLE X. - CALCULATED RAMAN BACKSCATTER RECEIVED SIGNAL FOR THE

 $\nu = 0 \rightarrow 1$ VIBRATIONAL BAND OF O_2 FOR A MOLECULAR ATMOSPHERE

Z (km)	$q(3400 \text{ \AA})_{M^*}$	$q(3600 \text{ \AA})_{M^*}$	n_{O_2} (meter ⁻³)	i_s (amperes)	V (volts)	n_s (ct/sec)
0.20	.9839	.9873	.5022	2.298308×10^{-11}	5.745770×10^{-2}	1.436442×10^8
0.40	.9681	.9748	.4926	5.475220×10^{-12}	13.688050×10^{-3}	3.422012×10^7
0.60	.9526	.9625	.4831	2.318660	5.796550	1.449162
0.80	.9372	.9503	.4737	1.263760	3.159400	.789850
1.00	.9222	.9383	.4646	7.575920×10^{-13}	18.939800×10^{-4}	4.734950×10^6
1.20	.9088	.9275	.4555	5.024560	12.561400	3.140350
1.40	.8955	.9168	.4466	3.525280	8.813200	2.203300
1.60	.8825	.9063	.4378	2.577560	6.443900	1.610975
1.80	.8696	.8959	.4291	1.944360	4.860900	1.215225
2.00	.8569	.8856	.4206	1.503720	3.759300	.939825
2.20	.8456	.8764	.4122	1.189360	2.973400	.743350
2.40	.8344	.8673	.4040	9.565200×10^{-14}	23.913000×10^{-5}	5.978250×10^5
2.60	.8234	.8583	.3958	7.797600	19.494000	4.873500
2.80	.8125	.8494	.3878	6.411200	16.028000	4.007000
3.00	.8018	.8405	.3800	5.362000	13.405000	3.351250
3.20	.7922	.8327	.3722	4.518400	11.296000	2.824000
3.40	.7828	.8249	.3646	3.837600	9.594000	2.398500
3.60	.7735	.8171	.3571	3.281600	8.204000	2.051000
3.80	.7643	.8095	.3497	2.823200	7.058000	1.764500
4.00	.7552	.8019	.3424	2.442000	6.105000	1.526250
4.20	.7471	.7951	.3352	2.126800	5.317000	1.329250
4.40	.7391	.7884	.3282	1.861200	4.653000	1.163250
4.60	.7311	.7817	.3212	1.634800	4.087000	1.021750
4.80	.7233	.7751	.3144	1.441600	3.604000	.901000
5.00	.7156	.7686	.3077	1.275600	3.189000	.797250
6.00	.6817	.7399	.2759	7.284000×10^{-15}	18.210000×10^{-6}	4.552500×10^4
7.00	.6528	.7151	.2466	4.424000	11.060000	2.765000
8.00	.6281	.6936	.2198	2.816000	7.040000	1.760000
9.00	.6068	.6751	.1952	1.860000	4.650000	1.162500
10.00	.5885	.6591	.1728	1.260000	3.150000	.787500
11.00	.5729	.6453	.1524	8.760000×10^{-16}	21.900000×10^{-7}	5.475000×10^3
12.00	.5596	.6334	.1304	6.040000	15.100000	3.775000
13.00	.5485	.6236	.1114	4.240000	10.600000	2.650000
14.00	.5392	.6152	.0952	3.000000	7.500000	1.875000

*Elterman, L.; AFCRL Environmental Research Paper No. 20, 1964

TABLE XI. CALCULATED RAMAN BACKSCATTER RECEIVED SIGNAL FOR THE ν_1
 SYMMETRIC VIBRATION LINE OF H_2O FOR ELTERMAN'S "CLEAR
 ATMOSPHERE." (ASSUMING CONSTANT MIXING RATIO OF
 1 gm/kg AND CROSS SECTION OF THE ORDER OF THE
 NITROGEN $\nu = 0 \rightarrow 1$ TRANSITION).

Z (km)	$q(3400 \text{ Å})_{T*}$	$q(4000 \text{ Å})_{T*}$	n_{H_2O} (meter ⁻³)	I_S (amperes)	V (volts)	n_S (ct/sec)
.20	.9505	.9637	.003886	8.197606×10^{-13}	20.494016×10^{-4}	5.123504×10^6
.40	.9034	.9287	.003812	1.841192	4.602980	1.150745
.60	.8586	.8949	.003738	7.349896×10^{-14}	18.374740×10^{-5}	4.593685×10^5
.80	.8161	.8624	.003666	3.713850	9.284626	2.321156
1.00	.7757	.8311	.003595	2.134962	5.337406	1.334351
1.20	.7529	.8146	.003525	1.382962	3.457406	.864351
1.40	.7308	.7985	.003456	9.478444×10^{-15}	23.696110×10^{-6}	5.924027×10^4
1.60	.7093	.7827	.003388	6.767984	16.919960	4.229990
1.80	.6885	.7672	.003321	4.987496	12.468740	3.117185
2.00	.6683	.7520	.003255	3.767333	9.418333	2.354583
2.20	.6552	.7429	.003190	2.955444	7.388610	1.847152
2.40	.6424	.7339	.003126	2.357184	5.892960	1.473240
2.60	.6298	.7250	.003063	1.906021	4.765053	1.191263
2.80	.6174	.7162	.003001	1.559384	3.898460	.974615
3.00	.6053	.7075	.002940	1.288874	3.222185	.805546
3.20	.5964	.7016	.002880	1.084236	2.710592	.677648
3.40	.5877	.6957	.002821	9.192073×10^{-16}	22.980183×10^{-7}	5.745045×10^3
3.60	.5790	.6899	.002763	7.845629	19.614073	4.903518
3.80	.5705	.6841	.002706	6.737333	16.843333	4.210833
4.00	.5621	.6784	.002650	5.817333	14.543333	3.635833
4.20	.5553	.6741	.002594	5.071110	12.677776	3.169444
4.40	.5486	.6698	.002540	4.440517	11.101293	2.775323
4.60	.5419	.6655	.002486	3.903184	9.757960	2.439490
4.80	.5354	.6613	.002433	3.444666	8.611666	2.152916
5.00	.5289	.6570	.002381	3.049406	7.623516	1.905879
6.00	.5026	.6395	.002135	1.755702	4.389256	1.097314
7.00	.4853	.6250	.001908	1.087925	2.719814	.679953
8.00	.4626	.6126	.001700	6.935554×10^{-17}	17.338886×10^{-8}	4.334721×10^2
9.00	.4466	.6023	.001510	4.620000	11.550000	2.887500
10.00	.4330	.5927	.001337	3.160740	7.901850	1.975462
11.00	.4215	.5851	.001179	2.214814	5.537036	1.384259
12.00	.4115	.5781	.001008	1.534814	3.837036	.959259
13.00	.4033	.5723	.000862	1.084444	2.711111	.677777
14.00	.3961	.5672	.000736	7.777777×10^{-18}	19.444443×10^{-9}	4.861110×10^1

*Elterman, L.; AFCRL Environmental Research Paper No. 20, 1964

TABLE XII.- CALCULATED RAMAN BACKSCATTER RECEIVED SIGNAL FOR THE ν_1 SYMMETRIC VIBRATION LINE OF H_2O FOR A MOLECULAR ATMOSPHERE. (ASSUMING CONSTANT MIXING RATIO OF 1 gm/kg AND CROSS SECTION OF THE ORDER OF THE NITROGEN $\nu = 0 \rightarrow 1$ TRANSITION)

Z (km)	$q(3400 \text{ \AA})_M$	$q(4000 \text{ \AA})_M$	n_{H_2O} (meter ⁻³)	i_s (amperes)	V (volts)	n_s (ct/sec)
.20	.9839	.9918	.003886	8.733096 x 10 ⁻¹³	21.832740 x 10 ⁻⁴	5.458185 x 10 ⁶
.40	.9681	.9837	.003812	2.089908	5.224770	1.306192
.60	.9526	.9757	.003738	8.890844 x 10 ⁻¹⁴	22.227110 x 10 ⁻⁵	5.556777 x 10 ⁵
.80	.9373	.9677	.003666	4.786214	11.965536	2.991384
1.00	.9222	.9598	.003595	2.931273	7.328183	1.832045
1.20	.9088	.9527	.003525	1.952337	4.880843	1.220210
1.40	.8955	.9457	.003456	1.375569	3.438923	.859730
1.60	.8825	.9386	.003388	1.009785	2.524464	.631116
1.80	.8696	.9317	.003321	7.650073 x 10 ⁻¹⁵	19.125183 x 10 ⁻⁶	4.781295 x 10 ⁴
2.00	.8569	.9248	.003255	5.940496	14.851240	3.712810
2.20	.8456	.9186	.003190	4.716392	11.790980	2.947745
2.40	.8344	.9124	.003126	3.806369	9.515923	2.378980
2.60	.8234	.9063	.003063	3.115088	7.787720	1.946930
2.80	.8125	.9002	.003001	2.579377	6.448443	1.612110
3.00	.8018	.8941	.002940	2.157569	5.393923	1.348480
3.20	.7922	.8887	.002880	1.824258	4.560646	1.140161
3.40	.7828	.8834	.002821	1.554688	3.886720	.971690
3.60	.7735	.8780	.002763	1.333888	3.334720	.833680
3.80	.7643	.8727	.002706	1.151436	2.878592	.719648
4.00	.7552	.8674	.002650	9.993333 x 10 ⁻¹⁶	24.983333 x 10 ⁻⁷	6.245833 x 10 ³
4.20	.7471	.8627	.002594	8.731554	21.828886	5.457221
4.40	.7391	.8580	.002540	7.663481	19.158703	4.789675
4.60	.7311	.8533	.002486	6.751925	16.879813	4.219953
4.80	.7233	.8486	.002433	5.971702	14.929256	3.732314
5.00	.7156	.8440	.002381	5.300148	13.250370	3.312592
6.00	.6817	.8236	.002135	3.066888	7.667220	1.916805
7.00	.6528	.8057	.001908	1.886592	4.716480	1.179120
8.00	.6281	.7901	.001700	1.214518	3.036296	.759074
9.00	.6068	.7764	.001510	8.092592 x 10 ⁻¹⁷	20.231480 x 10 ⁻⁸	5.057870 x 10 ²
10.00	.5885	.7645	.001337	5.541481	13.853703	3.463425
11.00	.5729	.7541	.001179	3.880000	9.700000	2.425000
12.00	.5596	.7452	.001008	2.690369	6.725923	1.681480
13.00	.5485	.7376	.000862	1.900740	4.751850	1.187962
14.00	.5392	.7313	.000736	1.365184	3.412960	.853240

*Elterman, L.: AFCRL Environmental Research Paper No. 20, 1964

$$n_S = \frac{i_S}{e}$$

where e is the electronic charge. These results have also been plotted and are shown in figures 2, 3, and 4.

IIF. Application of Raman Scattering to Measurements in the Atmosphere

If the water vapor mixing ratio, w , is defined as the mass of water vapor per unit mass of dry air, then from equation (69) the ratio of the signal returns from the atmosphere is related to w by

$$\frac{V(Z)_{H_2O}}{V(Z)_{N_2}} = \frac{i_S(Z)_{H_2O}}{i_S(Z)_{N_2}} = \frac{\gamma(3976 \text{ \AA}) E_{H_2O} \frac{d\phi}{d\Omega_{H_2O}} n_{H_2O}(Z)}{\gamma(3777 \text{ \AA}) E_{N_2} \frac{d\phi}{d\Omega_{N_2}} n_{N_2}(Z)} \propto w \quad (74)$$

assuming $\eta(3777 \text{ \AA}) = \eta(3976 \text{ \AA})$ and $q(3777 \text{ \AA}) = q(3976 \text{ \AA})$. In similar fashion an indication of the aerosol mixing ratio, a , can be shown to be proportional to the ratio of the elastic scattered return to the nitrogen return as

$$\frac{V(Z)_{Elastic}}{V(Z)_{N_2}} = \frac{i_S(Z)_{Elastic}}{i_S(Z)_{N_2}} = \frac{\gamma(3471.5 \text{ \AA}) E_{Elastic} \left(\frac{d\phi}{d\Omega_M} n_M(Z) + \frac{d\phi}{d\Omega_A} n_A(Z) \right)}{\gamma(3777 \text{ \AA}) E \frac{d\phi}{d\Omega_{N_2}} n_{N_2}(Z)} \propto c + a \quad (75)$$

where $\frac{d\phi}{d\Omega_M}$ is the cross section for molecular Rayleigh backscatter, n_M is the total molecular number density, $\frac{d\phi}{d\Omega_A}$ is the aerosol backscatter cross section, n_A is the aerosol number density, and c is a constant.

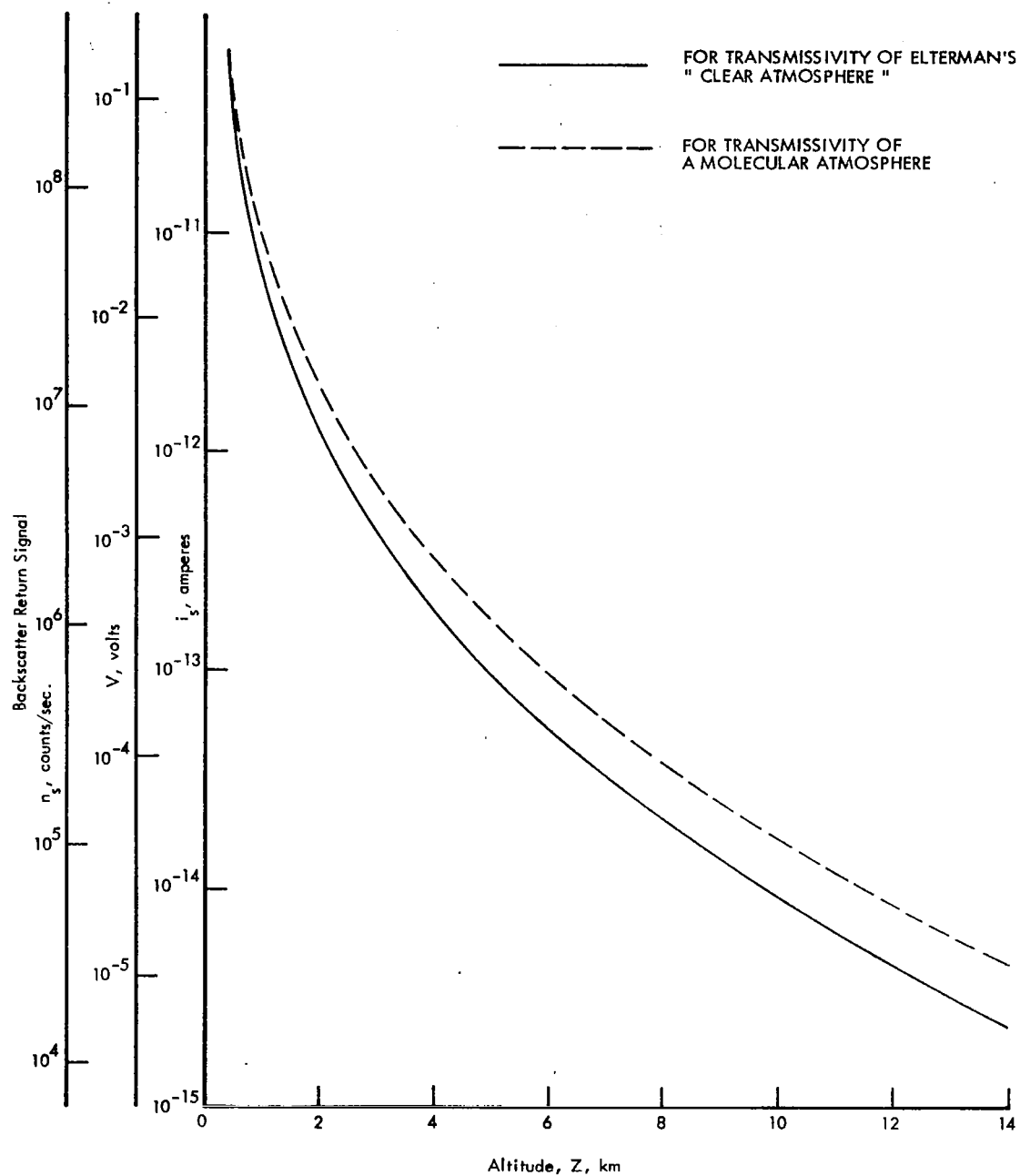


Figure 2.- Calculated Raman backscatter signal for nitrogen as a function of altitude using typical system parameters listed in table VI.

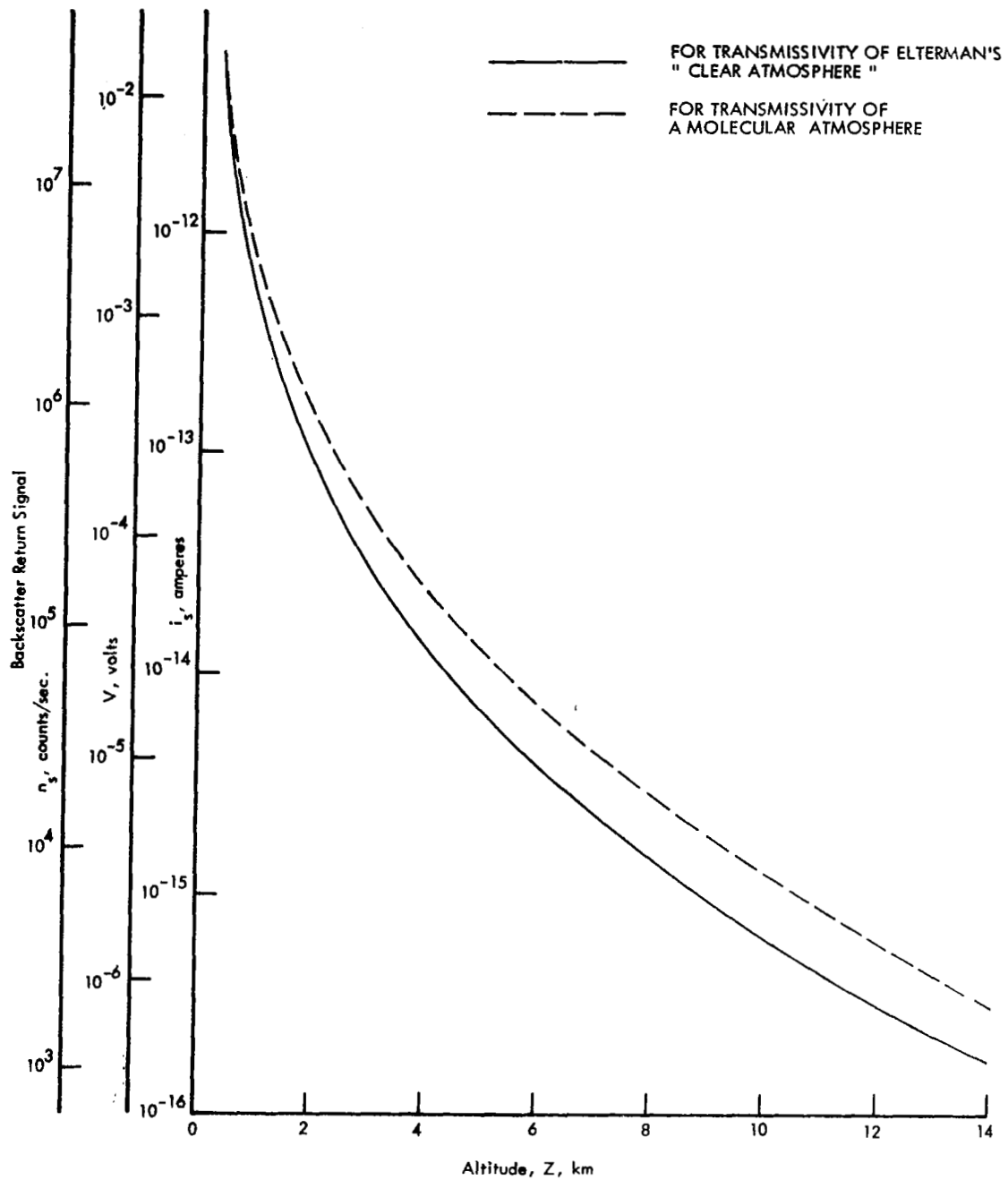


Figure 3.- Calculated Raman backscatter signal for oxygen as a function of altitude using typical system parameters listed in table VI.

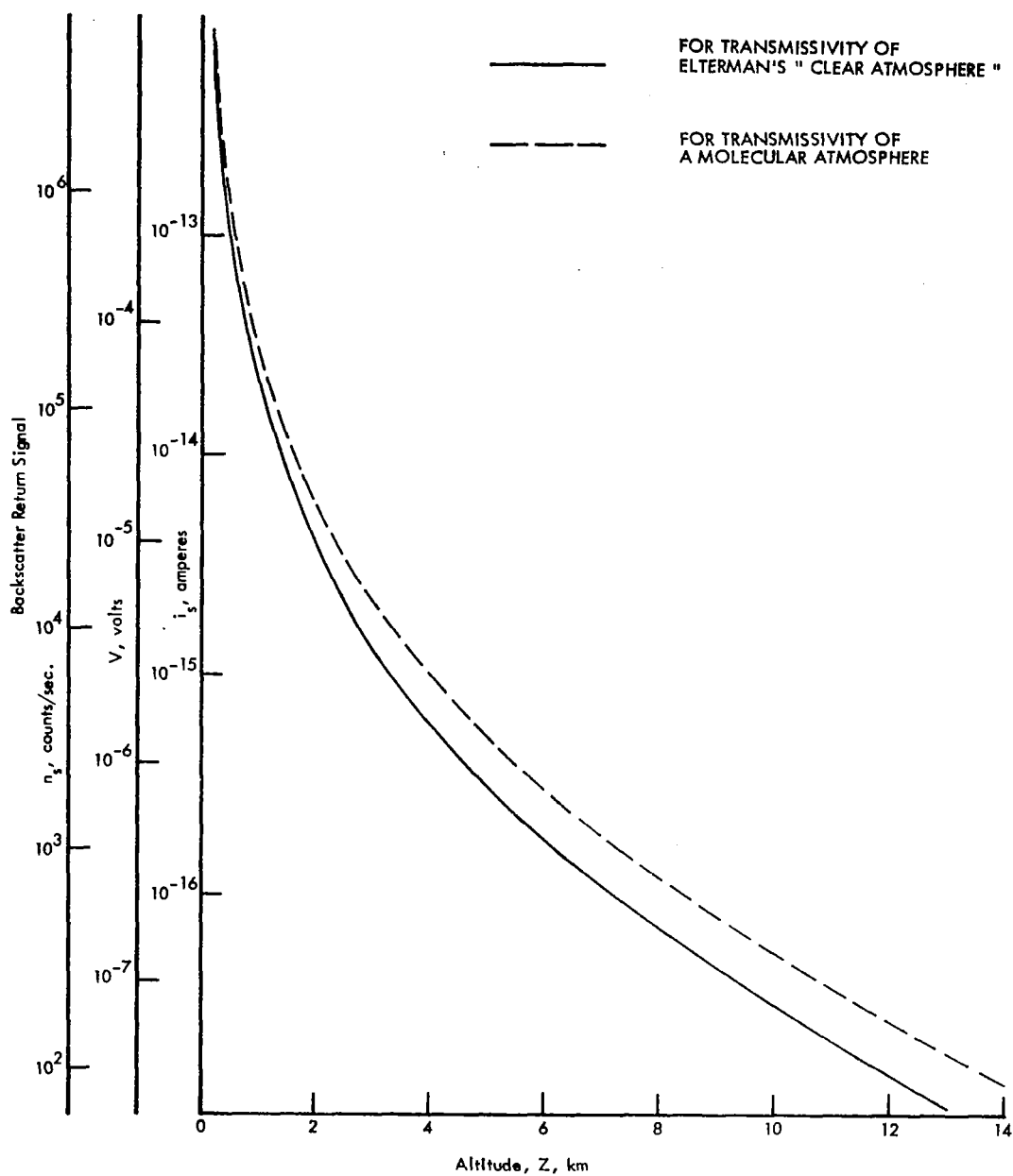


Figure 4.- Calculated Raman backscatter signal for water vapor as a function of altitude using typical system parameters listed in table VI. Calculations are based on a constant mixing ratio of 1 gm/kg.

The ratio of signals given in equation (75) will only provide an indication of aerosol mixing ratio since it neglects the interaction of aerosols with water vapor. This interaction may change the backscatter due to the aerosols changing size and index of refraction without a corresponding change in the aerosol number density.

III. MIXING IN THE EARTH'S LOWER ATMOSPHERE

The major mechanism for mixing in the lower atmosphere is turbulent diffusion. A complete analysis of turbulence and its effect on mixing must involve the equations of motion of the gas. Exact solutions of these equations have been obtained for a limited number of special cases considering only simple geometric configurations; consequently, the study of turbulent diffusion in the atmosphere has centered on the development and utilization of statistical models. The model for turbulent mixing to be discussed here was suggested independently by Prandtl⁽²⁹⁾ and Taylor⁽³⁰⁾ and is referred to as the mixing length theory. This model is an attempt to frame turbulent diffusion in terms similar to molecular diffusion of kinetic gas theory. In the mixing length theory the transfer entity is pictured as a volume of gas, called an eddy, which maintains its identity and characteristics from its creation until it has moved a distance l , referred to as its mixing length, at which point it is absorbed into its surroundings. No restrictions are placed on the size of an eddy or its mixing length. The mechanism of turbulent diffusion in analogy with molecular diffusion must be viewed with caution. Molecular diffusion is described by a model in which the distance and time scales are very small compared to the scales of the property being diffused. In turbulent transfer the scales of the turbulent motion are frequently of the same order as those of the property being transported, and never very much smaller. In addition, turbulence is a continuum phenomenon. The success of the

mixing length concept lies in the fact that only simple assumptions regarding l are required in order to obtain a useful analysis of many aspects of turbulent motion.

Consider that the concentration of a constituent in the atmosphere, such as water vapor or aerosols, has an instantaneous distribution given as $S(Z)$, then its average vertical transport (momentum flux) can be written as

$$F_S(Z) = \overline{\rho(Z)w(Z)S(Z)} \quad (76)$$

where F_S is the average vertical transport

ρ is the mass density of air

w is the instantaneous vertical velocity

S is the mixing ratio of the constituent

Z is the altitude

and

the bar denotes a time average

Due to random motions of the eddies, $w(Z)$ and $S(Z)$ may be divided into their respective average part and fluctuating or eddy part as

$$w(Z) = \overline{w(Z)} + w'(Z)$$

and

$$S(Z) = \overline{S(Z)} + S'(Z)$$

then equation (76) becomes

$$F_S(Z) = \overline{\rho(Z) \left[\overline{w(Z)} + w'(Z) \right] \left[\overline{S(Z)} + S'(Z) \right]} \quad (77)$$

Since only turbulent diffusion is to be considered, $\bar{w} = 0$ and

$$F_S(Z) = \overline{\rho(Z)w'(Z)S(Z)} + \rho(Z)\overline{w'(Z)S'(Z)}$$

From eddy to eddy $\rho(Z) \simeq \text{constant}$, therefore,

$$F_S(Z) = \rho(Z)\overline{w'(Z)S'(Z)} \quad (78)$$

since $\overline{w'(Z)} \equiv 0$.

Consider, now, a horizontal plane through which eddies are passing. For an eddy that originates a distance l above this plane, the fluctuating part of $S(Z)$ can be written as

$$S'(Z) = \bar{S}(Z) - \bar{S}(Z + l)$$

$$\simeq -l \frac{\partial \bar{S}(Z)}{\partial Z}$$

Using this for $S'(Z)$, equation (78) becomes

$$\begin{aligned} F_S(Z) &= -\rho(Z)\overline{w'(Z)l} \frac{\partial \bar{S}(Z)}{\partial Z} \\ &= -\rho(Z)K_S(Z) \frac{\partial \bar{S}(Z)}{\partial Z} \end{aligned} \quad (79)$$

where $K_S(Z) \equiv \overline{w'(Z)l}$ and is referred to as the eddy diffusion coefficient. In the framework of the mixing length theory, equation (79) is the equation that should determine turbulent mixing

in the atmosphere. Difficulties arise even in this simple model of turbulent diffusion when it is applied to studies of the atmosphere because of the complexity of the diffusion coefficient. Fleagle and Bussinger⁽³¹⁾ give for K :

$$K \propto \overline{v^2} \left[\left(\frac{\partial \overline{v}}{\partial Z} \right)^2 - \alpha \frac{g}{T} \left(\frac{\partial \overline{T}}{\partial Z} + \Gamma \right) \right]^{1/2} \quad (80)$$

where

v is the horizontal wind velocity

α is an unknown constant

g is the gravitational constant

T is temperature

and

Γ is the adiabatic lapse rate defined as the negative slope with altitude of the adiabatic temperature relationship, $TP^K = \text{constant}$, where P may be related to altitude, $\Gamma \equiv - \left(\frac{\partial T}{\partial Z} \right)_{ad}$

The atmosphere at an altitude Z is said to be adiabatic if

$-\frac{\partial T(Z)}{\partial Z} = \Gamma(Z)$, where $T(Z)$ is the true temperature profile. An

adiabatic atmosphere is neutrally stable since eddies expand adiabatically under vertical motion and are thus always in equilibrium with their surroundings. If $-\frac{\partial T(Z)}{\partial Z} < \Gamma(Z)$, the atmosphere is considered stable

at Z because of the restoring buoyant forces. Otherwise, if

$-\frac{\partial T(Z)}{\partial Z} > \Gamma(Z)$, the atmosphere is considered unstable.

Equation (79) indicates that mixing takes place, on the average, from regions of high concentration to regions of low concentration.

If the earth is the source of the atmospheric constituent, such as water vapor, aerosols, or pollutants, the tendency is for the mixing to be vertically upward.

The height up to which this mixing takes place is important, particularly in regard to aerosol and pollutant mixing. The higher this mixing height, the lower (on the average) is the concentration at the earth's surface. For an adiabatic atmosphere, from equation (80)

$$K(Z) \propto \overline{v^2} \left(\frac{\partial \overline{v}(Z)}{\partial Z} \right)$$

Thus, the mixing height for this case will be that altitude where $\frac{\partial \overline{v}(Z)}{\partial Z} \simeq 0$, or where the winds are not affected by the disturbing presence of the earth. This height is on the order of 1 to 2 km. The atmosphere, however, is seldom adiabatic; rather it is more often layered with each altitude layer having varying degrees of stability and instability. Equation (80) indicates that the magnitude of the eddy diffusion coefficient is altered by the stability of the atmosphere. In a stable layer $\left(\frac{\partial \overline{T}}{\partial Z} + \Gamma \right) > 0$ indicating that mixing is discouraged. For an unstable layer, mixing is encouraged since $\left(\frac{\partial \overline{T}}{\partial Z} + \Gamma \right) < 0$. Thus, if a very stable layer is present in the lower atmosphere, its height may determine the height of the mixing layer since it would tend to cap further upward mixing.

This analysis indicates that turbulent mixing within the framework of the mixing length theory is determined by the rms value of the mixing length, the horizontal wind gradient, and the stability layering in the atmosphere.

IV. NOISE ANALYSIS

The sources of noise or uncertainty in an optical radar system include shot noise, thermionic emission at the photocathode of the detector, sky background, variations in dynode amplification, and near-field scattering of fluorescence radiation produced by the laser and Johnson noise. Of these, only the first three will be considered in detail, since Johnson's noise and fluorescence are small and can be neglected. The shot noise of the signal current from the photomultiplier including these three effects is

$$\Delta i = G \left[2e(i_S + i_D + i_B)\Delta f \right]^{1/2} \quad (81)$$

where

G is the electron gain of the phototube

e is the electronic charge

i_S is the signal current at the photocathode

i_D is the thermionic emission current at the photocathode

i_B is the sky background current at the photocathode

and Δf is the electrical bandwidth

The signal-to-noise ratio is then:

$$\frac{S}{N} = \frac{i_S}{\Delta i} = \frac{i_S}{\left[2e(i_S + i_D + i_B)\Delta f \right]^{1/2}} \quad (82)$$

Assuming a $\frac{S}{N} = 2$ for minimum signal detection criterion, equation (82) can be rewritten as

$$i_S = 4e \Delta f + \left[16e^2 \Delta f^2 + 8e(i_D + i_B)\Delta f \right]^{1/2} \quad (83)$$

With $(i_D + i_B) \simeq 2 \times 10^{-15}$ amperes, as discussed in appendix F, and using the calculated signal current given in tables VII through XII, curves relating altitude limit and bandwidth, Δf , have been constructed for oxygen, nitrogen, and water vapor Raman returns and are shown in figure 5. The detection altitude and/or the altitude resolution can be increased by averaging returns from a number of laser transmissions. At any given altitude, or for any given altitude resolution, it will be shown for the photon counting case that S/N is increased by the square root of the number of laser firings; this result is also applicable here.

At higher altitudes the signal at the oscilloscope becomes a series of spikes corresponding to individual photon events. At this signal level it becomes convenient to count these events in successive altitude resolution windows and sum the results over a large number of laser transmissions as a measure of backscatter from the atmosphere. Since the rate of emission of photoelectrons from the photocathode of the detector is assumed to be Poisson, the fluctuation in the number of counts for a counting time τ can be written as⁽³²⁾

$$\Delta n = \left[\tau(n_S + n_D + n_B) \right]^{1/2} \quad (84)$$

where

n_S is the signal count rate

n_D is the thermionic emission count rate

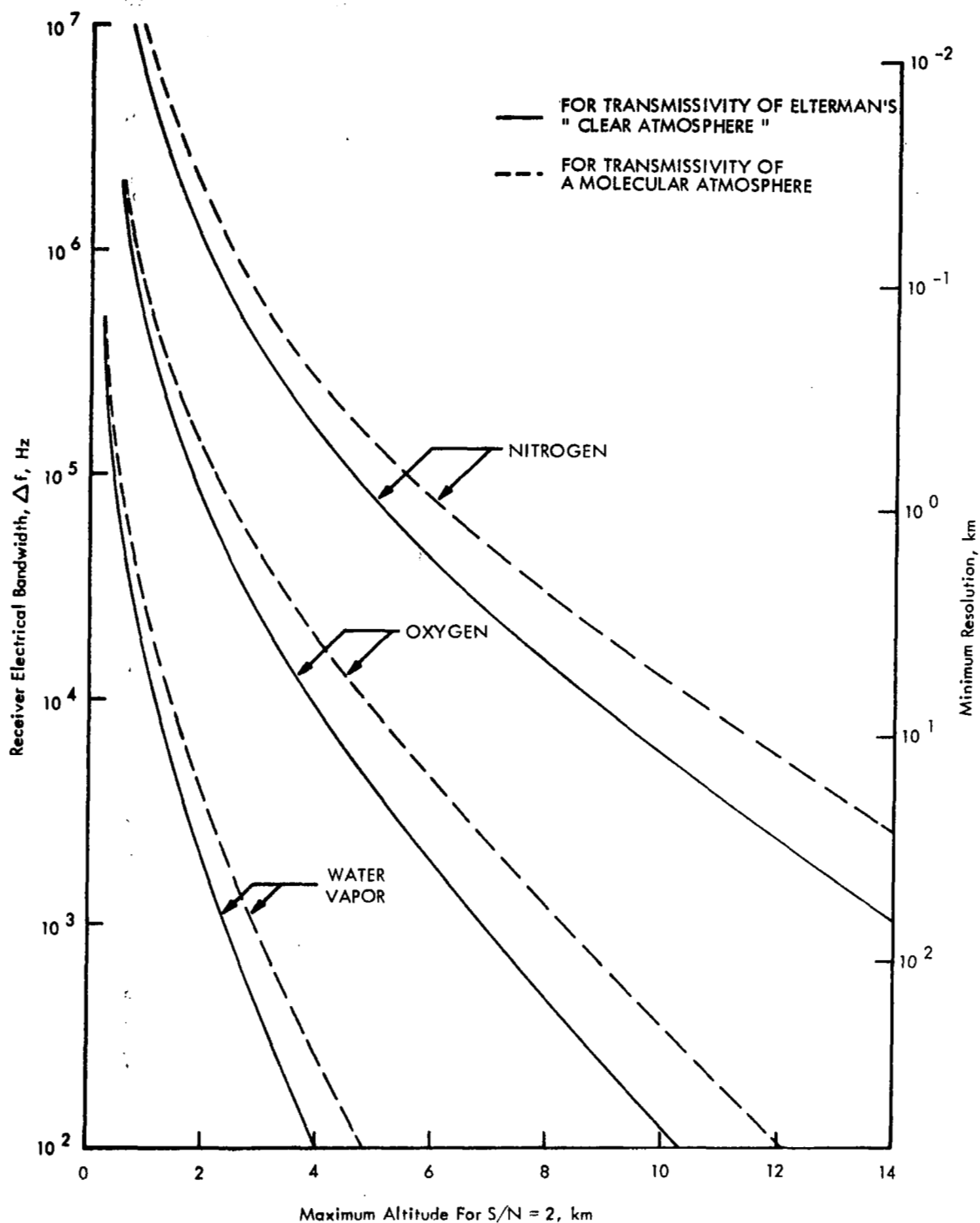


Figure 5.- A plot of receiver bandwidth and altitude resolution as a function of maximum altitude for nitrogen, oxygen, and water vapor with signal detection criterion $S/N = 2$.

and

n_B is the sky background count rate

The signal-to-noise ratio is then:

$$\frac{S}{N} = \frac{\tau n_S}{\Delta n} = \frac{\tau n_S}{\left[\tau (n_S + n_D + n_B) \right]^{1/2}} \quad (85)$$

If m successive laser firings are made and the photon counts are summed over successive counting times, τ , S/N can be increased by \sqrt{m} as

$$\frac{S}{N} = \frac{m \tau n_S}{\left[m \tau (n_S + n_D + n_B) \right]^{1/2}} \quad (86)$$

Again using as the minimum detection criterion $\frac{S}{N} = 2$, equation (86) may be rewritten as

$$n_S = \frac{2}{m\tau} + \left[\frac{4}{(m\tau)^2} + \frac{4}{m\tau} (n_D + n_B) \right]$$

Using the calculated count rate from the atmosphere given in tables VII through XII, a series of curves can be constructed relating the product $m\tau$ with maximum altitude. These are shown in figure 6 for oxygen, nitrogen, and water vapor, and provide the basis for establishing a relationship between laser pulse repetition rate, stability of the particular atmospheric phenomena being observed, altitude resolution, and maximum attainable altitude.

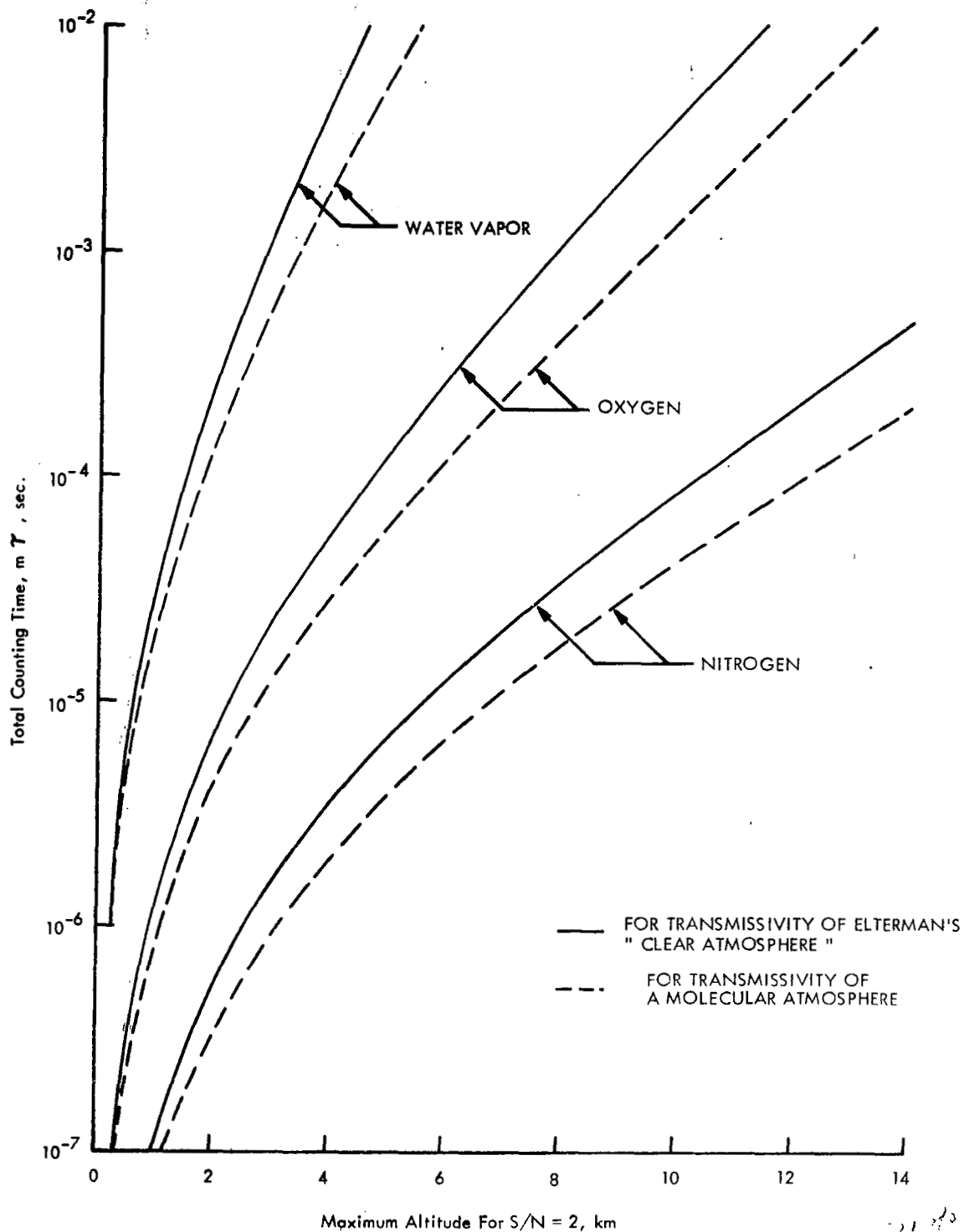


Figure 6.- A plot of the product of counting time and number of laser transmissions as a function of maximum altitude for nitrogen, oxygen, and water vapor with signal detection criterion $S/N = 2$.

V. EQUIPMENT

General

The optical radar system used in this investigation was installed in an environmentally controlled mobile van. A photograph of the van is given in figure 7 with its rear door open showing the laser system. The laser and telescope of the optical radar system are aligned parallel and pointed on the vertical directly below a hatch in the roof of the van. The laser pulse propagates through the hatch and vertically into the atmosphere. As this pulse of laser energy propagates upward through the atmosphere, part of it is scattered by molecules and aerosols. A small portion of the scattered energy is collected by the telescope and is spectrally analyzed to provide basic information concerning the earth's lower atmosphere.

VA. Laser Transmitter

The laser system used in this investigation is a frequency doubled Korad Kl-Q Q-switched ruby laser. A sketch of the laser transmitter is shown in figure 8. The cavity of the laser is defined by a totally reflecting rear reflector and a partially reflecting front sapphire etalon. Mounted within the cavity is a $9/16 \times 4$ inch ruby rod pumped by a helical xenon flash lamp, and a Pockels cell Q-switching device. The Pockels cell switches the Q of the laser cavity approximately 1.5 msec after the flash lamp fires, producing a nominal 1 joule pulse of 20 nsec duration at $6943 \overset{\circ}{\text{A}}$ contained in a beam of approximately 5 mrad. The Q-switching by the Pockels cell

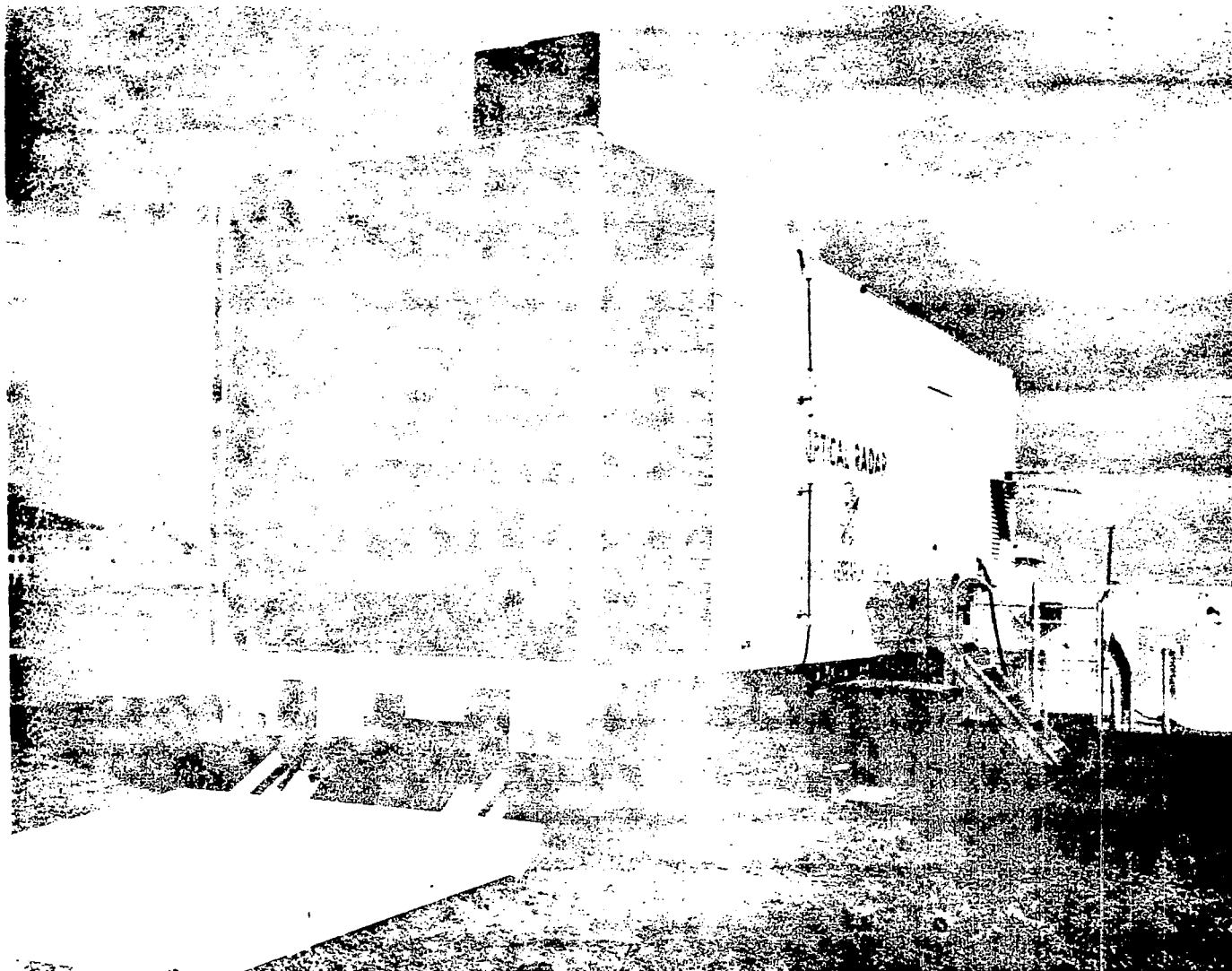


figure 7.- A photograph of the optical radar system installed in
a mobile van.

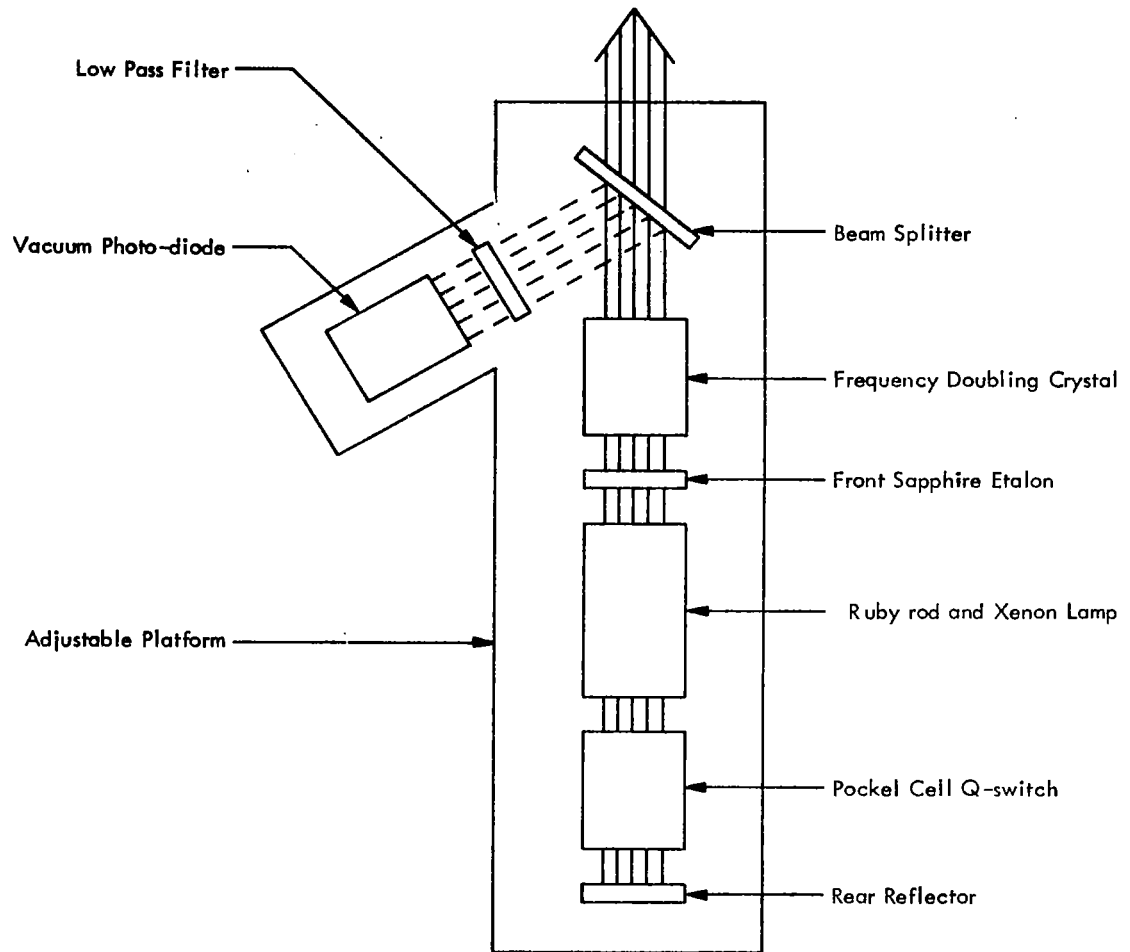


Figure 8.- A sketch of the laser transmitter.

produced a high level of rf noise which was eliminated by wrapping the unit in several layers of aluminum foil and double shielding the Pockels cell cable and signal cable.

The output of the ruby laser is frequency doubled (3471.5 \AA) by a nonlinear ADP crystal with conversion efficiency of about 4 percent. Temperature control of the ADP crystal to within $\pm 1^\circ \text{ F}$ was necessary to maintain peak conversion efficiency. A simple feedback temperature control system was designed that was able to meet the $\pm 1^\circ \text{ F}$ temperature control requirement.

The beam splitter shown in figure 8 directs a small portion of the emitted laser energy onto a vacuum photodiode whose spectral response is limited by a low-pass filter. The filter rejects the laser fundamental at 6943 \AA while passing the second harmonic at 3471.5 \AA . A test was performed to evaluate the rejection capability of the low-pass filter for the laser fundamental. The laser was pulsed both with and without the frequency doubler crystal placed in front of the laser. As was expected, the photodiode only responded when the laser was pulsed with the crystal in place, indicating that it is not sensitive to the laser fundamental. The signal from the photodiode is slightly integrated so that the peak of its output is proportional to the total energy of the laser pulse at 3471.5 \AA .

All laser components are mounted on a rigid platform which is adjustable in two degrees of freedom to permit alignment with the receiver system.

VB. Receiver System

The telescope that collects the backscattered radiation from the atmosphere was designed around an available $f/3$, 16-inch-diameter schlieren mirror. A drawing of the telescope is shown in figure 9. The telescope tube is made of rolled aluminum plate with mounting brackets at the rear and a flange at the bottom. Attached to the flange is a plate that supports the weight of the primary mirror. Nine support points are provided for the primary mirror to reduce the possibility of introducing optical distortion due to stressing. These nine support points are arranged in groups of three. Each group of support points is, in turn, supported and made adjustable by a micrometer. The secondary is a first surface flat mirror cut in an elliptical shape to match the cone of light from the primary mirror and to maintain minimum obscuration of the incident radiation. The secondary mirror is mounted with Eastman 510 optical cement on a brass cylinder cut at 45° . Three micrometers mounted above the cylinder provide angular adjustment of the secondary. An accessory optics cradle is mounted on the outside of the telescope tube.

For the initial experiments performed with a precision dual monochromator, the arrangement of the receiver system was as shown in figure 10. In this configuration the backscattered radiation from the atmosphere was focused by the primary mirror in the plane of a 0.3-inch adjustable stop. The collected radiation was refocused by two anti-reflective coated lenses onto the entrance slit of the monochromator. Both lenses were mounted in a Lansing mount which provided angular

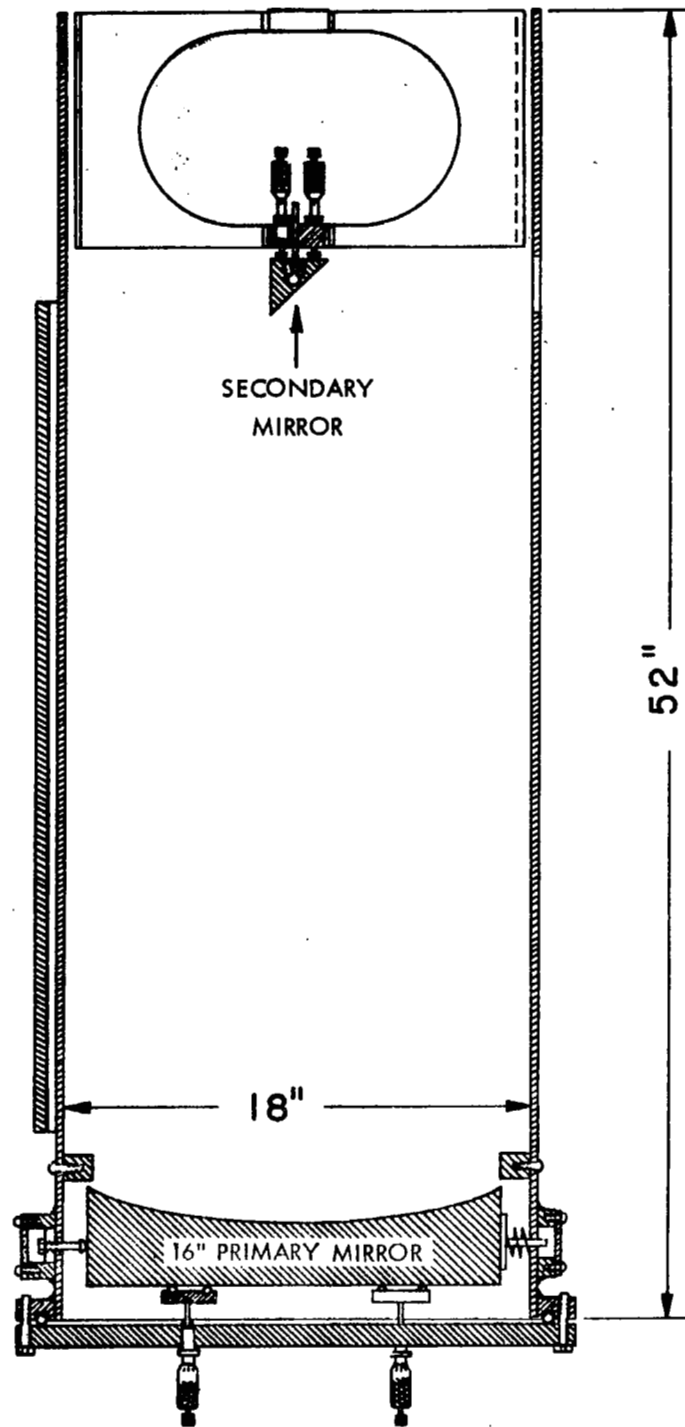


Figure 9.- A drawing of the telescope.

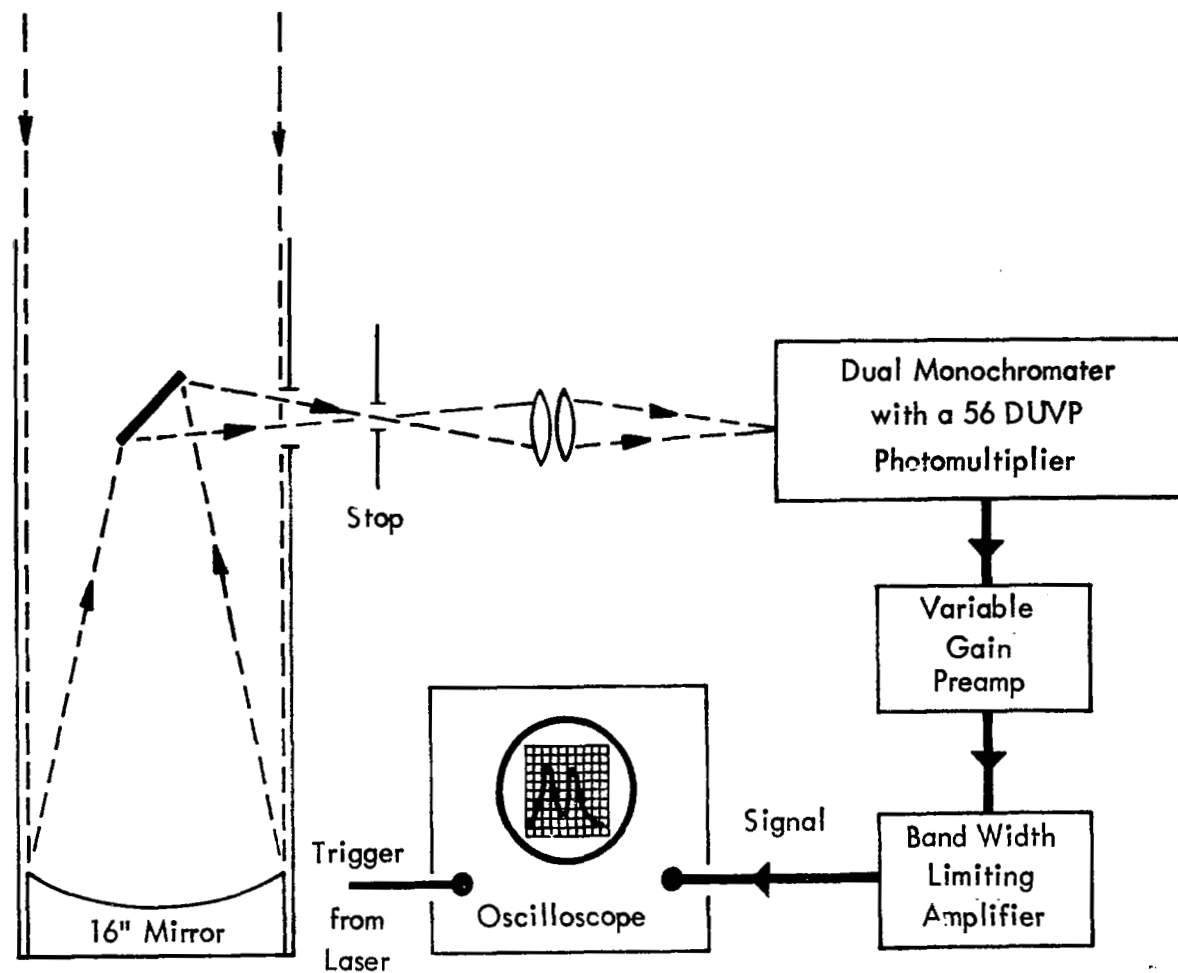


Figure 10.- The arrangement of the receiver system using a dual monochromator.

adjustment to minimize coma in the final image and translational adjustment to allow for precise focusing. The monochromator was mounted on two heavy aluminum plates separated by a teflon sheet. Eight positioning bolts attached to the lower plate and in contact with the upper plate provided three degrees of adjustment of the monochromator in the horizontal plane. The lower plate was supported by three bolts arranged in a triangular pattern providing vertical and tilt adjustments. A dual monochromator was selected for this investigation because of its ability to reject stray light. This is of particular importance in a Raman scattering experiment because of the presence of the relatively intense elastic scattered line near the Raman lines of interest. The dual monochromator used in this investigation was a Spex Model 1400-II, with straight slits 50 mm high, adjustable to 3 mm wide, and gratings blazed to give a maximum reflectance at 3000 \AA . It has a maximum stray light rejection greater than 10^{12} . The analyzed light is detected by an Amperex 56 DUVP, 14-stage photomultiplier tube placed at the exit slit of the dual monochromator. This phototube, in combination with the dynode circuitry provided by the manufacturer, produces a 2 to 3 nsec pulse for each photoelectron event, making it ideal as a detector in photon counting experiments. The linearity of the phototube was verified by comparing its output current with its output count rate over a range of light intensities of a tungsten lamp. The characteristics, as measured by the manufacturer for this phototube, indicate a gain of 10^8 when operating at 2000 V and a peak quantum efficiency of 16 percent. A 50 Ω anode load resistance at the phototube and a matching 50 Ω

impedance at the input of the preamplifier results in an effective load resistance of $25\ \Omega$. The preamplifier is a variable gain (up to 100) 100 MHz bandwidth amplifier made by Lecroy Research Systems. The signal is then presented to a variable bandwidth amplifier, which is a Tektronix type 0 oscilloscope preamplifier, and displayed on a Tektronix type 556 oscilloscope.

After the experiments performed with the monochromator were completed, the receiver system was modified to make use of the higher throughput of interference filters. Three interference filters, each $35\ \text{\AA}$ wide, were used in this phase of the experiment. The bandpass of the filters were centered at $3669\ \text{\AA}$, $3777\ \text{\AA}$, and $3976\ \text{\AA}$ which correspond to Raman bands from oxygen, nitrogen, and water vapor, respectively. Optical transmission curves were measured for the three filters on a Cary 14 spectrophotometer to determine their rejection of the relatively intense elastic scattered line at $3471.5\ \text{\AA}$. Since the Cary 14 instrument is not sensitive below 0.1 percent transmission, it was necessary to verify the rejection of the filters in the experimental setup. This check was performed by two methods. First, before the monochromator was removed from the system it was adjusted to select the elastic scattered radiation from the atmosphere at $3471.5\ \text{\AA}$. Each filter was then placed between the monochromator's exit slit and the phototube, and the laser was pulsed. If each filter was blocked at $3471.5\ \text{\AA}$, no backscatter signal from the atmosphere would be observed. This was determined to be the case when an additional blocking filter was provided for the nitrogen and oxygen interference filters. No

additional blocking was required for the water vapor filter. The peak transmission of each filter is given in Chapter II. The second test was performed after the monochromator was removed from the system. In this test an interference filter centered at 3471.5 \AA was used with each Raman band filter. The results of the second test were in agreement with the first. It should be stated that these tests could only check the blocking of the Raman band filters to within a factor of 5 since both the monochromator and the 3471.5 \AA filter have transmissions of the order of 20 percent. A sketch of the modified receiver system is shown in figure 11. The single lens, in a Lansing mount, collimates the backscatter return before it passes through the particular interference filter and is incident on the phototube. The external circuitry is identical to the original setup with the exception that the bandwidth limiting amplifier is a Tektronix type D oscilloscope preamplifier.

VC. Alignment of the Receiver and Laser Transmitter

The alignment of this system is difficult, since both the telescope receiver, and laser transmitter are rigidly fixed, pointing on the vertical. For alignment purposes an 18-inch-diameter mirror is mounted above the telescope, as shown in figure 12. Collimated light from a zirconium arc lamp is directed down the mechanical axis of the telescope. This collimated light is produced by replacing the telescope primary with an optical flat. The arc source is then positioned to be coincident with its return tangential image. With the primary again in place, the telescope and stop position are aligned. In the initial setup shown in

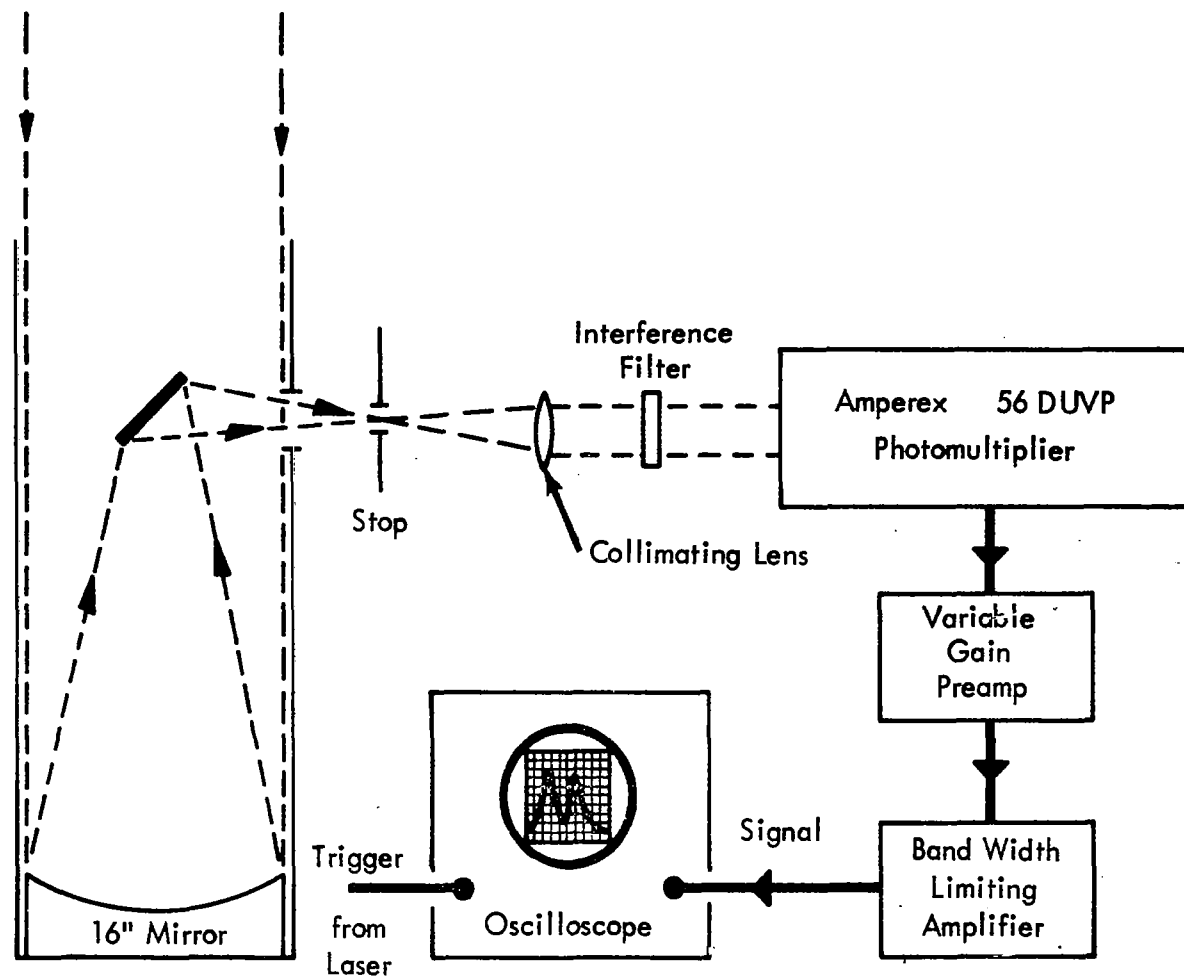


Figure 11.- A sketch of the modified receiver system using interference filters.

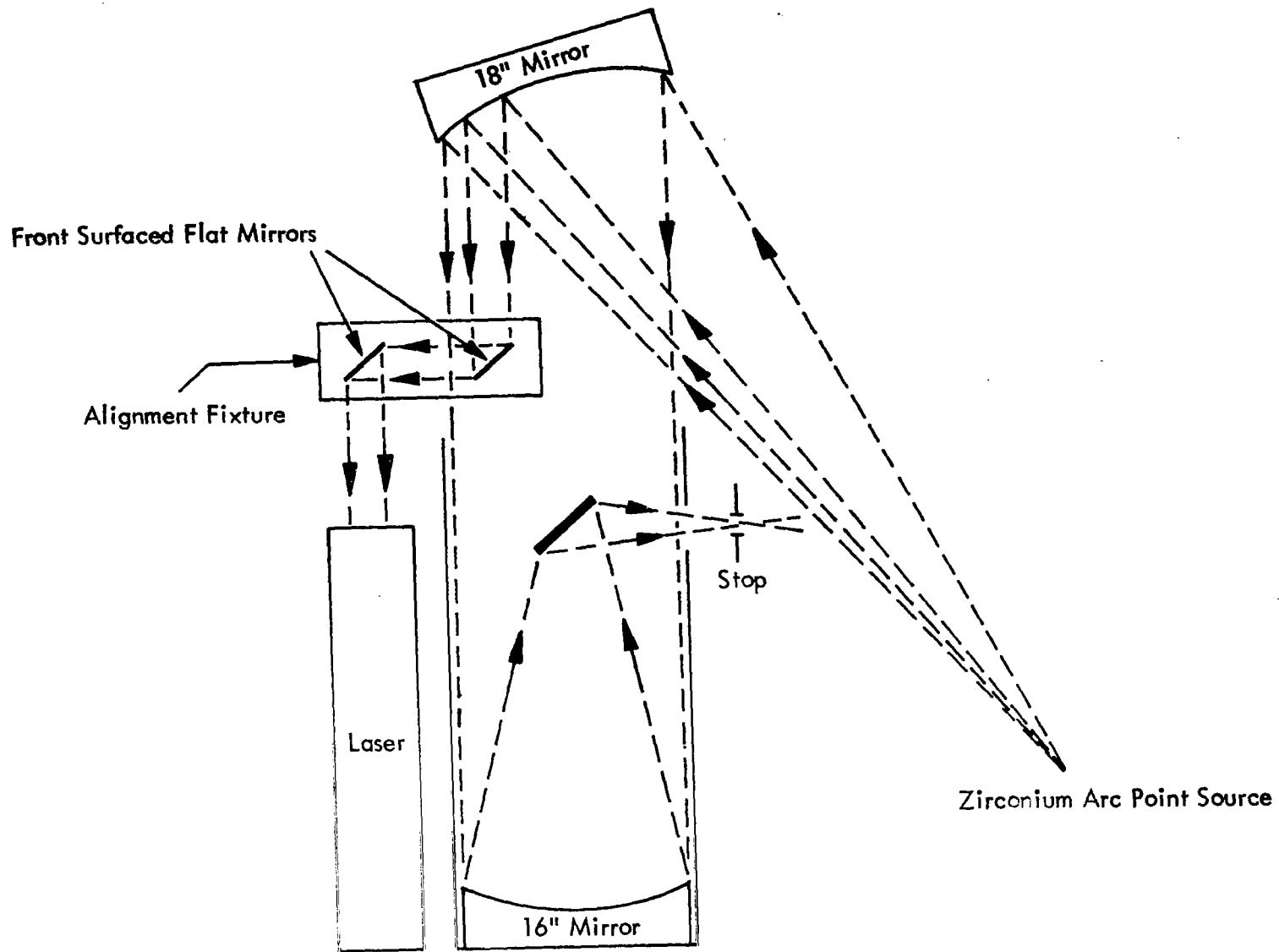


Figure 12.- Arrangement for aligning optical radar system.

figure 10, the two lenses are adjusted, using standard retro-reflective techniques, to minimize coma and to produce a sharp image at the entrance slit of the monochrometer. In the modified receiver system shown in figure 11, retro-reflective techniques are again utilized to assure maximum collimation and proper orientation of the interference filters.

The alignment of the laser's optical axis to the telescope's optical axis is accomplished using an alignment fixture shown in figure 12. The two front surfaced mirrors on the alignment fixture are adjusted to be parallel using an independent source of parallel light. The fixture is then positioned in the collimated beam from the 18-inch mirror. Again utilizing retro-reflective techniques, the laser table is adjusted until the laser's front mirror is perpendicular to the optical axis of the telescope. Final alignment of the laser and telescope is performed by adjusting the orientation of the laser transmitter until a maximum backscatter return is received from the atmosphere.

VD. Supporting Equipment

Radiosondes: Environmental Sciences Services Administration personnel assigned to NASA, Wallops Island, Virginia, launched standard U.S. Weather Bureau radiosondes in support of this research. The radiosonde provides a measure of pressure, temperature, relative humidity, and wind velocity as a function of altitude. The relative humidity used to calculate water vapor mixing ratio has stated accuracies of ± 5 percent and ± 10 percent down to equivalent dewpoint temperatures of -10°C and -40°C , respectively.

Aerosol Measurements: Two balloons with particle scattering instrument packages attached were launched April 17, 1970, by Dr. J. M. Rosen of the University of Wyoming. In the first package, referred to as a particle sampler, individual light pulses produced by aerosols pumped through a scattering chamber were detected by a phototube, pulse height analyzed, and counted in two channels: (1) aerosols larger than 0.25μ diameter, and (2) aerosols larger than 0.4μ diameter. The second package, termed a dust photometer, measured the ratio of total elastic scattering to molecular Rayleigh scattering by alternately filtering and not filtering the atmospheric gas sample being pumped through the scattering chamber.

VI. DATA ANALYSIS AND EXPERIMENTAL RESULTS

General

A typical analog Raman return from atmospheric nitrogen is shown as the top trace in figure 13(a). The bottom trace in 13(a) is the integrated output of the laser energy monitor. Its peak is a relative measure of the laser energy at 3471.5 \AA . The maximum return signal from the atmosphere occurs shortly after the laser pulse moves into the field of view of the telescope. After crossover, the signal from the atmosphere obeys the optical radar equation for Raman backscatter (eq. (69)).

VIA. Data Analysis

Each oscillogram of the analog signal is analyzed using a film reader. Computer punch cards are obtained for each significant datum point, are compiled and computer plotted in relative units as shown in figure 14. The oscillogram and computer plot are compared as a check on film reading accuracy. The initial data are analyzed further to provide a plot of normalized backscatter signal as a function of altitude, as shown in figure 15. The square symbols in figure 15 represent linear interpolations of the data at 50 m intervals. The Z^2 dependence of the signal is removed by forming the quantity $Z^2 V/E$, which is also computer plotted, and a typical example is given in figure 16. A number of signal profiles are used to obtain an average return from the atmosphere.

An increase in bandwidth and external gain of the receiver electronics produced oscillograms of the Raman return signal which

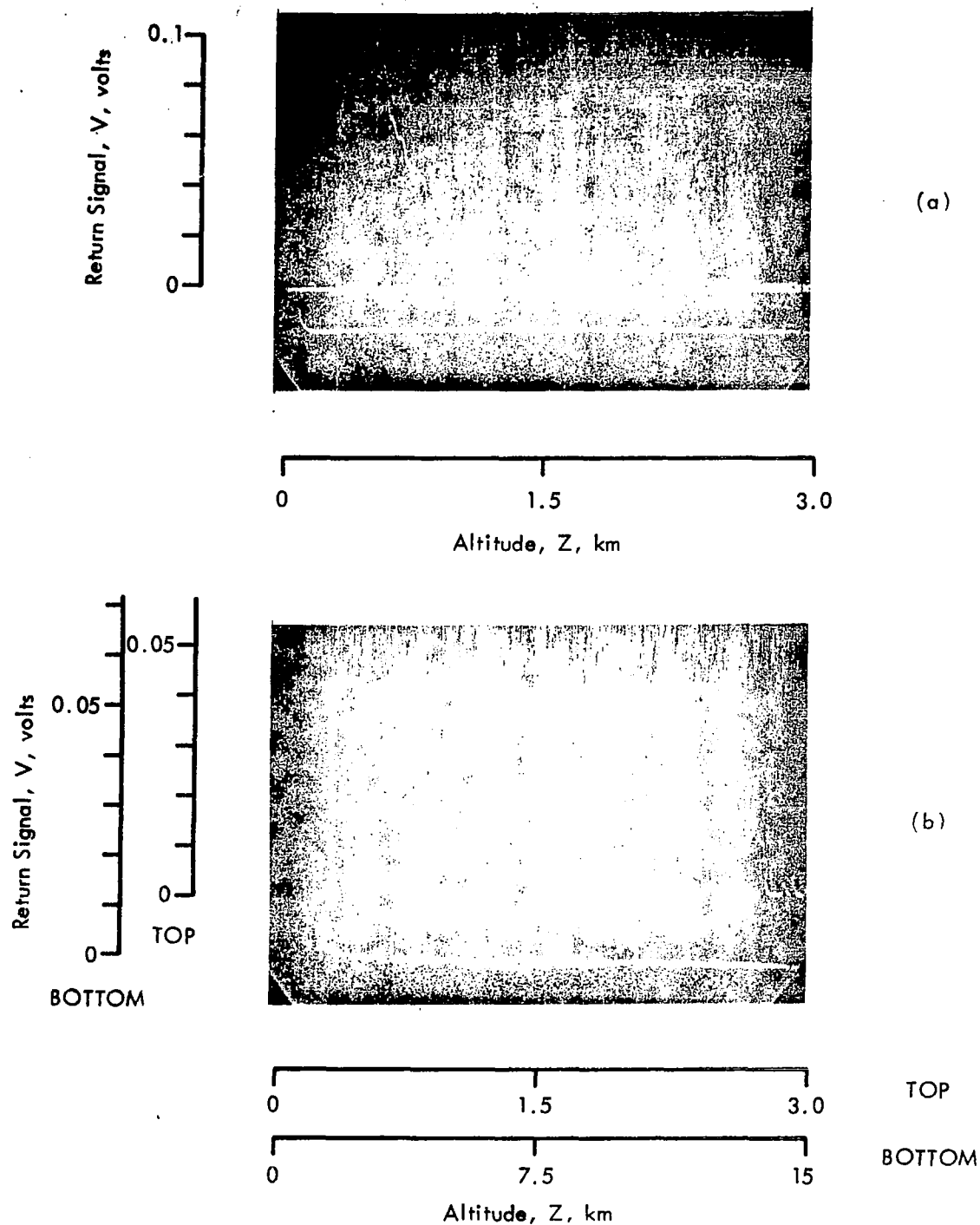


Figure 13.- (a) Typical analog Raman return from atmospheric nitrogen.
 (b) A typical oscillogram taken for the purposes of photon counting.

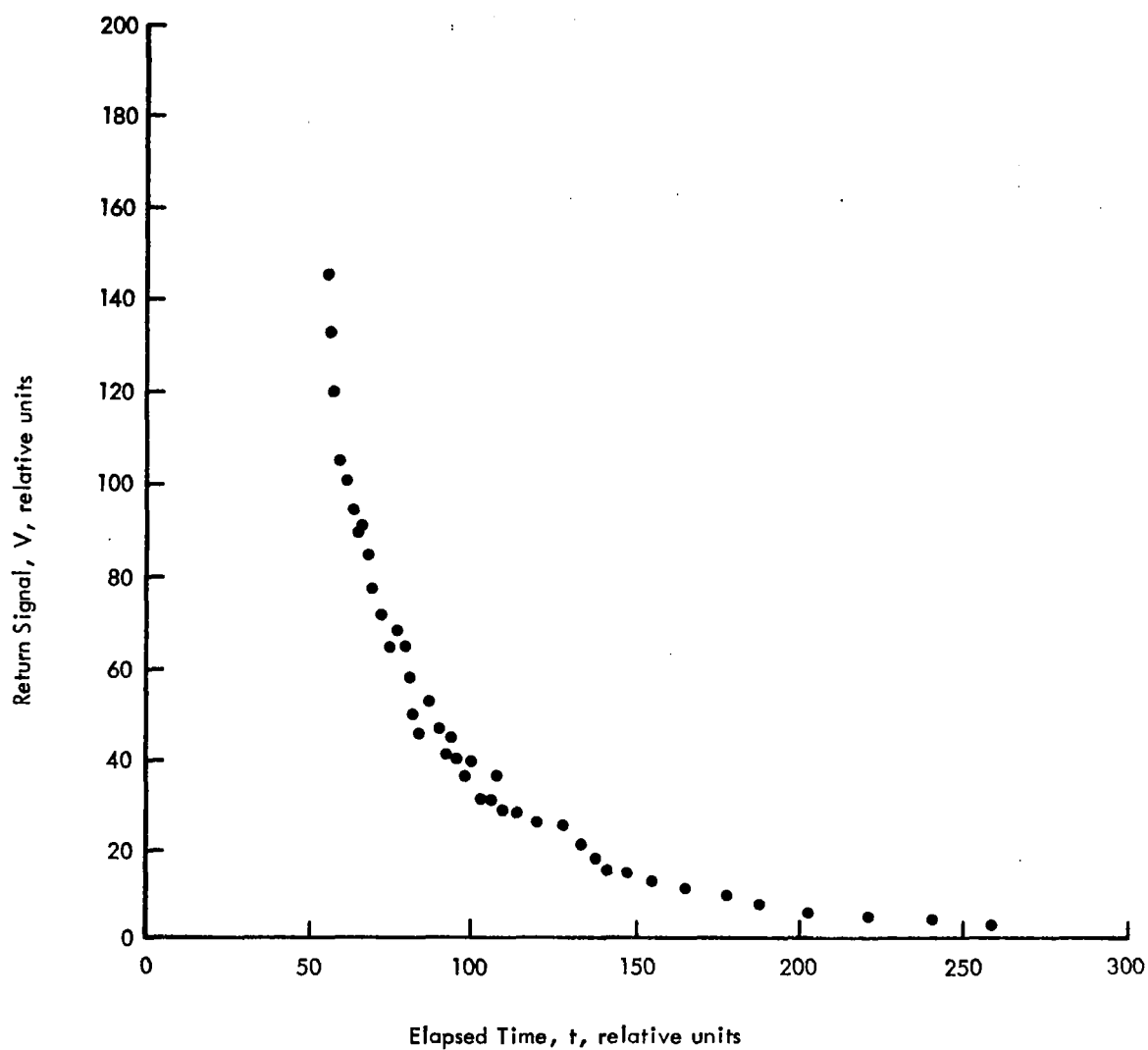


Figure 14.- Initial computer plot of data from oscillogram given in figure 13(a).

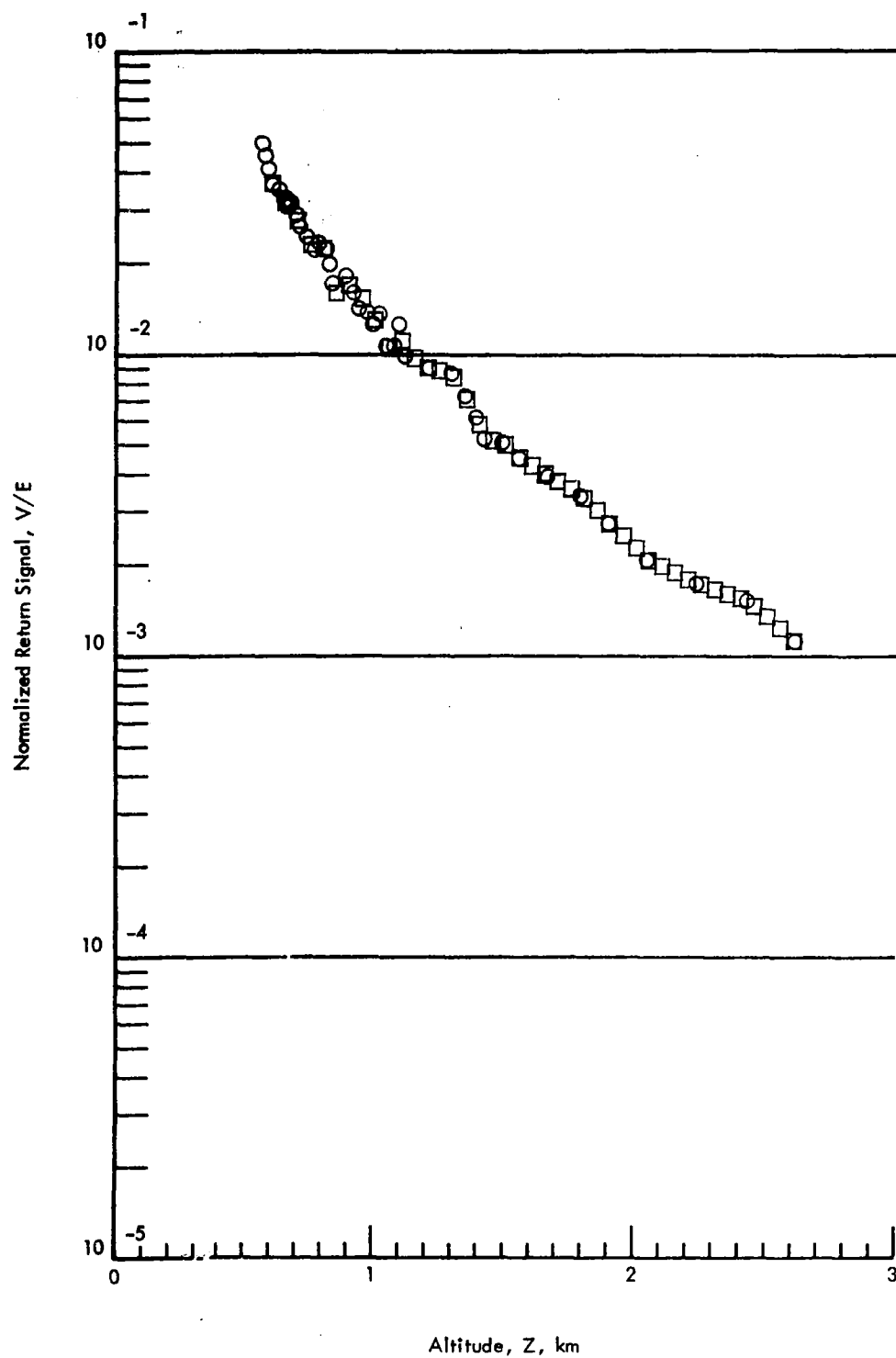


Figure 15... Backscatter signal normalized to relative laser energy as a function of altitude (data from fig. 13(a)).

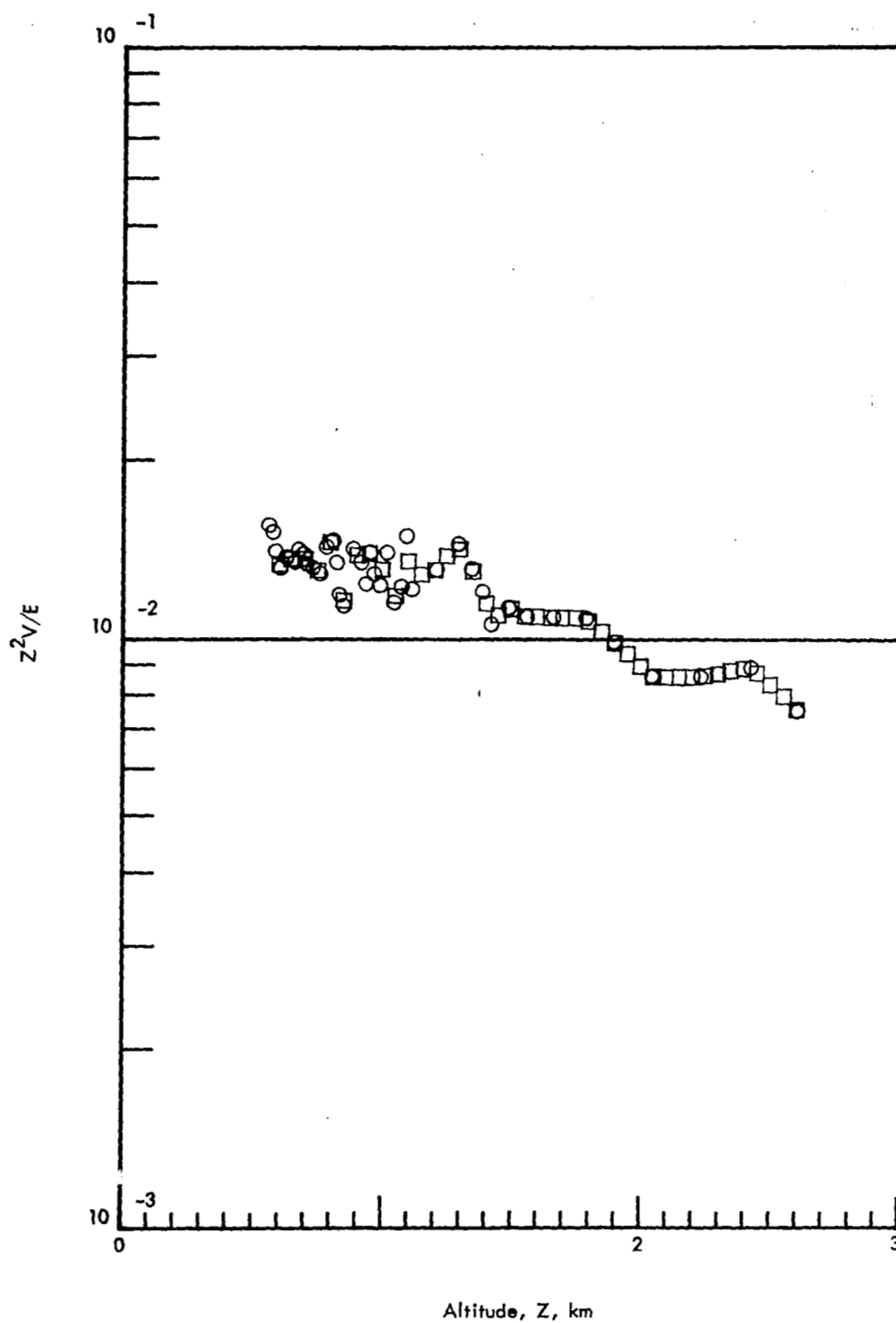


Figure 16.- The quantity Z^2V/E as a function of altitude (data from fig. 13(a)).

were used to count individual photon events. A typical oscillogram of the nitrogen signal taken for the purpose of photon counting is shown in figure 13(b). The individual pulses are counted in successive 4 μ sec time windows which corresponds to an altitude resolution of 0.6 km. The photon count return signal from many (usually 50 or more) laser probings are added together to obtain the final profile of backscatter from the atmosphere.

VIB. Early Experimental Results Using a Monochromator to Select Spectral Bandpass

In August 1969, the initial Raman atmospheric backscatter experiments were conducted using a dual monochromator. A spectrum of the atmospheric backscatter was compiled by firing the laser while the monochromator was adjusted in 10 \AA increments. Over the spectral range 3400 \AA to 4000 \AA , four bands were observed; the elastically scattered band at 3471.5 \AA , the 0-1 vibration-rotation bands of N_2 and O_2 at 3777 \AA and 3669 \AA , respectively, and the ν_1 symmetric vibration line of water vapor at 3976 \AA . The observation of Raman scattering by water vapor in this series of experiments constituted the first remote measurement of a minor atmospheric constituent using an optical radar system and was reported in reference 14.

Typical Raman returns from the atmosphere are shown in figure 17, which were obtained with the monochromator set at the wavelength indicated. These profiles were measured over Hampton, Virginia, on the night of August 11, 1969, under the following surface conditions: temperature, 71 $^\circ$ F; relative humidity, 88 percent; barometric pressure,

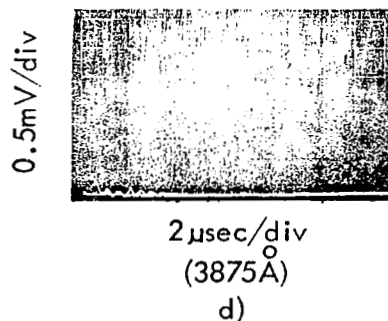
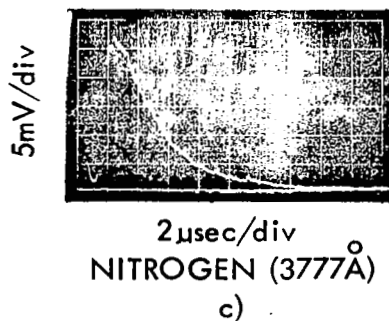
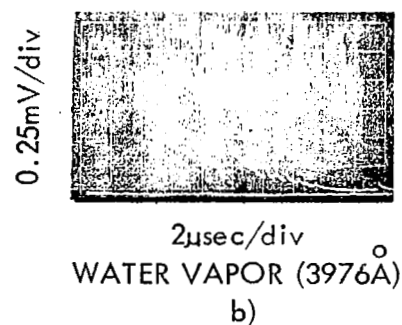
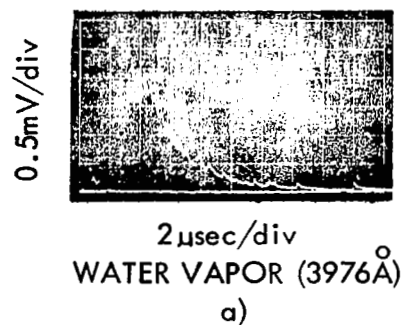


Figure 17.- Typical Raman backscatter returns from the atmosphere versus time after laser emission taken using the dual monochromator.

29.92 in. Hg; winds, less than 5 knots from the northeast. To verify the rejection of stray light by the monochromator, a number of measurements were made at the wavelengths 3570, 3875, 3922, and 4050 Å for which no Raman backscatter by atmospheric constituents was expected. Given in figure 17(d) is an oscillogram obtained at 3875 Å which is identical to the oscillograms obtained at the other three wavelengths. This oscillogram is also identical with that obtained with the entrance slit of the monochromator closed and, in consequence, represents a measure of the system noise. The ratio $V_{H_2O}(Z)/V_{N_2}(Z)$ for the two oscillograms (17(a) and 17(c)) is shown in figure 18, along with its estimated rms error. Also shown in the figure is the water vapor mixing ratio obtained from the Wallops Island, Virginia, radiosonde taken the night of August 11, 1969. Wallops Island is located approximately 75 miles northeast of Hampton; however, in view of the wind direction that prevailed at the time of the experiment, the radiosonde measurements should be indicative of the moisture profile in the atmosphere over the test site. Because of the good agreement obtained, additional experiments were planned using interference filters to increase the optical efficiency of the receiver system.

VIC. Experimental Results Using Interference Filters as Spectral Band Selectors

After the receiver system was modified to make use of interference filters, the mobile van containing the optical radar equipment was moved to Wallops Island, Virginia. This relocation was made because of the availability of extensive meteorological support at Wallops Island.

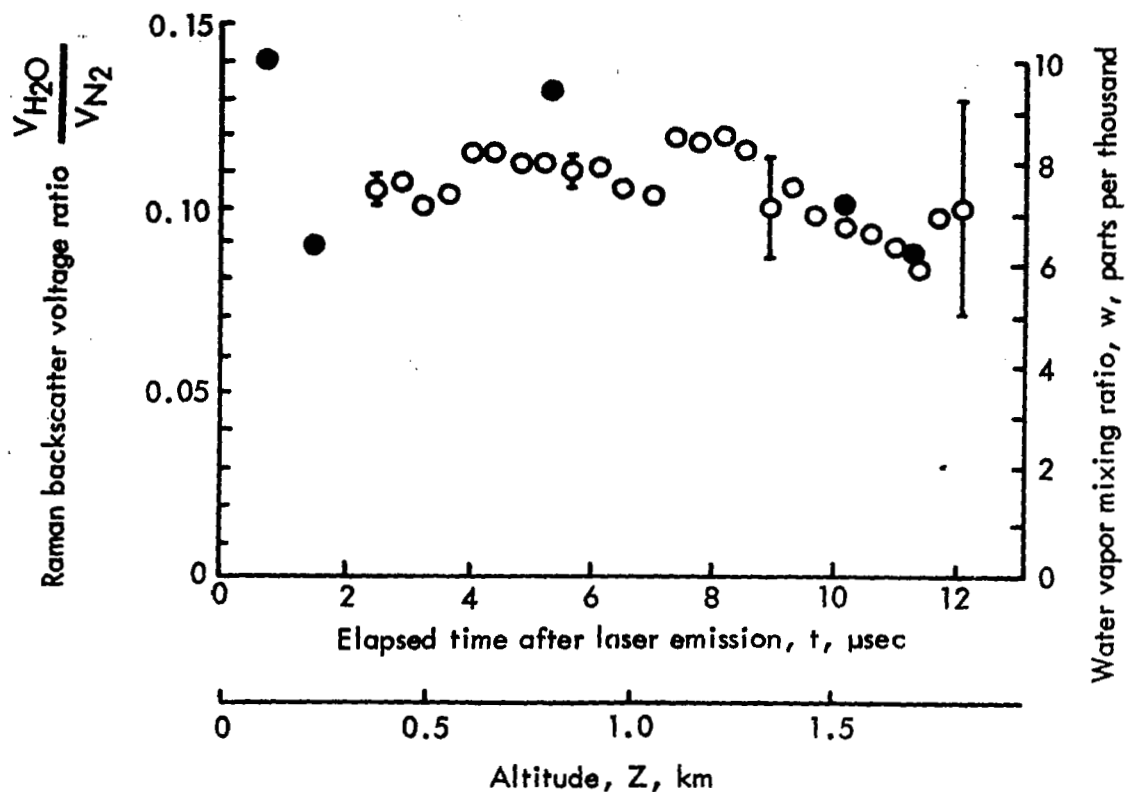


Figure 18.- A comparison of the ratio, $V_{H_2O}(Z)/V_{N_2}(Z)$, with water vapor mixing ratio w obtained from a radiosonde.
 O, $V_{H_2O}(Z)/V_{N_2}(Z)$ (left scale). ●, w (right scale)

A number of tests were performed at Wallops Island during December 1969, February, April, and June 1970.

VIC1. Examples of Average Analog Backscatter From the Atmosphere

Shown in figure 19 are typical examples of the analog average profiles for nitrogen and water vapor taken on the night of December 4, 1969. These average profiles for N_2 and H_2O were constructed from seven and eight oscillograms, respectively. The bars represent the 1 σ variation of the experimental data. The curves are the calculated signal return from a "clear atmosphere" normalized individually to the experimental data at the points indicated. Comparing the H_2O data with the calculated return for a constant mixing ratio of 1 gm/kg indicates that the water vapor mixing ratio may not have been constant with altitude as assumed in the calculations.

In February 1970, average oxygen profiles were obtained. Shown in figure 20 are typical examples of the average profiles for N_2 , O_2 , and H_2O compared with their respective calculated signals. The elastic scattered return was observed during the April 1970 experiment and an average profile is shown in figure 21 along with average profiles of N_2 and H_2O . A statistically significant aerosol layer is apparent on the elastic scattered return at an altitude of 1 km.

The variations in atmospheric attenuation are clearly indicated in figure 22, which is a normalized comparison of nitrogen profiles made in February and June 1970. The attenuation in the lower atmosphere in the June data was apparently higher and is indicated by the larger slope of the profile below an altitude of 1 km. Above this altitude the slopes of the two profiles are similar.

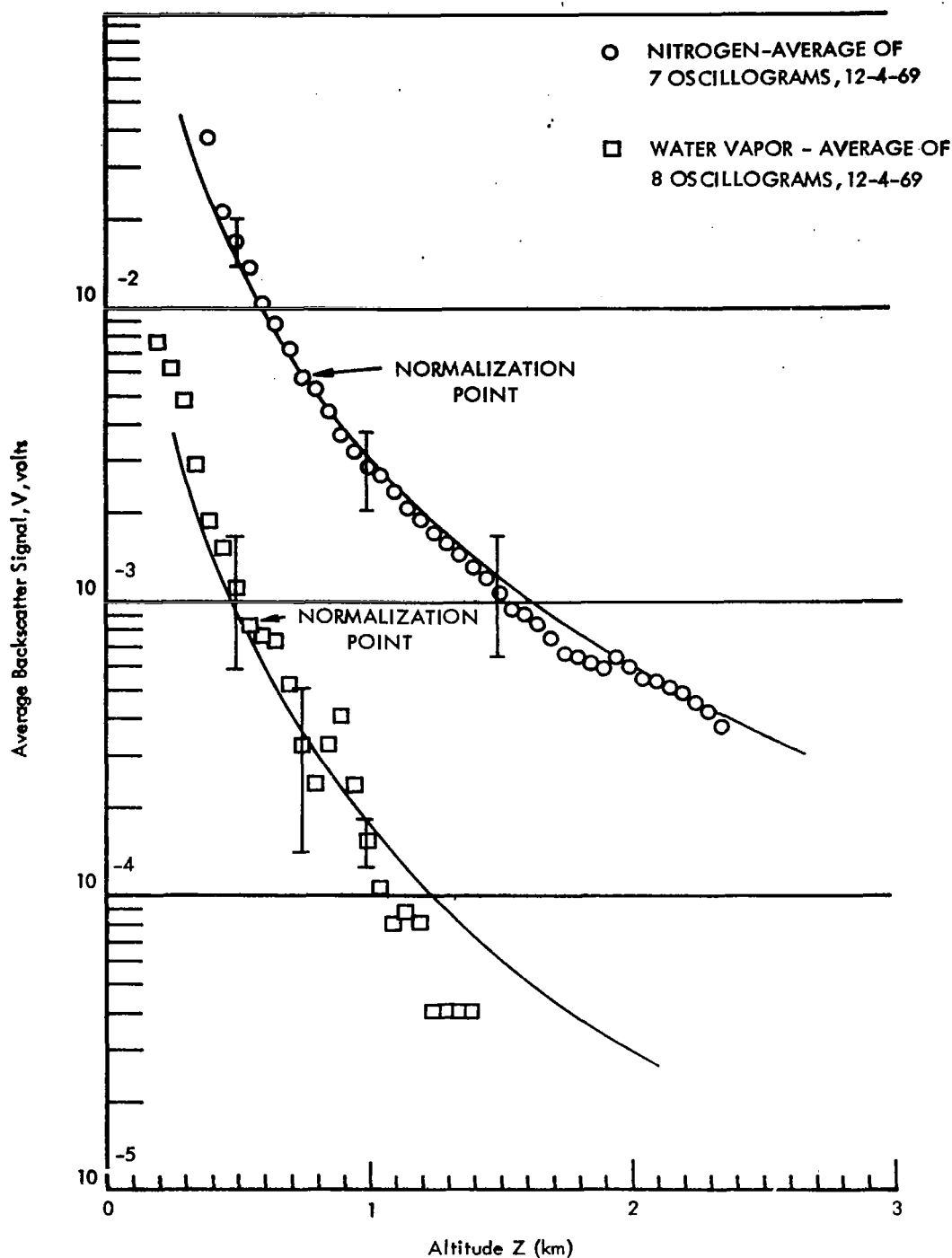


Figure 19.- Typical examples of average analog profiles for nitrogen and water vapor taken the night of December 4, 1969. The curves are the calculated nitrogen and water vapor signal returns normalized individually to the experimental data at the points indicated. The water vapor calculations were performed for a constant mixing ratio of 1 gm/kg.

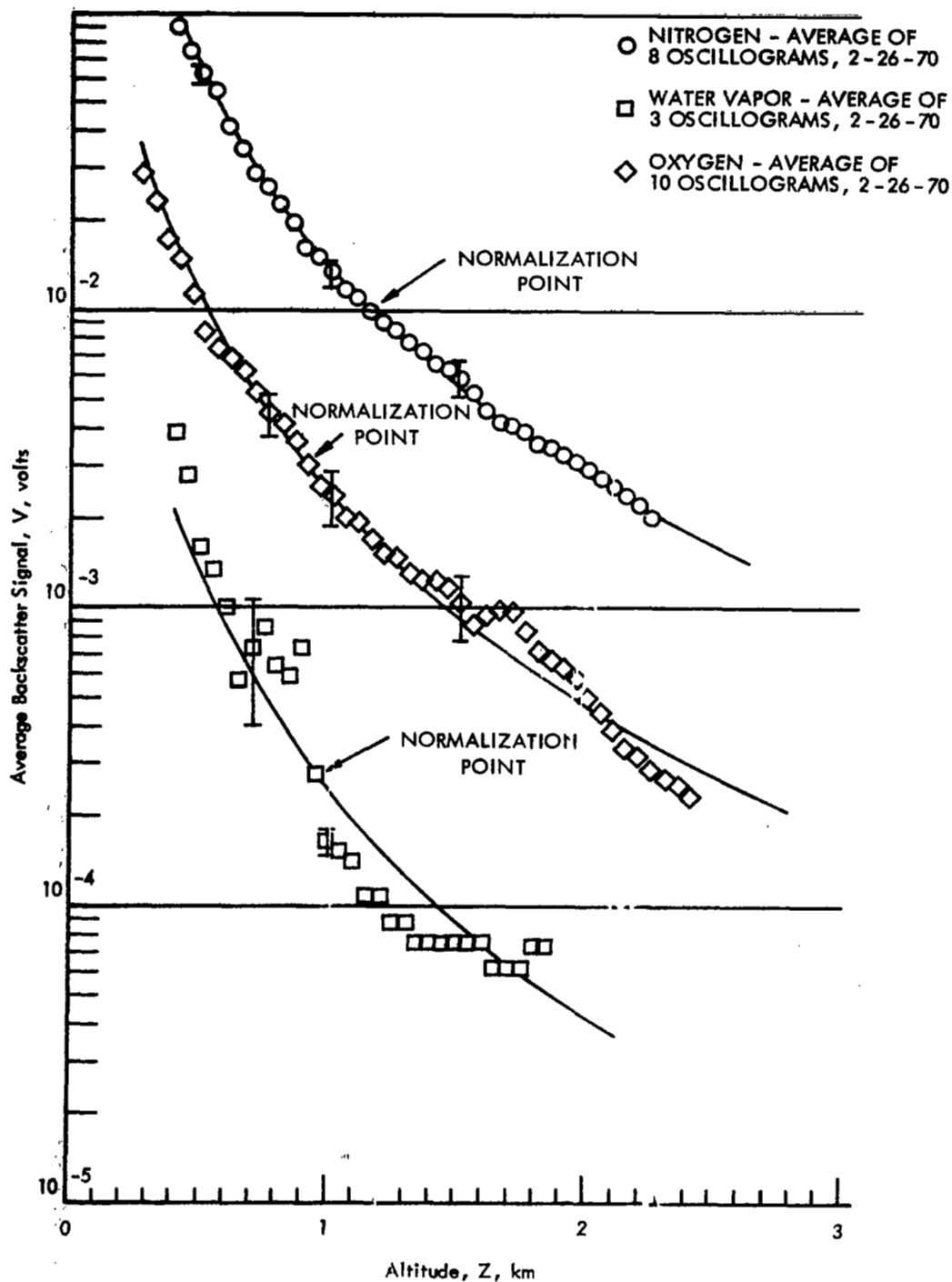


Figure 20.- Typical examples of average analog profiles for nitrogen, oxygen, and water vapor taken the night of February 26, 1970. The curves represent calculated signal returns individually normalized to the experimental data at the points indicated. Water vapor calculations are for a constant mixing ratio of 1 gm/kg.

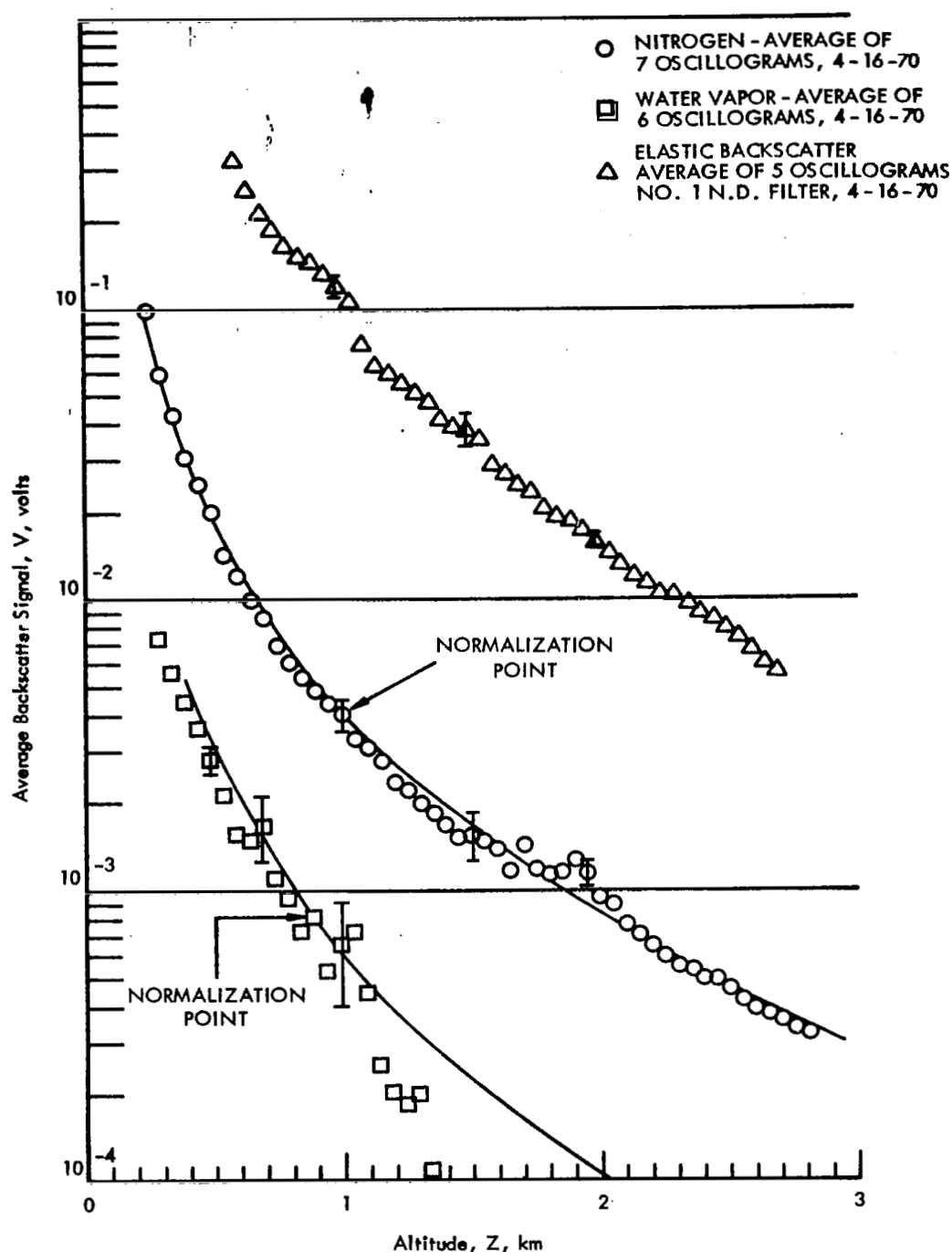


Figure 21.- Typical examples of analog average profiles for nitrogen, water vapor, and elastic backscatter taken the night of April 16, 1970. The curves represent calculated signal returns individually normalized to the experimental data at the points indicated. Water vapor calculations are for a constant mixing ratio of 1 gm/kg.

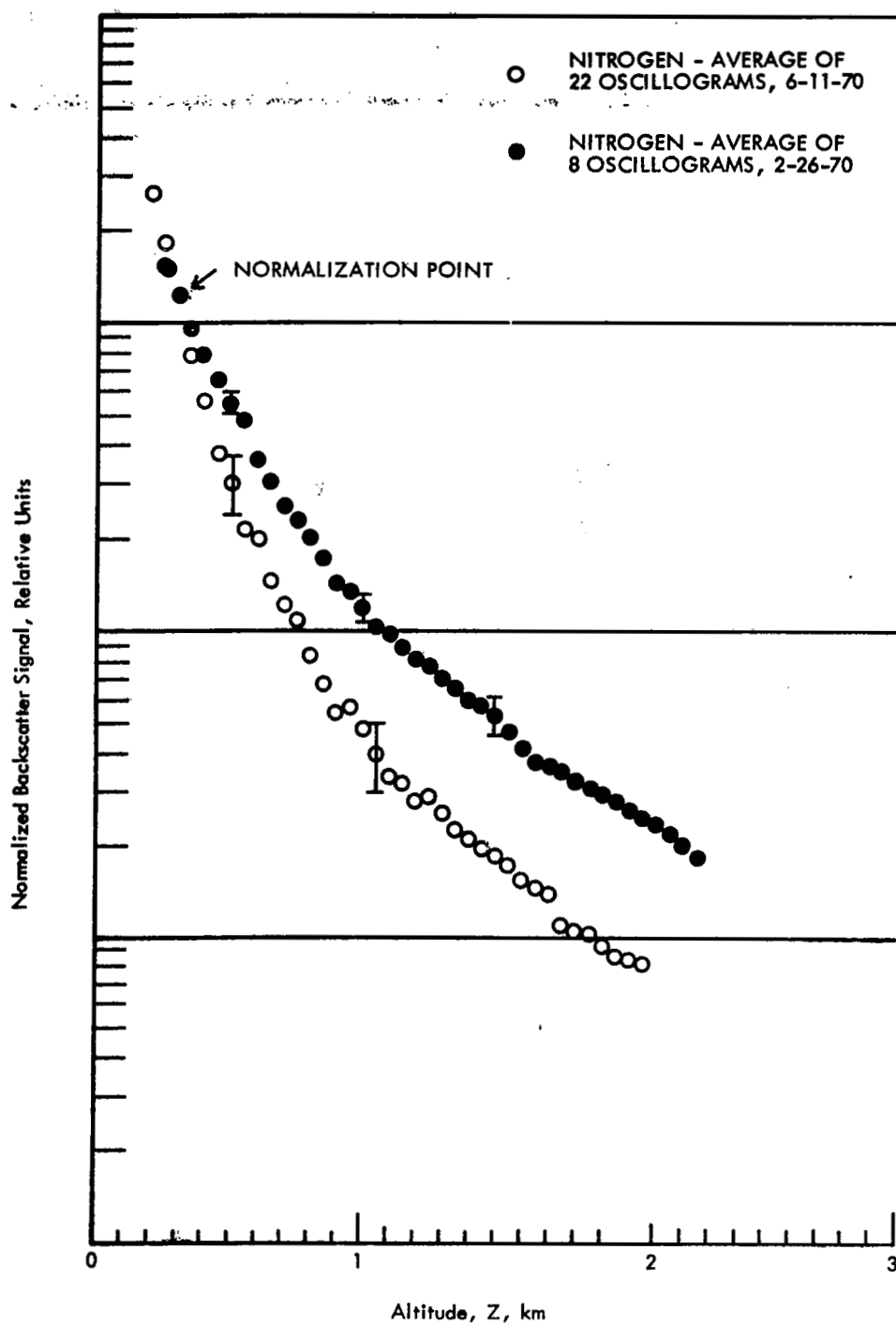


Figure 22.- Normalized comparison of nitrogen returns taken the nights of December 4, 1969, and June 11, 1970.

VIC2. Examples of Photon Counting Backscatter From the Atmosphere

Shown in figure 23 are the return signal profiles using the photon counting method for N_2 and H_2O taken the night of April 16, 1970. Each datum point represents the sum of photon counts in a 4 μ sec time window over 50 laser firings. A number one neutral density filter with a transmission ≈ 9 percent at 3777 \AA was used in front of the phototube for the N_2 return to keep the count rate measurable at low altitudes. The horizontal bars indicate the 0.6 km altitude resolution and the vertical bars indicate \pm the square root of the total counts for each datum point. The curve in this figure represents the calculated photon count rate for N_2 from the atmosphere normalized to the experimental data at the point indicated. In comparing the shape of the N_2 and H_2O profiles, it is apparent that the concentration of water vapor decreases in the altitude range 1-2 km and is nearly constant from 2 to above 3 km. Figure 24 shows the photon counting return taken the night of April 16, 1970, for nitrogen and for elastic backscatter. The nitrogen and elastic scatter returns were reduced in intensity using a number 0.3 and two number 1 neutral density filters, respectively. At low altitudes the shape of the profile does not follow the calculated curve for nitrogen. This behavior is due to an inability to visually distinguish individual photon events for the relatively high count rates obtained. From the nitrogen return in figure 24, an indication of nitrogen Raman backscatter is apparent to above an altitude of 10 km. The elastic scattered return shows an indication of an aerosol layer centered at 5.8 km.

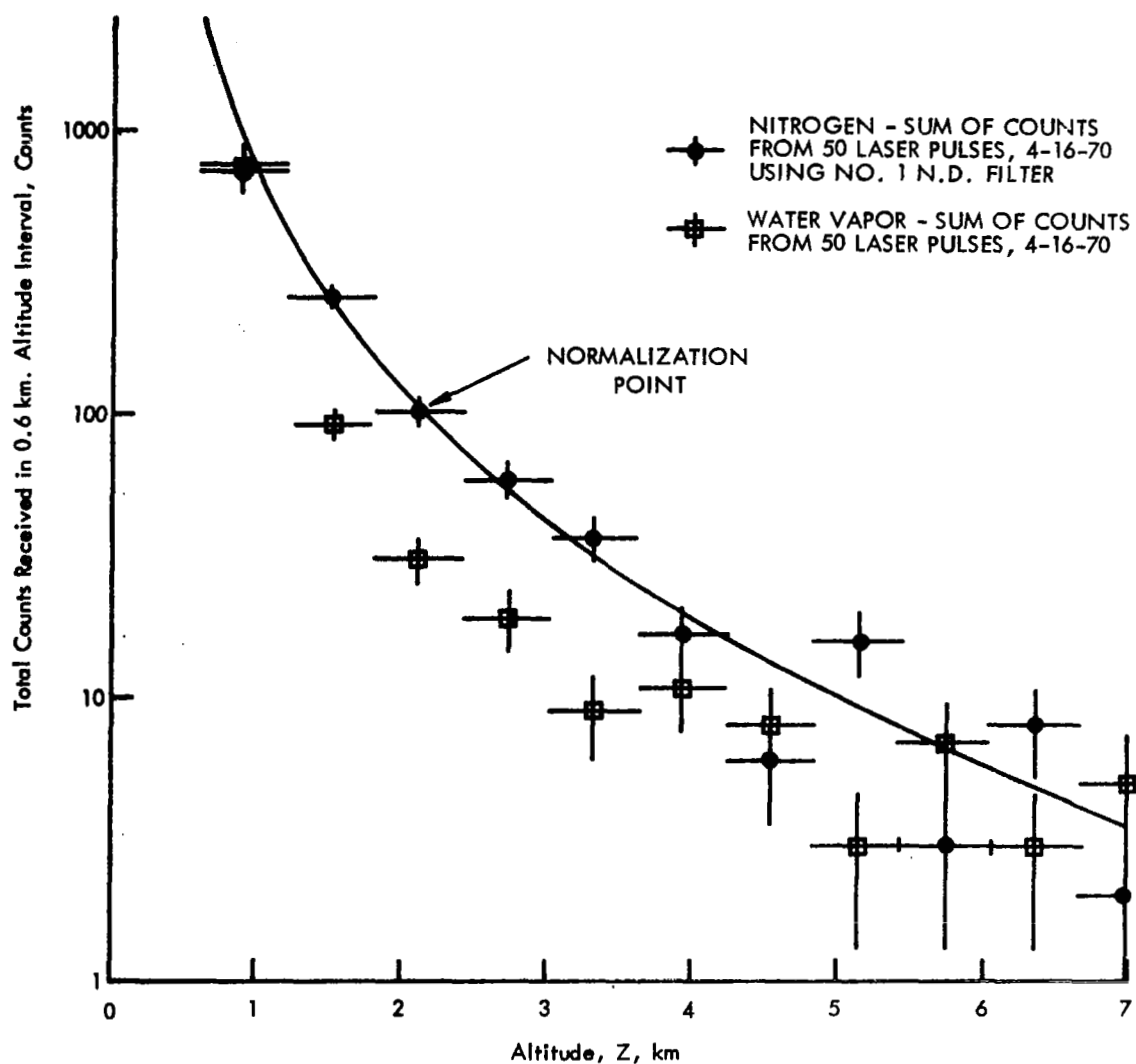


Figure 23.- Nitrogen and water vapor profiles using photon counting taken the night of April 16, 1970. The curve is the calculated photon count rate as a function of altitude for N_2 normalized to the experimental data at the point indicated.

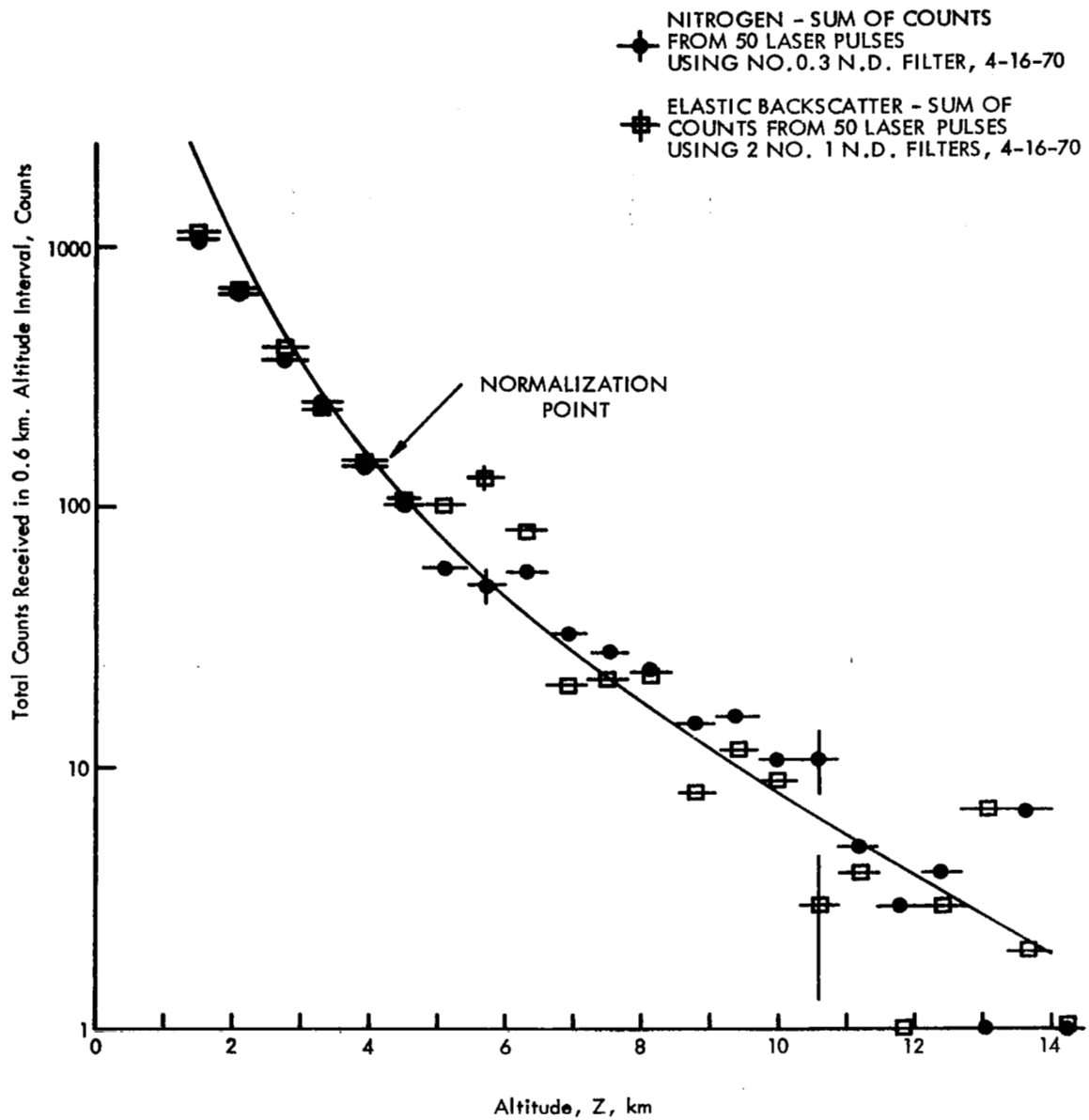


Figure 24.- Nitrogen and elastic backscatter profiles using photon counting, taken the night of April 16, 1970. The curve is the calculated photon count rate as a function of altitude for N_2 normalized to the N_2 experimental data at the point indicated.

VIC3. Comparison of the Optical Radar Data With Independent Meteorological Measurements

As was indicated in Chapter II (eq. (74)), the ratio of the water vapor to nitrogen Raman backscatter signals is proportional to water vapor mixing ratio. Optical radar measurements of this ratio have been compared to independent radiosonde measurements of water vapor in the atmosphere. Figure 25 shows the ratio of water vapor to nitrogen signals taken the night of February 26, 1970, normalized to the water vapor mixing ratio obtained from a radiosonde launched earlier the same evening.

Although these Raman data generally agree with the independent measurement of the radiosonde, there are some differences in shape of the profiles below 1 kilometer. This low altitude disagreement may be due to changes in the atmosphere since there was a 3-hour difference between the time of balloon launch and the initiation of the Raman experiment. Another possible explanation is that the elastic scattered band is not totally rejected by the interference filters. If rejection is the cause of the disagreement, it would be most apparent in the lowest layers of the atmosphere where the aerosol scattering is greatest. Also shown in figure 25 is a temperature profile obtained by the same radiosonde and, for comparison purposes, the temperature profiles for an adiabatic atmosphere. As was mentioned in Chapter III, stable regions of the atmosphere tend to discourage mixing. Comparing the two temperature profiles, it is apparent that a very stable layer was present that evening. The temperature profile indicates that the base of this layer is at an altitude of 0.8 km, and its presence has effectively prevented

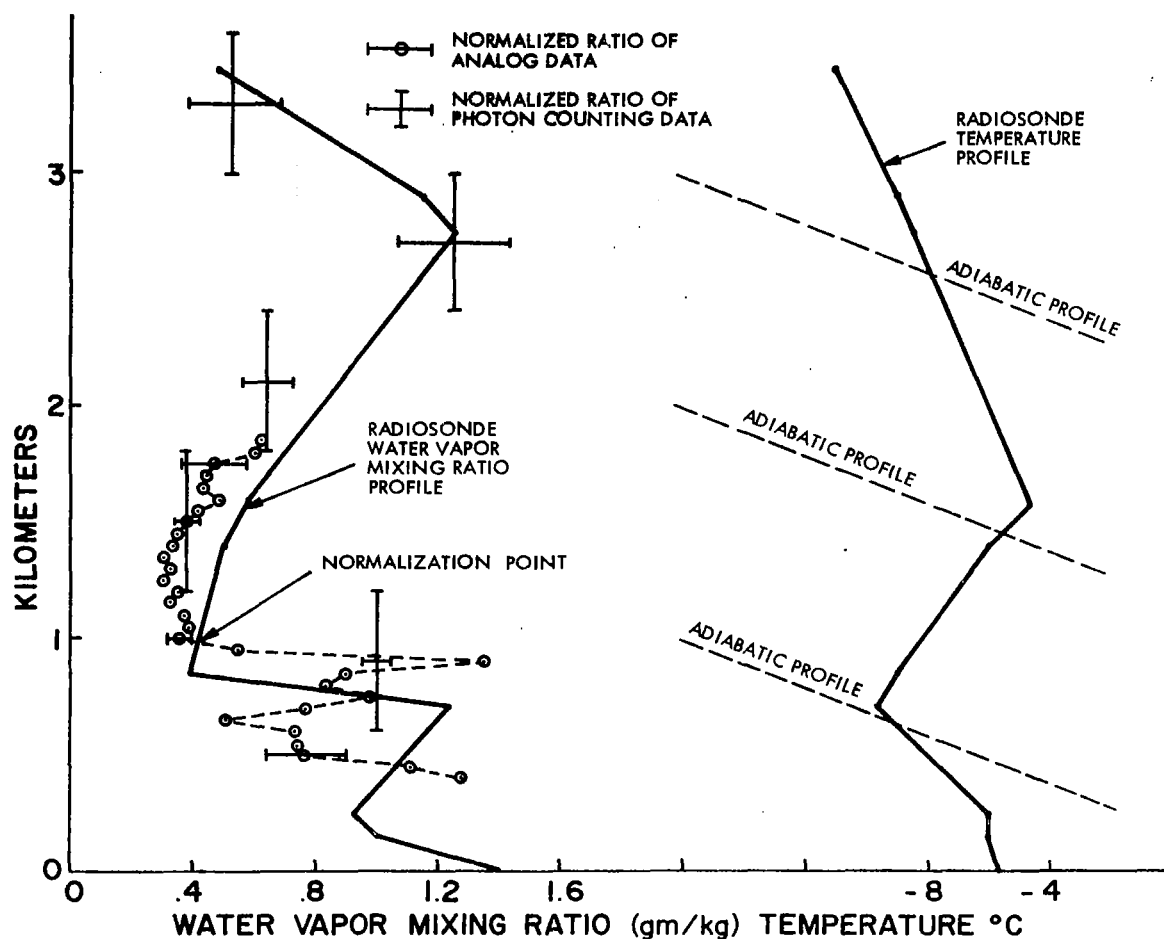


Figure 25.- The ratio of water vapor to nitrogen return signals normalized to the water vapor mixing ratio measured by a radiosonde at the point indicated. Both measurements made the night of February 26, 1970. Also shown is the radiosonde temperature profile and adiabatic temperature profiles.

upward mixing, as can be seen by the corresponding sharp decrease in water vapor above this altitude. Above 1 km and throughout the stable layer, the water vapor mixing ratio is small and nearly constant. The relative peak in the water vapor profile at 2.8 km may be a remnant of the base of a previous stable layer, an indication of the top of the adiabatic mixing layer described in Chapter II, or an indication of the early stages of cloud formation.

Figure 26 is a plot of the ratio of oxygen to nitrogen return signal obtained the night of February 26, 1970, as a function of altitude. This ratio was expected to be nearly constant with altitude, since the ratio of oxygen to nitrogen number densities is constant, and thus serves as a preliminary check on the assumptions $q_{\lambda_{R1}}(Z) = q_{\lambda_{R2}}(Z)$ in equations (74) and (75). Above 0.5 km the ratio is approximately constant, as expected. Below 0.5 km the departure from a constant value may again be explained on the basis of elastic scattering not totally rejected by the interference filters.

Figure 27 shows another comparison of Raman ratio data with radiosonde measurements. This experiment was conducted the night of April 16, 1970. Again, there was a time difference between the balloon launch and the Raman experiment. The balloon was launched approximately 4 hours prior to the initiation of the experiment. Again, agreement between the Raman data and the radiosonde measurement above 0.8 km is very good. A possible explanation for the disagreement below this altitude would be the same as given previously in regard to figure 25. The true temperature profile in figure 27 indicates the existence of a

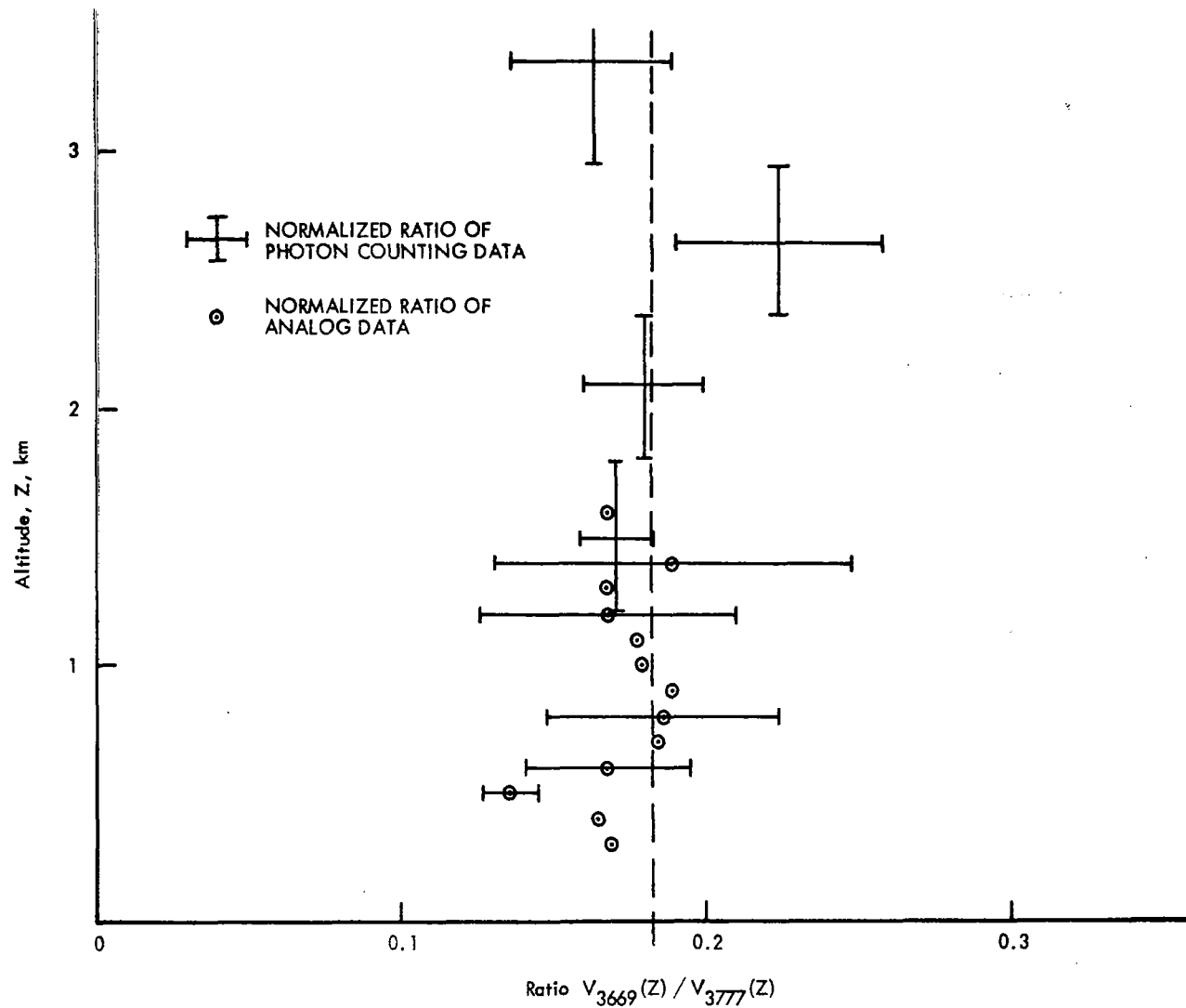


Figure 26.- The ratio of oxygen to nitrogen return signals as a function of altitude.

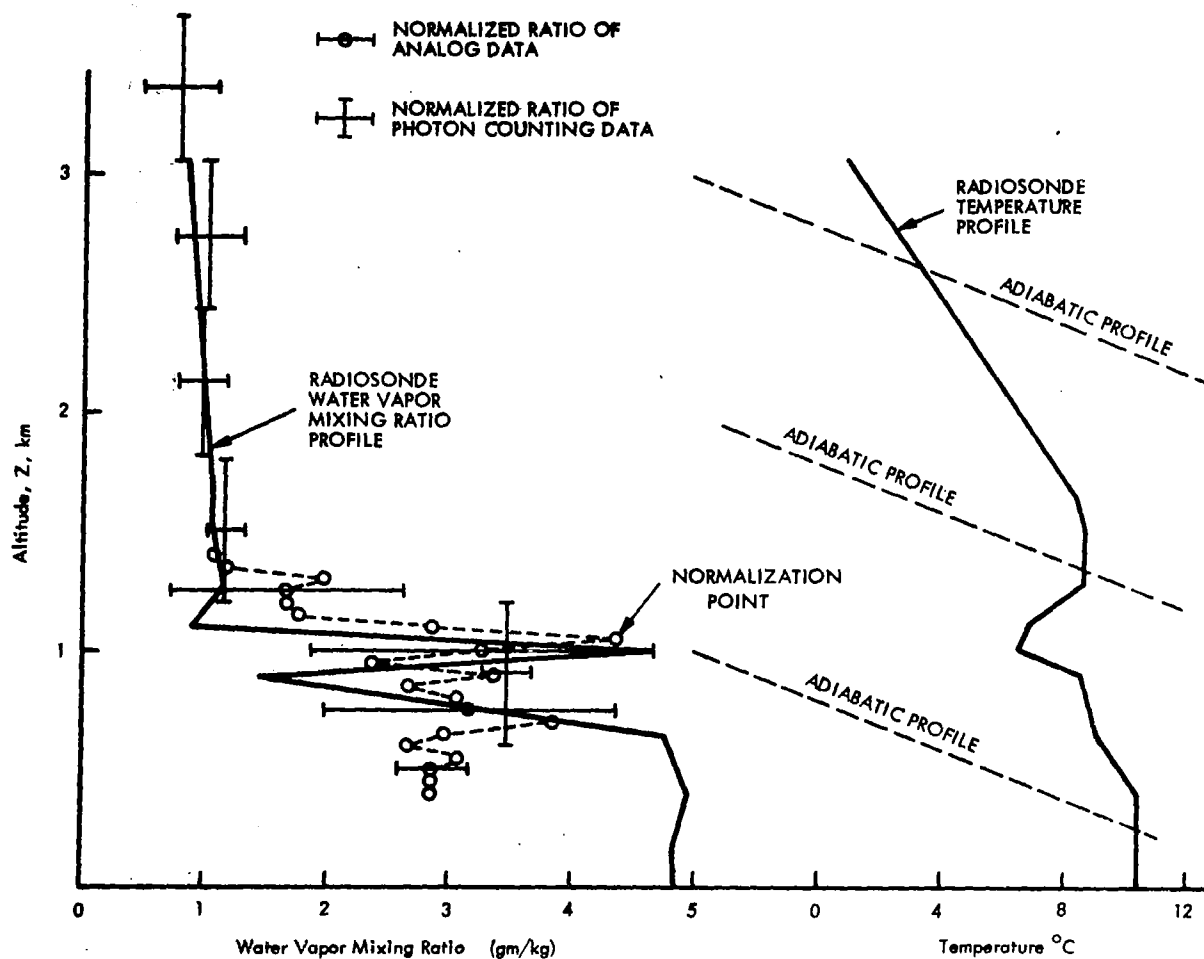


Figure 27.- The ratio of water vapor to nitrogen return signals normalized to the water vapor mixing ratio measured by a radiosonde. Both measurements made the night of April 16, 1970. Also shown is the radiosonde temperature profile and adiabatic temperature profiles.

stable layer extending from 1 km to approximately 1.5 km above a thin (100 m) slightly unstable layer. The sharp peak in the water vapor profile near the boundary between the stable and unstable layers may have a simple explanation. Eddies mixing from below move into the unstable layer and are quickly mixed to the top of this layer. A process of this type would create a minimum concentration below the unstable layer, which is also evident in the water vapor profile.

During the April 16, 1970, experiment, two balloons with particle sampling instrument packages, described in Chapter V, were launched by Dr. J. M. Rosen of the University of Wyoming. Figure 28 shows a comparison between the optical radar data and the results of the balloon-borne dust photometer as a function of altitude. The optical radar data are the ratio of the elastic backscattered return to the nitrogen return, which may provide a preliminary indication of the mixing ratio of aerosols in the lower atmosphere, as shown by equation (75). The optical radar ratio profile is equated to 1 at an altitude of approximately 2 km. If the elastic backscattered return at this altitude is predominantly due to Rayleigh molecular scattering values of the ratio greater than 1 must be assumed to be due to aerosols. The agreement between the two independent measurements is evident. The peak in the apparent aerosol concentration within the unstable layer is also apparent. In general, the altitude profiles of the water vapor mixing ratio and the aerosol scattering ratio in figures 27 and 28 are similar.

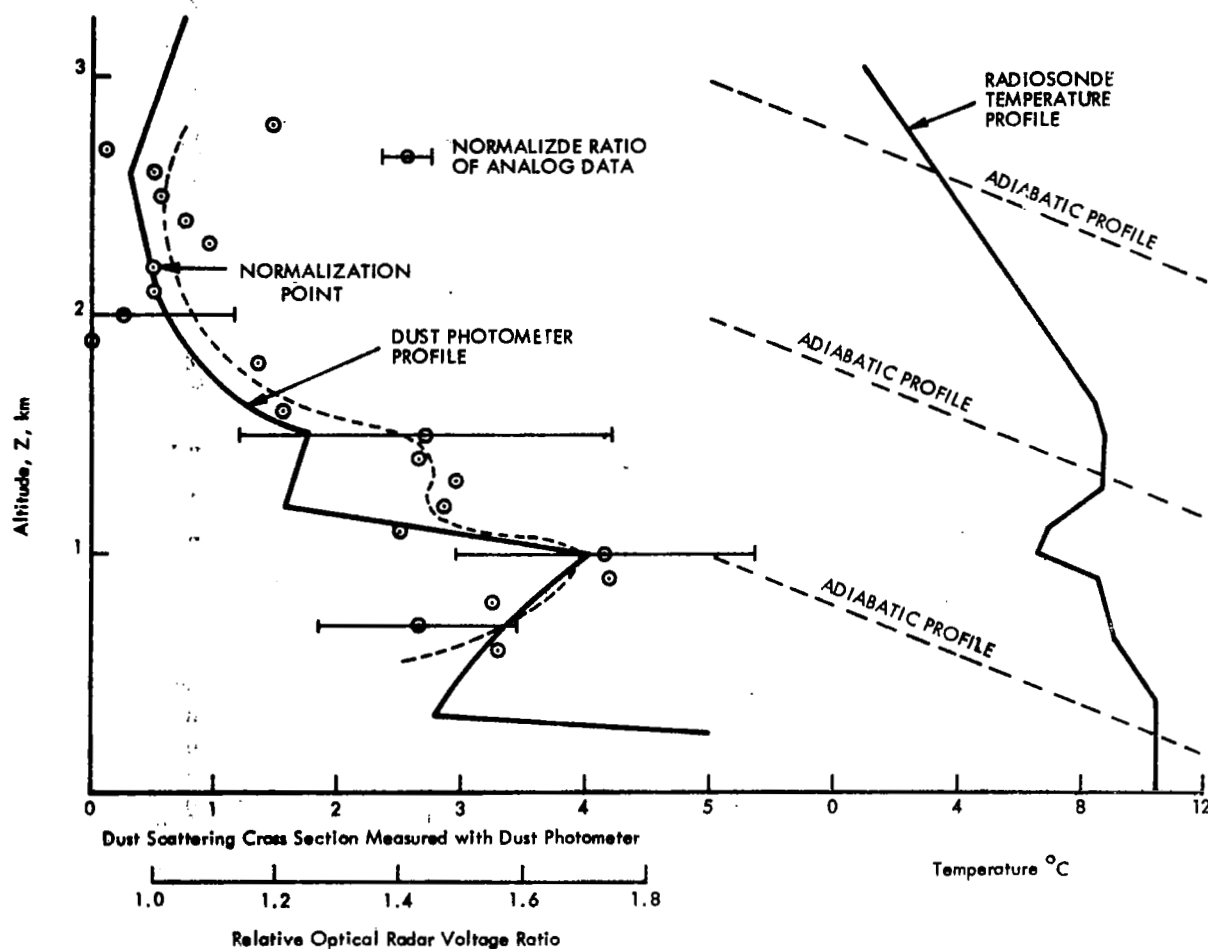


Figure 28.- The ratio of the elastic scattered to nitrogen return signals measured by a balloon-borne dust photometer. Both measurements made the night of April 16, 1970. Also shown is a radiosonde temperature profile taken the same night and adiabatic temperature profiles.

VII. CONCLUSIONS

This research has demonstrated conclusively that the Raman optical radar technique may be used to obtain quantitative measurements of the profiles of individual atmospheric molecular trace constituents, in particular water vapor, as well as those of the major constituents, N_2 and O_2 .

A concise treatment of Rayleigh and Raman scattering by molecules has resulted in an approximate value for backscatter cross sections of nitrogen and oxygen. These calculations have included rotational fine structure and its effect on the effective cross section in an optical radar experiment. Using these cross sections, the optical radar signal return from Raman backscatter in the atmosphere has been calculated for the first time.

In general, the experimental results show good agreement with independent meteorological measurements. Using a dual monochrometer, optical radar data was obtained from altitudes above 1 km which agree well with radiosonde measurements of relative humidity. Using interference filters to select Raman bands:

(1) Water vapor mixing ratio profiles were measured which agreed with radiosonde measurements to an altitude of 3.3 km.

(2) Some disagreement between Raman optical radar profiles and radiosonde results was evident below an altitude of 1 km. A possible explanation of this disagreement is that the filters are not totally rejecting the relatively intense aerosol scattering at low altitudes.

(3) An indication of Raman backscatter from molecular nitrogen has been observed for altitudes above 10 km.

(4) An indication of aerosol mixing ratio to an altitude above 3 km has been obtained that agreed well with independent measurements by a balloon-borne dust photometer.

(5) Changes in the slope of the nitrogen return signals obtained in February and June 1970 indicate the ability of this technique to monitor variations in atmospheric attenuation.

(6) Raman optical radar measurements of water vapor and aerosol profiles agree with a qualitative treatment of turbulent mixing in the lower atmosphere.

The analysis of the Raman optical radar technique presented has indicated the potential of the method to remotely measure other molecular species in the atmosphere, such as pollutants, and to observe on a local basis turbulent diffusion, pollution dissipation, and cloud formation in the earth's lower atmosphere. In addition, the possibility exists of using this technique to distinguish between cloud formations consisting of water droplets or ice crystals.

A natural extension of this research program would be the installation of a Raman optical radar system in an aircraft to measure high altitude molecular profiles of water vapor and other trace constituents; and, as the technique is developed, experiments can be performed from a space platform to monitor upper atmospheric constituents on a global basis.

APPENDIX A

TRANSFORMATION OF THE POLARIZABILITY AND DIFFERENTIAL POLARIZABILITY TENSORS FROM A RANDOMLY ORIENTED MOLECULAR COORDINATE SYSTEM TO A LABORATORY COORDINATE SYSTEM

The matrix for the transformation of a vector in the laboratory coordinate system (x_i') to a molecular coordinate system (x_i) is:

$$T = \begin{bmatrix} \cos(x_1, x_1') & \cos(x_1, x_2') & \cos(x_1, x_3') \\ \cos(x_2, x_1') & \cos(x_2, x_2') & \cos(x_2, x_3') \\ \cos(x_3, x_1') & \cos(x_3, x_2') & \cos(x_3, x_3') \end{bmatrix} \quad (A-1)$$

where (x_i, x_i') indicates the angle between the coordinate axis x_i and x_i' . The transformation of polarizability tensor is then:

$$\begin{aligned} \alpha_{\Omega, \Sigma} &= \left[T^{-1} (\alpha_{\mu\nu}) T \right]_{\Omega, \Sigma} \\ &= \sum_{\mu, \nu} \alpha_{\mu, \nu} \cos(\mu, \Sigma) \cos(\nu, \Omega) \end{aligned} \quad (A-2)$$

The $\alpha_{\mu\nu}$ matrix can be diagonalized. Denoting the principal values as α_i with $i = 1, 2, \text{ or } 3$, equation (A-2) becomes:

$$\alpha_{\Omega, \Sigma} = \sum_i \alpha_i \cos(i, \Sigma) \cos(i, \Omega) \quad (A-3)$$

The average of the square of equation (A-3) can be written as:

$$\overline{\langle |\alpha_{\Omega\Sigma}|^2 \rangle} = \sum_{i,j} \alpha_i \alpha_j \langle \cos(i,\Sigma) \cos(i,\Omega) \cos(j,\Sigma) \cos(j,\Omega) \rangle \quad (\text{A-4})$$

Simplification of equation (A-4) involves using well-known values for the average of products of cosine functions⁽³³⁾ such as:

$$\langle \cos^4 \theta \rangle = \frac{1}{5}$$

$$\langle \cos^2 \theta_1 \cos^2 \theta_2 \rangle = \frac{1}{15}$$

and

$$\langle \cos \theta_1 \cos \theta_2 \cos \theta_3 \cos \theta_4 \rangle = -\frac{1}{30}$$

Using these values for the cosine function averages, equation (A-4) can be written as:

$$\overline{\langle |\alpha_{\Omega,\Sigma}|^2 \rangle} = \frac{1}{45} \begin{bmatrix} 45\alpha^2 + 4\beta^2 & 3\beta^2 & 3\beta^2 \\ 3\beta^2 & 45\alpha^2 + 4\beta^2 & 3\beta^2 \\ 3\beta^2 & 3\beta^2 & 45\alpha^2 + 4\beta^2 \end{bmatrix} \quad (\text{A-5})$$

where

$$\alpha = \frac{1}{3}(\alpha_1 + \alpha_2 + \alpha_3)$$

and

$$\beta^2 = \frac{1}{2}[(\alpha_1 - \alpha_2)^2 + (\alpha_2 - \alpha_3)^2 + (\alpha_1 - \alpha_3)^2]$$

and in a similar fashion:

$$\underbrace{\langle |\alpha'_{\Omega\Sigma}|^2 \rangle}_{\cdot} = \frac{1}{45} \begin{bmatrix} 45\alpha'^2 + 4\beta'^2 & 3\beta'^2 & 3\beta'^2 \\ 3\beta'^2 & 45\alpha'^2 + 4\beta'^2 & 3\beta'^2 \\ 3\beta'^2 & 3\beta'^2 & 45\alpha'^2 + 4\beta'^2 \end{bmatrix} \quad (\text{A-6})$$

where

$$\alpha' = \frac{1}{3}(\alpha'_1 + \alpha'_2 + \alpha'_3)$$

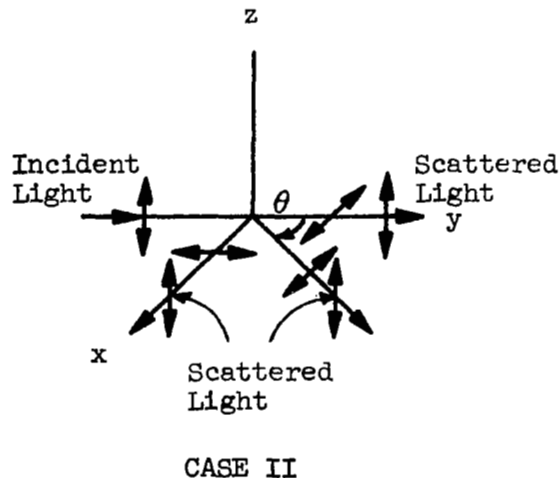
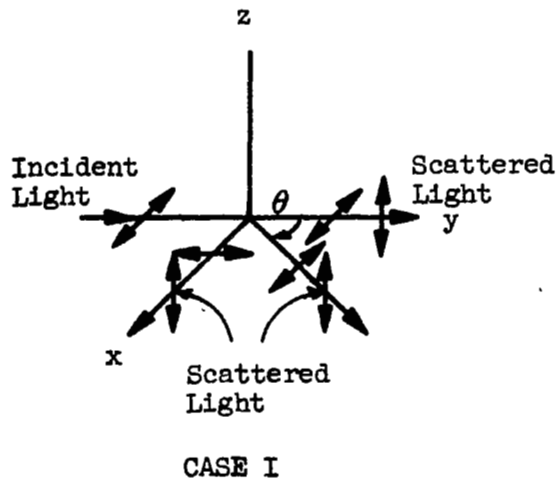
and

$$\beta'^2 = \frac{1}{2}[(\alpha'_1 - \alpha'_2)^2 + (\alpha'_2 - \alpha'_3)^2 + (\alpha'_1 - \alpha'_3)^2]$$

APPENDIX B

DERIVATION OF RAYLEIGH AND RAMAN VIBRATIONAL CROSS SECTIONS FOR ALL POLARIZATIONS AS A FUNCTION OF SCATTERING ANGLE

Assume in the laboratory coordinate system that the incident light is moving in the positive y direction polarized in the x direction, Case I and the z direction, Case II as shown below:



CASE I

If the Rayleigh scattered light is observed along the x direction (90° scattering) the cross sections for the two polarizations will be:

$$\frac{d\sigma}{d\Omega}(x, z, \omega_0)_s = \frac{\omega_0^4}{c^4} \langle |\alpha_{xz}|^2 \rangle \quad (B-1)$$

and

$$\frac{d\varphi}{d\Omega}(x, y, \omega_o)_p = \frac{\omega_o^4}{c^4} \langle |\alpha_{xy}|^2 \rangle \quad (B-2)$$

where the subscript s refers to the scattered component polarized perpendicular to the scattering plane and the subscript p refers to the scattered component polarized parallel to the scattering plane. The scattering plane is that plane which contains both the incident and scattered rays. The two components of the Rayleigh scatter cross section along the y axis (forward scattering) can be written in a similar manner as:

$$\frac{d\varphi}{d\Omega}(x, z, \omega_o)_s = \frac{\omega_o^4}{c^4} \langle |\alpha_{xz}|^2 \rangle \quad (B-3)$$

and

$$\frac{d\varphi}{d\Omega}(x, x, \omega_o)_p = \frac{\omega_o^4}{c^4} \langle |\alpha_{xx}|^2 \rangle \quad (B-4)$$

at any other angle θ equations (B-1), (B-2), (B-3) and (B-4) can be combined to yield

$$\frac{d\varphi}{d\Omega}(\theta_x, \omega_o)_s = \frac{\omega_o^4}{c^4} \langle |\alpha_{xz}|^2 \rangle \quad (B-5)$$

and

$$\frac{d\varphi}{d\Omega}(\theta_x, \omega_o)_p = \frac{\omega_o^4}{c^4} \left[\langle |\alpha_{xy}|^2 \rangle \sin^2 \theta_x + \langle |\alpha_{xx}|^2 \rangle \cos^2 \theta \right] \quad (B-6)$$

where θ_x is the scattering angle for incident light polarized in the x direction.

Substituting the appropriate values of $\langle |\alpha_{\Omega\Sigma}|^2 \rangle$ from equation (35) equation (B-5) and (B-6) become:

$$\frac{d\varphi}{d\Omega}(\theta_x, \omega_o)_p = \frac{\omega_o^4}{c^4} \left(\frac{3}{45} \beta^2 \right) \quad (B-7)$$

and

$$\frac{d\varphi}{d\Omega}(\theta_x, \omega_o)_s = \frac{\omega_o^4}{c^4} \left[\left(\alpha^2 + \frac{1}{45} \beta^2 \right) \cos^2 \theta_x + \frac{3}{45} \beta^2 \right] \quad (B-8)$$

In similar fashion, the cross sections for the vibrational Raman effect are:

$$\frac{d\varphi}{d\Omega}(\theta_x, \omega)_p = \frac{\omega^4}{c^4} \frac{n}{2m\omega_j} \frac{\frac{3}{45} \beta'^2}{1 - e^{-n\omega_j/KT}} \quad (B-9)$$

and

$$\frac{d\varphi}{d\Omega}(\theta_x, \omega)_s = \frac{\omega^4}{c^4} \frac{n}{2m\omega_j} \frac{\left[\left(\alpha'^2 + \frac{1}{45} \beta'^2 \right) \cos^2 \theta_x + \frac{3}{45} \beta'^2 \right]}{1 - e^{-n\omega_j/KT}} \quad (B-10)$$

for

$$\Delta V = +1 \quad \text{and} \quad \omega = (\omega_o - \omega_j)$$

CASE II

The Rayleigh cross sections for Case II which correspond to equations (B-7) and (B-8) can be shown to be:

$$\frac{d\varphi}{d\Omega}(\theta_z, \omega_o)_p = \frac{\omega_o^4}{c^4} (\alpha^2 + \frac{4}{45} \beta^2) \quad (B-11)$$

and

$$\frac{d\varphi}{d\Omega}(\theta_z, \omega_o)_s = \frac{\omega_o^4}{c^4} \left(\frac{3}{45} \beta^2 \right) \quad (B-12)$$

where θ_z is the scattering angle for incident light polarized in the z direction and the Raman vibration cross sections for Case II are:

$$\frac{d\varphi}{d\Omega}(\theta_z, \omega)_p = \frac{\omega^4}{c^4} \frac{\pi}{2m\omega_j} \frac{\alpha'^2 + \frac{4}{45} \beta'^2}{1 - e^{-\hbar\omega_j/KT}} \quad (B-13)$$

and

$$\frac{d\varphi}{d\Omega}(\theta_z, \omega)_s = \frac{\omega^4}{c^4} \frac{\pi}{2m\omega_j} \frac{\frac{3}{45} \beta'^2}{1 - e^{-\hbar\omega_j/KT}} \quad (B-14)$$

for

$$\Delta V = +1 \quad \text{and} \quad \omega = (\omega_o - \omega_j)$$

By taking the average of the sum of equations (B-7), (B-8), (B-11), and (B-12), the well-known equation for Rayleigh scattering by unpolarized incident light is obtained, (cf. van de Hulst)⁽³⁴⁾

$$\frac{d\varphi}{d\Omega}(\theta, \omega) = \frac{\omega_o^4}{c^4} \frac{(1 + \cos^2 \theta)}{2} \langle |\alpha|^2 \rangle$$

with β small.

0

APPENDIX C

REDUCTION OF THE PURE ROTATIONAL RAMAN CROSS SECTION EQUATION

The pure rotational Raman cross section from equation (49) is:

$$\frac{d\sigma}{d\Omega}(\Omega, \Sigma, \omega, J) = \frac{\omega^4}{c^4} \frac{g_J(2J+1)e^{-B_0 J(J+1)hc/KT}}{\sum_J g_J(2J+1)e^{-B_0 J(J+1)hc/KT}} \times \sum_i \alpha_i \langle \psi_r^* | \cos(i, \Sigma) \cos(i, \Omega) | \psi_r \rangle \quad (49)$$

Let g_J^+ be the nuclear degeneracy for J even and g_J^- that for J odd. Then the denominator in equation (49) becomes:

$$\begin{aligned} \sum_{J=0}^{\infty} g_J(2J+1)e^{-B_0 J(J+1)hc/KT} &= g_J^+ \sum_{J=0}^{\infty} (4J+1)e^{-B_0(4J^2+2J)hc/KT} \\ &+ g_J^- \sum_{J=0}^{\infty} (4J+3)e^{-B_0(4J^2+6J+2)hc/KT} \quad (C-1) \end{aligned}$$

Since the increment in J is small compared to the range, equation (C-1) may be written

$$\begin{aligned} \sum_{J=0}^{\infty} g_J(2J+1)e^{-B_0 J(J+1)hc/KT} &= g_J^+ \int_0^{\infty} (4J+1)e^{-B_0(4J^2+2J)hc/KT} dJ \\ &+ g_J^- \int_0^{\infty} (4J+3)e^{-B_0(4J^2+6J+2)hc/KT} dJ \end{aligned}$$

$$\begin{aligned}
&= \frac{g_J^+ KT}{2Bhc} e^{Bhc/4KT} + \frac{g_J^- KT}{2Bhc} e^{9Bhc/4KT} \\
&\approx \frac{KT}{2Bhc} (g_J^+ + g_J^-) \quad (C-2)
\end{aligned}$$

assuming $KT \ll Bhc$. Substituting equation (3-2) into equation (49) gives:

$$\begin{aligned}
\frac{d\varphi}{d\Omega}(\Omega, \Sigma, \omega, J) &= \frac{\omega^4}{c^4} \frac{2B_0 hc}{KT} \frac{g_J(2J+1)e^{-B_0 J(J+1)hc/KT}}{g_J^+ + g_J^-} \\
&\times \sum_i \alpha_i \left\langle \psi_r^* \left| \cos(i, \Sigma) \cos(1\Omega) \right| \psi_r \right\rangle \quad (C-3)
\end{aligned}$$

APPENDIX D

SAMPLE CALCULATION OF ONE TERM IN THE ROTATIONAL RAMAN CROSS SECTION

From equation (51) the matrix elements to be calculated are:

$$(\alpha_{\Omega\Sigma})_{J_m, J'_m} = \sum_1 \alpha_1 \langle Y_{J_m}^{*m}(\theta, \varphi) | \cos(i\Sigma) \cos(i\Omega) | Y_{J'_m}^{m'}(\theta, \varphi) \rangle \quad (D-1)$$

The transformation matrix given in equation (A-1) can be rewritten in terms of Euler angles (cf. Goldstein):

$$T = \begin{pmatrix} \cos \psi \cos \varphi - \cos \theta \sin \varphi \sin \psi & -\sin \psi \cos \varphi - \cos \theta \sin \varphi \cos \psi & \sin \theta \sin \varphi \\ \cos \psi \sin \varphi + \cos \theta \cos \varphi \sin \psi & -\sin \psi \sin \varphi + \cos \theta \cos \varphi \cos \psi & -\sin \theta \cos \varphi \\ \sin \theta \sin \psi & \sin \theta \cos \psi & \cos \theta \end{pmatrix} \quad (D-2)$$

Using this transformation matrix the $\Omega = \Sigma = 3$ term of equation (D-1) becomes:

$$\begin{aligned} (\alpha_{3,3})_{J_m J'_m} &= \alpha_1 \langle Y_{J_m}^{*m}(\theta, \varphi) | \sin^2 \theta \sin^2 \varphi | Y_{J'_m}^{m'}(\theta, \varphi) \rangle \\ &+ \alpha_2 \langle Y_{J_m}^{*m}(\theta, \varphi) | \sin^2 \theta \cos^2 \varphi | Y_{J'_m}^{m'}(\theta, \varphi) \rangle \\ &+ \alpha_3 \langle Y_{J_m}^{*m}(\theta, \varphi) | \cos^2 \theta | Y_{J'_m}^{m'}(\theta, \varphi) \rangle \end{aligned} \quad (D-3)$$

Only the third term on the right side of equation (D-3) will be examined. This term can be written

$$\begin{aligned}
& \alpha_3 \langle Y_J^{*m}(\theta, \varphi) | \cos^2 \theta | Y_{J'}^{m'}(\theta, \varphi) \rangle \\
&= \left\langle \sqrt{\frac{2J+1}{4\pi}} \frac{(J-m)!}{(J+m)!} P_J^{*m}(\cos \theta) e^{-im\varphi} \middle| \cos^2 \theta \middle| \sqrt{\frac{2J'+1}{4\pi}} \frac{(J'-m')!}{(J'+m')!} P_{J'}^{m'}(\cos \theta) e^{im'\varphi} \right\rangle
\end{aligned}
\tag{D-4}$$

A well-known recursion relation for Associated Legendre polynomials is:

$$\cos \theta P_J^m(\cos \theta) = (2J+1)^{-1} [(J+m)P_{J-1}^m(\cos \theta) + (J-m+1)P_{J+1}^m(\cos \theta)]
\tag{D-5}$$

multiplying by $\cos \theta$ results in:

$$\cos^2 \theta P_J^m(\cos \theta) = \frac{J+m}{2J+1} \cos \theta P_{J-1}^m(\cos \theta) + \frac{(J-m+1)}{2J+1} \cos \theta P_{J+1}^m(\cos \theta)
\tag{D-6}$$

Combining equations (D-5) and (D-6) and collecting terms:

$$\begin{aligned}
\cos^2 \theta P_J^m(\cos \theta) &= \left[\frac{(J+m)(J-m)}{(2J+1)(2J-1)} + \frac{(J-m+1)(J+m+1)}{(2J+1)(2J+3)} \right] P_J^m(\cos \theta) \\
&+ \frac{(J-m+1)(J-m+2)}{(2J+1)(2J+3)} P_{J+2}^m(\cos \theta) \\
&+ \frac{(J+m)(J+m-1)}{(2J+1)(2J-1)} P_{J-2}^m(\cos \theta)
\end{aligned}
\tag{D-7}$$

When equation (D-7) is substituted into equation (D-4), the selection rules $\Delta J = 0, \pm 2$, $\Delta m = 0$ are apparent from the orthogonality of the $Y_J^{m'}$ s.

APPENDIX E

A LISTING OF THE ROTATIONAL RAMAN FINE STRUCTURE BACKSCATTER CROSS SECTIONS OF N₂ AND O₂

Tables E1 through E8 list the normalized backscatter cross sections for the rotational fine structure of Rayleigh scattering and $v = 0 \rightarrow 1$ vibrational Raman scattering.

Tables E9 through E16 list the calculated backscatter cross sections for the rotational fine structure of Rayleigh scattering and $v = 0 \rightarrow 1$ vibrational Raman scattering.

The notation in these tables such as 1.481E+27 is to be interpreted as 1.481×10^{27} and 9.12379E-31 as 9.12379×10^{-31} .

TABLE E1.- NORMALIZED BACKSCATTER CROSS SECTIONS FOR PURE ROTATIONAL RAMAN

FINE STRUCTURE OF O_2 . $\Delta J = +2$

J	Relative cross section $\Delta J = +2$	Normalized cross section	Running sum of normalized cross section	$\lambda, (\mu)$
0	1.481E+27	1.84216E-02	1.480754E+27	3.47254E-01
1	0.	0.	1.480754E+27	3.47323E-01
2	3.647E+27	4.53741E-02	5.127990E+27	3.47393E-01
3	0.	0.	5.127990E+27	3.47462E-01
4	5.259E+27	6.54275E-02	1.038715E+28	3.47539E-01
5	0.	0.	1.038715E+28	3.47601E-01
6	6.174E+27	7.68133E-02	1.656152E+28	3.47671E-01
7	0.	0.	1.656152E+28	3.47740E-01
8	6.358E+27	7.90928E-02	2.291911E+28	3.47810E-01
9	0.	0.	2.291911E+28	3.47879E-01
10	5.915E+27	7.35873E-02	2.883416E+28	3.47949E-01
11	0.	0.	2.883416E+28	3.48019E-01
12	5.048E+27	6.28020E-02	3.388228E+28	3.48088E-01
13	0.	0.	3.388228E+28	3.48158E-01
14	3.986E+27	4.95935E-02	3.786868E+28	3.48228E-01
15	0.	0.	3.786868E+28	3.48297E-01
16	2.929E+27	3.64367E-02	4.079751E+28	3.48367E-01
17	0.	0.	4.079751E+28	3.48437E-01
18	2.009E+27	2.49986E-02	4.280694E+28	3.48507E-01
19	0.	0.	4.280694E+28	3.48577E-01
20	1.291E+27	1.60576E-02	4.469767E+28	3.48647E-01
21	0.	0.	4.469767E+28	3.48716E-01
22	7.777E+26	9.67523E-03	4.487538E+28	3.48786E-01
23	0.	0.	4.487538E+28	3.48856E-01
24	4.402E+26	5.47615E-03	4.531550E+28	3.48926E-01
25	0.	0.	4.531550E+28	3.48996E-01
26	2.343E+26	2.91477E-03	4.556988E+28	3.49066E-01
27	0.	0.	4.556988E+28	3.49137E-01
28	1.170E+26	1.46625E-03	4.566723E+28	3.49207E-01
29	0.	0.	4.566723E+28	3.49277E-01
30	5.539E+25	6.89039E-04	4.572262E+28	3.49347E-01
31	0.	0.	4.572262E+28	3.49417E-01
32	2.463E+25	3.06412E-04	4.574725E+28	3.49487E-01
33	0.	0.	4.574725E+28	3.49558E-01
34	1.033E+25	1.28474E-04	4.575758E+28	3.49628E-01
35	0.	0.	4.575758E+28	3.49698E-01
36	4.084E+24	5.08092E-05	4.576166E+28	3.49769E-01
37	0.	0.	4.576166E+28	3.49839E-01
38	1.524E+24	1.89597E-05	4.576319E+28	3.49909E-01
39	0.	0.	4.576319E+28	3.49980E-01
40	5.367E+23	6.67738E-06	4.576372E+28	3.50050E-01
41	0.	0.	4.576372E+28	3.50121E-01
42	1.785E+23	2.22009E-06	4.576390E+28	3.50191E-01
43	0.	0.	4.576390E+28	3.50262E-01
44	5.602E+22	6.96971E-07	4.576396E+28	3.50332E-01
45	0.	0.	4.576396E+28	3.50403E-01
46	1.661E+22	2.06642E-07	4.576397E+28	3.50474E-01
47	0.	0.	4.576397E+28	3.50544E-01
48	4.652E+21	5.78700E-08	4.576398E+28	3.50615E-01
49	0.	0.	4.576398E+28	3.50686E-01
50	1.231E+21	1.53101E-08	4.576398E+28	3.50757E-01

TABLE E1.- (Cont'd)

J	Relative cross section $\Delta J = +2$	Normalized cross section	Running sum of normalized cross section	$\lambda, (\mu)$
51	0.	0.	4.576398E+28	3.50827E-01
52	3.076E+20	3.82690E-09	4.576398E+28	3.50898E-01
53	0.	0.	4.576398E+28	3.50969E-01
54	7.265E+19	9.03877E-10	4.576398E+28	3.51040E-01
55	0.	0.	4.576398E+28	3.51111E-01
56	1.622E+19	2.01747E-10	4.576398E+28	3.51181E-01
57	0.	0.	4.576398E+28	3.51252E-01
58	3.421E+18	4.25579E-11	4.576398E+28	3.51323E-01
59	0.	0.	4.576398E+28	3.51394E-01
60	6.821E+17	8.48520E-12	4.576398E+28	3.51465E-01
61	0.	0.	4.576398E+28	3.51536E-01
62	1.285E+17	1.59913E-12	4.576398E+28	3.51608E-01
63	0.	0.	4.576398E+28	3.51679E-01
64	2.290E+16	2.84890E-13	4.576398E+28	3.51750E-01
65	0.	0.	4.576398E+28	3.51821E-01
66	3.857E+15	4.79805E-14	4.576398E+28	3.51892E-01
67	0.	0.	4.576398E+28	3.51963E-01
68	6.141E+14	7.63960E-15	4.576398E+28	3.52035E-01
69	0.	0.	4.576398E+28	3.52106E-01
70	9.244E+13	1.15005E-15	4.576398E+28	3.52177E-01
71	0.	0.	4.576398E+28	3.52249E-01
72	1.316E+13	1.63691E-16	4.576398E+28	3.52320E-01
73	0.	0.	4.576398E+28	3.52391E-01
74	1.771E+12	2.20298E-17	4.576398E+28	3.52463E-01
75	0.	0.	4.576398E+28	3.52534E-01
76	2.253E+11	2.80345E-18	4.576398E+28	3.52606E-01
77	0.	0.	4.576398E+28	3.52677E-01
78	2.712E+10	3.37354E-19	4.576398E+28	3.52749E-01
79	0.	0.	4.576398E+28	3.52820E-01
80	3.080E+09	3.83888E-20	4.576398E+28	3.52892E-01
81	0.	0.	4.576398E+28	3.52964E-01
82	3.521E+08	4.13106E-21	4.576398E+28	3.53035E-01
83	0.	0.	4.576398E+28	3.53107E-01
84	3.379E+07	4.20407E-22	4.576398E+28	3.53179E-01
85	0.	0.	4.576398E+28	3.53250E-01
86	3.252E+06	4.04614E-23	4.576398E+28	3.53322E-01
87	0.	0.	4.576398E+28	3.53394E-01
88	2.960E+05	3.68287E-24	4.576398E+28	3.53466E-01
89	0.	0.	4.576398E+28	3.53538E-01
90	2.548E+04	3.17040E-25	4.576398E+28	3.53610E-01
91	0.	0.	4.576398E+28	3.53682E-01
92	2.075E+03	2.58128E-26	4.576398E+28	3.53754E-01
93	0.	0.	4.576398E+28	3.53826E-01
94	1.598E+02	1.98774E-27	4.576398E+28	3.53898E-01
95	0.	0.	4.576398E+28	3.53970E-01
96	1.104E+01	1.44774E-28	4.576398E+28	3.54042E-01
97	0.	0.	4.576398E+28	3.54114E-01
98	8.017E-01	9.97338E-30	4.576398E+28	3.54186E-01
99	0.	0.	4.576398E+28	3.54258E-01
00	5.224E-02	6.49657E-31	4.576398E+28	3.54330E-01

TABLE E2.- NORMALIZED BACKSCATTER CROSS SECTIONS FOR PURE ROTATIONAL RAMAN

FINE STRUCTURE OF O_2 . $\Delta J = -2$.

J	Relative cross section $\Delta J = -2$	Normalized cross section	Running sum of normalized cross section	$\lambda, (\mu)$
2	1.424E+27	1.77161E-02	1.424046E+27	3.47046E-01
3	0.	0.	1.424046E+27	3.46977E-01
4	3.330E+27	4.14220E-02	4.753654E+27	3.46908E-01
5	0.	0.	4.753654E+27	3.46838E-01
6	4.558E+27	5.60993E-02	9.311228E+27	3.46768E-01
7	0.	0.	9.311228E+27	3.46700E-01
8	5.079E+27	6.31890E-02	1.439046E+28	3.46631E-01
9	0.	0.	1.439046E+28	3.46562E-01
10	4.905E+27	6.17633E-02	1.935508E+28	3.46493E-01
11	0.	0.	1.935508E+28	3.46424E-01
12	4.385E+27	5.45487E-02	2.373978E+28	3.46355E-01
13	0.	0.	2.373978E+28	3.46286E-01
14	3.552E+27	4.41120E-02	2.729199E+28	3.46217E-01
15	0.	0.	2.729199E+28	3.46148E-01
16	2.663E+27	3.31271E-02	2.995479E+28	3.46079E-01
17	0.	0.	2.995479E+28	3.46010E-01
18	1.857E+27	2.31039E-02	3.181192E+28	3.45941E-01
19	0.	0.	3.181192E+28	3.45872E-01
20	1.209E+27	1.56470E-02	3.302142E+28	3.45804E-01
21	0.	0.	3.302142E+28	3.45735E-01
22	7.375E+26	9.17495E-03	3.375692E+28	3.45666E-01
23	0.	0.	3.375692E+28	3.45598E-01
24	6.218E+26	5.28773E-03	3.418974E+28	3.45529E-01
25	0.	0.	3.418974E+28	3.45460E-01
26	2.266E+26	2.81951E-03	3.440737E+28	3.45392E-01
27	0.	0.	3.440737E+28	3.45323E-01
28	1.145E+26	1.42459E-03	3.452186E+28	3.45254E-01
29	0.	0.	3.452186E+28	3.45186E-01
30	5.446E+25	6.77487E-04	3.457636E+28	3.45117E-01
31	0.	0.	3.457636E+28	3.45049E-01
32	2.439E+25	3.03674E-04	3.460073E+28	3.44980E-01
33	0.	0.	3.460073E+28	3.44912E-01
34	1.030E+25	1.28102E-04	3.461103E+28	3.44844E-01
35	0.	0.	3.461103E+28	3.44775E-01
36	4.098E+24	5.08863E-05	3.461513E+28	3.44707E-01
37	0.	0.	3.461513E+28	3.44639E-01
38	1.539E+24	1.91412E-05	3.461667E+28	3.44570E-01
39	0.	0.	3.461667E+28	3.44502E-01
40	5.450E+23	6.78027E-06	3.461721E+28	3.44434E-01
41	0.	0.	3.461721E+28	3.44366E-01
42	1.822E+23	2.26678E-06	3.461739E+28	3.44297E-01
43	0.	0.	3.461739E+28	3.44229E-01
44	5.751E+22	7.15421E-07	3.461745E+28	3.44161E-01
45	0.	0.	3.461745E+28	3.44093E-01
46	1.714E+22	2.13204E-07	3.461747E+28	3.44025E-01
47	0.	0.	3.461747E+28	3.43957E-01
48	4.823E+21	6.00050E-08	3.461747E+28	3.43889E-01
49	0.	0.	3.461747E+28	3.43821E-01
50	1.282E+21	1.59518E-08	3.461748E+28	3.43753E-01
51	0.	0.	3.461748E+28	3.43685E-01
52	3.220E+20	4.00611E-09	3.461748E+28	3.43617E-01

TABLE E2.- (Cont'd)

J	Relative cross section $\Delta J = -2$	Normalized cross section	Running sum of normalized cross section	$\lambda, (\mu)$
53	0.	0.	3.461748E+28	3.43549E-01
54	7.641E+19	9.50562E-10	3.461748E+28	3.43481E-01
55	0.	0.	3.461748E+28	3.43413E-01
56	1.713E+19	2.13123E-10	3.461748E+28	3.43346E-01
57	0.	0.	3.461748E+28	3.43278E-01
58	3.630E+18	4.51562E-11	3.461748E+28	3.43210E-01
59	0.	0.	3.461748E+28	3.43142E-01
60	7.268E+17	9.04229E-12	3.461748E+28	3.43075E-01
61	0.	0.	3.461748E+28	3.43007E-01
62	1.376E+17	1.71139E-12	3.461748E+28	3.42939E-01
63	0.	0.	3.461748E+28	3.42872E-01
64	2.461E+16	3.06168E-13	3.461748E+28	3.42804E-01
65	0.	0.	3.461748E+28	3.42736E-01
66	4.162E+15	5.17774E-14	3.461748E+28	3.42669E-01
67	0.	0.	3.461748E+28	3.42601E-01
68	6.654E+14	8.27782E-15	3.461748E+28	3.42534E-01
69	0.	0.	3.461748E+28	3.42466E-01
70	1.006E+14	1.25115E-15	3.461748E+28	3.42399E-01
71	0.	0.	3.461748E+28	3.42332E-01
72	1.437E+13	1.76791E-16	3.461748E+28	3.42264E-01
73	0.	0.	3.461748E+28	3.42197E-01
74	1.942E+12	2.41569E-17	3.461748E+28	3.42130E-01
75	0.	0.	3.461748E+28	3.42062E-01
76	2.481E+11	3.08614E-18	3.461748E+28	3.41995E-01
77	0.	0.	3.461748E+28	3.41928E-01
78	2.997E+10	3.72809E-19	3.461748E+28	3.41860E-01
79	0.	0.	3.461748E+28	3.41793E-01
80	3.423E+09	4.25861E-20	3.461748E+28	3.41726E-01
81	0.	0.	3.461748E+28	3.41659E-01
82	3.698E+08	4.60018E-21	3.461748E+28	3.41592E-01
83	0.	0.	3.461748E+28	3.41525E-01
84	3.777E+07	4.69916E-22	3.461748E+28	3.41458E-01
85	0.	0.	3.461748E+28	3.41391E-01
86	3.649E+06	4.53960E-23	3.461748E+28	3.41324E-01
87	0.	0.	3.461748E+28	3.41257E-01
88	3.334E+05	4.14741E-24	3.461748E+28	3.41190E-01
89	0.	0.	3.461748E+28	3.41123E-01
90	2.880E+04	3.58352E-25	3.461748E+28	3.41056E-01
91	0.	0.	3.461748E+28	3.40989E-01
92	2.354E+03	2.92838E-26	3.461748E+28	3.40922E-01
93	0.	0.	3.461748E+28	3.40855E-01
94	1.819E+02	2.26327E-27	3.461748E+28	3.40788E-01
95	0.	0.	3.461748E+28	3.40722E-01
96	1.330E+01	1.65443E-28	3.461748E+28	3.40655E-01
97	0.	0.	3.461748E+28	3.40588E-01
98	9.194E-01	1.14385E-29	3.461748E+28	3.40522E-01
99	0.	0.	3.461748E+28	3.40455E-01
100	6.013E-02	7.48014E-31	3.461748E+28	3.40388E-01
101	0.	0.	3.461748E+28	3.40322E-01
102	3.719E-03	4.62673E-32	3.461748E+28	3.40255E-01

TABLE E3.- NORMALIZED BACKSCATTER CROSS SECTIONS FOR PURE ROTATIONAL RAMAN

FINE STRUCTURE OF N_2 . $\Delta J = +2$

J	Relative cross section $\Delta J = +2$	Normalized cross section	Running sum of normalized cross section	$\lambda, (\mu)$
0	1.373E+27	1.71618E-02	1.373002E+27	3.47295E-01
1	1.211E+27	1.51347E-02	2.583228E+27	3.47391E-01
2	3.325E+27	4.15647E-02	5.909149E+27	3.47488E-01
3	2.032E+27	2.54021E-02	7.941405E+27	3.47585E-01
4	4.614E+27	5.76717E-02	1.255534E+28	3.47681E-01
5	2.480E+27	3.09944E-02	1.503500E+28	3.47778E-01
6	5.101E+27	6.37570E-02	2.013578E+28	3.47875E-01
7	2.526E+27	3.15762E-02	2.266198E+28	3.47972E-01
8	4.840E+27	6.04953E-02	2.750182E+28	3.48069E-01
9	2.248E+27	2.81031E-02	2.975010E+28	3.48166E-01
10	4.061E+27	5.07558E-02	3.381080E+28	3.48263E-01
11	1.785E+27	2.23087E-02	3.559557E+28	3.48360E-01
12	3.051E+27	3.82259E-02	3.865377E+28	3.48457E-01
13	1.278E+27	1.59744E-02	3.993178E+28	3.48554E-01
14	2.086E+27	2.60684E-02	4.201734E+28	3.48651E-01
15	8.312E+26	1.03890E-02	4.284850E+28	3.48749E-01
16	1.295E+27	1.61860E-02	4.414344E+28	3.48846E-01
17	4.931E+26	6.16406E-03	4.463658E+28	3.48943E-01
18	7.347E+26	9.18394E-03	4.537133E+28	3.49041E-01
19	2.678E+26	3.34684E-03	4.563969E+28	3.49138E-01
20	3.820E+26	4.77434E-03	4.602105E+28	3.49236E-01
21	1.333E+26	1.66663E-03	4.615439E+28	3.49334E-01
22	1.823E+26	2.22832E-03	4.633077E+28	3.49431E-01
23	6.100E+25	7.62416E-04	4.639760E+28	3.49529E-01
24	7.996E+25	9.99436E-04	4.646761E+28	3.49627E-01
25	2.567E+25	3.20803E-04	4.650328E+28	3.49725E-01
26	3.228E+25	4.03472E-04	4.653557E+28	3.49823E-01
27	9.943E+24	1.24281E-04	4.656550E+28	3.49921E-01
28	1.200E+25	1.50027E-04	4.655750E+28	3.50019E-01
29	3.549E+24	4.43035E-05	4.656105E+28	3.50117E-01
30	4.114E+24	5.14192E-05	4.656517E+28	3.50215E-01
31	1.168E+24	1.46608E-05	4.656634E+28	3.50313E-01
32	1.360E+24	1.62528E-05	4.656764E+28	3.50411E-01
33	3.546E+23	4.43286E-06	4.656799E+28	3.50509E-01
34	3.792E+23	4.74401E-06	4.656837E+28	3.50608E-01
35	9.957E+22	1.24263E-06	4.656847E+28	3.50706E-01
36	1.021E+23	1.27603E-06	4.656857E+28	3.50805E-01
37	2.570E+22	3.21274E-07	4.656860E+28	3.50903E-01
38	2.531E+22	3.17180E-07	4.656862E+28	3.51002E-01
39	6.140E+21	7.67448E-08	4.656866E+28	3.51100E-01
40	5.820E+21	7.28179E-08	4.656863E+28	3.51199E-01
41	1.355E+21	1.69343E-08	4.656864E+28	3.51298E-01
42	1.236E+21	1.54442E-08	4.656864E+28	3.51397E-01
43	2.762E+20	3.65243E-09	4.656864E+28	3.51495E-01
44	2.422E+20	3.02675E-09	4.656864E+28	3.51594E-01
45	5.204E+19	6.50942E-10	4.656864E+28	3.51693E-01
46	4.380E+19	5.48215E-10	4.656864E+28	3.51792E-01
47	9.062E+18	1.13264E-10	4.656864E+28	3.51891E-01
48	7.343E+18	9.17825E-11	4.656864E+28	3.51990E-01
49	1.459E+18	1.82323E-11	4.656864E+28	3.52089E-01
50	1.137E+18	1.42057E-11	4.656864E+28	3.52189E-01

TABLE E3.- (Cont'd)

J	Relative cross section $\Delta J = +2$	Normalized cross section	Running sum of normalized cross section	$\lambda, (\mu)$
51	2.171E+17	2.71339E-12	4.656864E+28	3.52288E-01
52	1.626E+17	2.03289E-12	4.656864E+28	3.52387E-01
53	2.987E+16	3.73385E-13	4.656864E+28	3.52487E-01
54	2.152E+16	2.69007E-13	4.656864E+28	3.52586E-01
55	3.801E+15	4.75139E-14	4.656864E+28	3.52686E-01
56	2.634E+15	3.29195E-14	4.656864E+28	3.52785E-01
57	4.474E+14	5.59170E-15	4.656864E+28	3.52885E-01
58	2.981E+14	3.72580E-15	4.656864E+28	3.52985E-01
59	4.869E+13	6.08645E-16	4.656864E+28	3.53084E-01
60	3.120E+13	3.90032E-16	4.656864E+28	3.53184E-01
61	4.903E+12	6.12793E-17	4.656864E+28	3.53284E-01
62	3.022E+12	3.77682E-17	4.656864E+28	3.53384E-01
63	4.566E+11	5.70719E-18	4.656864E+28	3.53484E-01
64	2.707E+11	3.38318E-18	4.656864E+28	3.53584E-01
65	3.934E+10	4.91720E-19	4.656864E+28	3.53684E-01
66	2.243E+10	2.80365E-19	4.656864E+28	3.53784E-01
67	3.136E+09	3.91945E-20	4.656864E+28	3.53884E-01
68	1.720E+09	2.14954E-20	4.656864E+28	3.53985E-01
69	2.512E+08	2.89045E-21	4.656864E+28	3.54085E-01
70	1.220E+08	1.52479E-21	4.656864E+28	3.54185E-01
71	1.578E+07	1.97225E-22	4.656864E+28	3.54286E-01
72	8.007E+06	1.00079E-22	4.656864E+28	3.54386E-01
73	9.902E+05	1.24518E-23	4.656864E+28	3.54487E-01
74	4.863E+05	6.07792E-24	4.656864E+28	3.54587E-01
75	5.820E+04	7.27433E-25	4.656864E+28	3.54688E-01
76	2.733E+04	3.41501E-25	4.656864E+28	3.54789E-01
77	3.140E+03	3.93243E-26	4.656864E+28	3.54889E-01
78	1.421E+03	1.77822E-26	4.656864E+28	3.54990E-01
79	1.574E+02	1.90722E-27	4.656864E+28	3.55091E-01
80	6.839E+01	8.54778E-28	4.656864E+28	3.55192E-01
81	7.286E+00	9.10710E-29	4.656864E+28	3.55293E-01
82	3.040E+00	3.80075E-29	4.656864E+28	3.55394E-01
83	3.122E-01	3.90173E-30	4.656864E+28	3.55495E-01
84	1.255E-01	1.56895E-30	4.656864E+28	3.55596E-01
85	1.238E-02	1.54701E-31	4.656864E+28	3.55698E-01
86	4.788E-03	5.98456E-32	4.656864E+28	3.55799E-01
87	4.542E-04	5.67681E-33	4.656864E+28	3.55900E-01
88	1.690E-04	2.11207E-33	4.656864E+28	3.56002E-01
89	1.542E-05	1.92796E-34	4.656864E+28	3.56103E-01
90	5.522E-06	6.90272E-35	4.656864E+28	3.56205E-01
91	4.848E-07	6.06014E-36	4.656864E+28	3.56306E-01
92	1.670E-07	2.08740E-36	4.656864E+28	3.56408E-01
93	1.411E-08	1.76307E-37	4.656864E+28	3.56509E-01
94	4.674E-09	5.84240E-38	4.656864E+28	3.56611E-01
95	3.798E-10	4.74751E-39	4.656864E+28	3.56713E-01
96	1.211E-10	1.51356E-39	4.656864E+28	3.56815E-01
97	9.466E-12	1.18326E-40	4.656864E+28	3.56917E-01
98	2.904E-12	3.62933E-41	4.656864E+28	3.57019E-01
99	2.184E-13	2.72973E-42	4.656864E+28	3.57121E-01
00	6.445E-14	8.05530E-43	4.656864E+28	3.57223E-01

TABLE E4.- NORMALIZED BACKSCATTER CROSS SECTIONS FOR PURE ROTATIONAL RAMAN

FINE STRUCTURE OF N₂. $\Delta J = -2$

J	Relative cross section $\Delta J = -2$	Normalized cross section	Running sum of normalized cross section	$\lambda, (\mu)$
2	1.300E+27	1.62541E-02	1.300387E+27	3.47005E-01
3	1.106E+27	1.33243E-02	2.406375E+27	3.40988E-01
4	2.929E+27	3.60152E-02	5.335724E+27	3.40813E-01
5	1.727E+27	2.15812E-02	7.062291E+27	3.40717E-01
6	3.780E+27	4.72537E-02	1.084275E+28	3.40620E-01
7	1.959E+27	2.44920E-02	1.280210E+28	3.40524E-01
8	3.887E+27	4.85888E-02	1.666096E+28	3.40428E-01
9	1.867E+27	2.32670E-02	1.850617E+28	3.40332E-01
10	3.631E+27	4.28811E-02	2.149768E+28	3.40236E-01
11	1.537E+27	1.92117E-02	2.351389E+28	3.40140E-01
12	2.677E+27	3.30630E-02	2.619096E+28	3.40044E-01
13	1.135E+27	1.41847E-02	2.732579E+28	3.40048E-01
14	1.875E+27	2.34408E-02	2.926110E+28	3.40053E-01
15	7.558E+26	9.44727E-03	2.995605E+28	3.40057E-01
16	1.190E+27	1.48685E-02	3.114684E+28	3.40062E-01
17	4.572E+26	5.71470E-03	3.160308E+28	3.40066E-01
18	6.870E+26	8.58008E-03	3.229064E+28	3.40070E-01
19	2.523E+26	3.15370E-03	3.254295E+28	3.40075E-01
20	3.625E+26	4.53159E-03	3.290549E+28	3.40080E-01
21	1.274E+26	1.59266E-03	3.303201E+28	3.40084E-01
22	1.753E+26	2.19114E-03	3.320821E+28	3.40089E-01
23	5.902E+25	7.37673E-04	3.326722E+28	3.40094E-01
24	1.781E+25	2.2540E-04	3.334503E+28	3.40098E-01
25	2.511E+25	3.13872E-04	3.337014E+28	3.40103E-01
26	3.175E+25	3.90811E-04	3.340180E+28	3.40108E-01
27	9.828E+24	1.22839E-04	3.341171E+28	3.40113E-01
28	1.192E+25	1.48997E-04	3.342363E+28	3.40118E-01
29	3.541E+24	4.42025E-05	3.342718E+28	3.40123E-01
30	4.123E+24	5.15311E-05	3.343130E+28	3.40128E-01
31	1.176E+24	1.46958E-05	3.343247E+28	3.40133E-01
32	1.314E+24	1.64271E-05	3.343537E+28	3.40138E-01
33	3.599E+23	4.49864E-06	3.343415E+28	3.40144E-01
34	3.864E+23	4.82948E-06	3.343453E+28	3.40149E-01
35	1.016E+23	1.27035E-06	3.343464E+28	3.40154E-01
36	1.048E+23	1.31006E-06	3.343474E+28	3.40159E-01
37	2.649E+22	3.31059E-07	3.343477E+28	3.40165E-01
38	2.624E+22	3.28023E-07	3.343479E+28	3.40171E-01
39	6.372E+21	7.96500E-08	3.343480E+28	3.40176E-01
40	6.067E+21	7.58376E-08	3.343481E+28	3.40182E-01
41	1.416E+21	1.76968E-08	3.343481E+28	3.40188E-01
42	1.296E+21	1.61939E-08	3.343481E+28	3.40193E-01
43	2.906E+20	3.63202E-09	3.343481E+28	3.40199E-01
44	2.556E+20	3.19459E-09	3.343481E+28	3.40205E-01
45	5.510E+19	6.88720E-10	3.343481E+28	3.40211E-01
46	4.659E+19	5.82320E-10	3.343481E+28	3.40217E-01
47	9.655E+18	1.20688E-10	3.343481E+28	3.40223E-01
48	7.848E+18	9.81009E-11	3.343481E+28	3.40229E-01
49	1.564E+18	1.95471E-11	3.343481E+28	3.40235E-01
50	1.222E+18	1.52263E-11	3.343481E+28	3.40241E-01
51	2.341E+17	2.92662E-12	3.343481E+28	3.40247E-01
52	1.759E+17	2.19916E-12	3.343481E+28	3.40253E-01

TABLE E4.- (Cont'd)

J	Relative cross section $\Delta J = -2$	Normalized cross section	Running sum of normalized cross section	$\lambda, (\mu)$
53	3.241E+16	4.05111E-13	3.343481E+28	3.42160E-01
54	2.342E+16	2.92715E-13	3.343481E+28	3.42036E-01
55	4.148E+15	5.18507E-14	3.343481E+28	3.41972E-01
56	2.882E+15	3.60271E-14	3.343481E+28	3.41879E-01
57	4.910E+14	6.13697E-15	3.343481E+28	3.41785E-01
58	3.281E+14	4.10066E-15	3.343481E+28	3.41692E-01
59	5.374E+13	6.71750E-16	3.343481E+28	3.41598E-01
60	3.454E+13	4.31676E-16	3.343481E+28	3.41505E-01
61	5.441E+12	6.80096E-17	3.343481E+28	3.41412E-01
62	3.363E+12	4.20315E-17	3.343481E+28	3.41318E-01
63	5.095E+11	6.36877E-18	3.343481E+28	3.41225E-01
64	3.024E+11	3.78561E-18	3.343481E+28	3.41132E-01
65	4.414E+10	5.51397E-19	3.343481E+28	3.41039E-01
66	2.523E+10	3.15407E-19	3.343481E+28	3.40946E-01
67	3.537E+09	4.42112E-20	3.343481E+28	3.40853E-01
68	1.945E+09	2.43112E-20	3.343481E+28	3.40760E-01
69	2.622E+08	3.27775E-21	3.343481E+28	3.40667E-01
70	1.387E+08	1.73366E-21	3.343481E+28	3.40574E-01
71	1.799E+07	2.24829E-22	3.343481E+28	3.40481E-01
72	9.151E+06	1.14384E-22	3.343481E+28	3.40389E-01
73	1.142E+06	1.42607E-23	3.343481E+28	3.40296E-01
74	5.587E+05	6.98285E-24	3.343481E+28	3.40203E-01
75	6.703E+04	8.37898E-25	3.343481E+28	3.40111E-01
76	3.156E+04	3.94441E-25	3.343481E+28	3.40018E-01
77	3.642E+03	4.55200E-26	3.343481E+28	3.39925E-01
78	1.649E+03	2.08173E-26	3.343481E+28	3.39833E-01
79	1.831E+02	2.28925E-27	3.343481E+28	3.39741E-01
80	7.978E+01	9.87232E-28	3.343481E+28	3.39649E-01
81	8.522E+00	1.06518E-28	3.343481E+28	3.39556E-01
82	3.571E+00	4.46305E-29	3.343481E+28	3.39464E-01
83	3.009E-01	4.58654E-30	3.343481E+28	3.39372E-01
84	1.479E-01	1.84896E-30	3.343481E+28	3.39280E-01
85	1.462E-02	1.82767E-31	3.343481E+28	3.39188E-01
86	5.671E-03	7.08794E-32	3.343481E+28	3.39096E-01
87	5.392E-04	6.74020E-33	3.343481E+28	3.39004E-01
88	2.012E-04	2.51466E-33	3.343481E+28	3.38912E-01
89	1.840E-05	2.30049E-34	3.343481E+28	3.38820E-01
90	6.606E-06	8.25083E-35	3.343481E+28	3.38728E-01
91	5.814E-07	7.26690E-36	3.343481E+28	3.38636E-01
92	2.007E-07	2.50923E-36	3.343481E+28	3.38544E-01
93	1.700E-08	2.12457E-37	3.343481E+28	3.38453E-01
94	5.646E-09	7.05768E-38	3.343481E+28	3.38361E-01
95	4.599E-10	5.74903E-39	3.343481E+28	3.38269E-01
96	1.470E-10	1.83734E-39	3.343481E+28	3.38178E-01
97	1.152E-11	1.43989E-40	3.343481E+28	3.38086E-01
98	3.542E-12	4.42722E-41	3.343481E+28	3.37995E-01
99	2.670E-13	3.33795E-42	3.343481E+28	3.37904E-01
100	7.900E-14	9.87402E-43	3.343481E+28	3.37812E-01
101	5.730E-15	7.16236E-44	3.343481E+28	3.37721E-01
102	1.631E-15	2.03839E-44	3.343481E+28	3.37630E-01

TABLE E5.- NORMALIZED BACKSCATTER CROSS SECTIONS FOR ROTATIONAL FINE STRUCTURE

ON THE $v = 0 \rightarrow 1$ RAMAN VIBRATIONAL TRANSITION OF O_2 . $\Delta J = +2$

J	Relative cross section $\Delta J = +2$	Normalized cross section	Running sum of normalized cross section	$\lambda, (\mu)$
0	1.186E+27	1.84157E-02	1.185977E+27	3.67070E-01
1	0.	0.	1.185977E+27	3.67146E-01
2	2.921E+27	4.53569E-02	4.106979E+27	3.67222E-01
3	0.	0.	4.106979E+27	3.67298E-01
4	4.212E+27	6.54601E-02	8.318770E+27	3.67373E-01
5	0.	0.	8.318770E+27	3.67447E-01
6	4.945E+27	7.67795E-02	1.326339E+28	3.67521E-01
7	0.	0.	1.326339E+28	3.67595E-01
8	5.091E+27	7.90577E-02	1.835474E+28	3.67669E-01
9	0.	0.	1.835474E+28	3.67742E-01
10	4.737E+27	7.35558E-02	2.309175E+28	3.67814E-01
11	0.	0.	2.309175E+28	3.67887E-01
12	4.043E+27	6.27772E-02	2.713463E+28	3.67959E-01
13	0.	0.	2.713463E+28	3.68030E-01
14	3.193E+27	4.95766E-02	3.032738E+28	3.68101E-01
15	0.	0.	3.032738E+28	3.68172E-01
16	2.346E+27	3.64269E-02	3.267328E+28	3.68242E-01
17	0.	0.	3.267328E+28	3.68312E-01
18	1.610E+27	2.49941E-02	3.428291E+28	3.68381E-01
19	0.	0.	3.428291E+28	3.68450E-01
20	1.034E+27	1.60505E-02	3.531696E+28	3.68519E-01
21	0.	0.	3.531696E+28	3.68587E-01
22	6.231E+26	9.67577E-03	3.594008E+28	3.68655E-01
23	0.	0.	3.594008E+28	3.68723E-01
24	3.527E+26	5.47726E-03	3.629282E+28	3.68790E-01
25	0.	0.	3.629282E+28	3.68850E-01
26	1.878E+26	2.91584E-03	3.648060E+28	3.68923E-01
27	0.	0.	3.648060E+28	3.68988E-01
28	9.409E+25	1.46105E-03	3.657469E+28	3.69054E-01
29	0.	0.	3.657469E+28	3.69119E-01
30	4.441E+25	6.89558E-04	3.661910E+28	3.69183E-01
31	0.	0.	3.661910E+28	3.69248E-01
32	1.975E+25	3.06710E-04	3.663885E+28	3.69311E-01
33	0.	0.	3.663885E+28	3.69375E-01
34	8.284E+24	1.28630E-04	3.664713E+28	3.69438E-01
35	0.	0.	3.664713E+28	3.69500E-01
36	3.277E+24	5.08841E-05	3.665041E+28	3.69562E-01
37	0.	0.	3.665041E+28	3.69624E-01
38	1.223E+24	1.89929E-05	3.665163E+28	3.69685E-01
39	0.	0.	3.665163E+28	3.69746E-01
40	4.309E+23	6.09106E-06	3.665207E+28	3.69807E-01
41	0.	0.	3.665207E+28	3.69867E-01
42	1.433E+23	2.22534E-06	3.665221E+28	3.69927E-01
43	0.	0.	3.665221E+28	3.69986E-01
44	4.501E+22	6.98854E-07	3.665225E+28	3.70045E-01
45	0.	0.	3.665225E+28	3.70103E-01
46	1.335E+22	2.07274E-07	3.665227E+28	3.70161E-01
47	0.	0.	3.665227E+28	3.70219E-01
48	3.740E+21	5.80685E-08	3.665227E+28	3.70276E-01
49	0.	0.	3.665227E+28	3.70333E-01
50	9.897E+20	1.53686E-08	3.665227E+28	3.70389E-01

TABLE E5.- (Cont'd)

J	Relative cross section $\Delta J = +2$	Normalized cross section	Running sum of normalized cross section	$\lambda, (\mu)$
51	0.	0.	3.665227E+28	3.70445E-01
52	2.475E+20	3.84311E-09	3.665227E+28	3.70501E-01
53	0.	0.	3.665227E+28	3.70556E-01
54	5.848E+19	9.08095E-10	3.665227E+28	3.70610E-01
55	0.	0.	3.665227E+28	3.70665E-01
56	1.306E+19	2.02780E-10	3.665227E+28	3.70719E-01
57	0.	0.	3.665227E+28	3.70772E-01
58	2.756E+18	4.27957E-11	3.665227E+28	3.70825E-01
59	0.	0.	3.665227E+28	3.70878E-01
60	5.498E+17	8.53676E-12	3.665227E+28	3.70930E-01
61	0.	0.	3.665227E+28	3.70982E-01
62	1.037E+17	1.60967E-12	3.665227E+28	3.71033E-01
63	0.	0.	3.665227E+28	3.71084E-01
64	1.848E+16	2.86917E-13	3.665227E+28	3.71134E-01
65	0.	0.	3.665227E+28	3.71184E-01
66	3.114E+15	4.83481E-14	3.665227E+28	3.71234E-01
67	0.	0.	3.665227E+28	3.71283E-01
68	4.960E+14	7.70247E-15	3.665227E+28	3.71332E-01
69	0.	0.	3.665227E+28	3.71381E-01
70	7.472E+13	1.16019E-15	3.665227E+28	3.71428E-01
71	0.	0.	3.665227E+28	3.71476E-01
72	1.064E+13	1.65234E-16	3.665227E+28	3.71523E-01
73	0.	0.	3.665227E+28	3.71570E-01
74	1.433E+12	2.22512E-17	3.665227E+28	3.71616E-01
75	0.	0.	3.665227E+28	3.71662E-01
76	1.825E+11	2.83344E-18	3.665227E+28	3.71707E-01
77	0.	0.	3.665227E+28	3.71752E-01
78	2.197E+10	3.41187E-19	3.665227E+28	3.71797E-01
79	0.	0.	3.665227E+28	3.71841E-01
80	2.502E+09	3.88513E-20	3.665227E+28	3.71885E-01
81	0.	0.	3.665227E+28	3.71928E-01
82	2.694E+08	4.18375E-21	3.665227E+28	3.71971E-01
83	0.	0.	3.665227E+28	3.72013E-01
84	2.744E+07	4.26076E-22	3.665227E+28	3.72055E-01
85	0.	0.	3.665227E+28	3.72097E-01
86	2.643E+06	4.10371E-23	3.665227E+28	3.72138E-01
87	0.	0.	3.665227E+28	3.72179E-01
88	2.407E+05	3.73808E-24	3.665227E+28	3.72219E-01
89	0.	0.	3.665227E+28	3.72259E-01
90	2.074E+04	3.22043E-25	3.665227E+28	3.72298E-01
91	0.	0.	3.665227E+28	3.72337E-01
92	1.696E+03	2.62410E-26	3.665227E+28	3.72376E-01
93	0.	0.	3.665227E+28	3.72414E-01
94	1.302E+02	2.02235E-27	3.665227E+28	3.72452E-01
95	0.	0.	3.665227E+28	3.72489E-01
96	9.494E+00	1.47418E-28	3.665227E+28	3.72526E-01
97	0.	0.	3.665227E+28	3.72563E-01
98	6.546E-01	1.01641E-29	3.665227E+28	3.72599E-01
99	0.	0.	3.665227E+28	3.72634E-01
00	4.269E-02	6.62864E-31	3.665227E+28	3.72669E-01

TABLE E6.- NORMALIZED BACKSCATTER CROSS SECTIONS FOR ROTATIONAL FINE STRUCTURE

ON THE $v = 0 \rightarrow 1$ RAMAN VIBRATIONAL TRANSITION OF O_2 . $\Delta J = -2$

J	Relative cross section $\Delta J = -2$	Normalized cross section	Running sum of normalized cross section	$\lambda, (\mu)$
2	1.141E+27	1.77126E-02	1.140698E+27	3.66839E-01
3	0.	0.	1.140698E+27	3.66761E-01
4	2.667E+27	4.14188E-02	3.808081E+27	3.66685E-01
5	0.	0.	3.808081E+27	3.66604E-01
6	3.652E+27	5.67011E-02	7.459650E+27	3.66525E-01
7	0.	0.	7.459650E+27	3.66446E-01
8	4.070E+27	6.32000E-02	1.152975E+28	3.66366E-01
9	0.	0.	1.152975E+28	3.66286E-01
10	3.979E+27	6.17838E-02	1.550865E+28	3.66206E-01
11	0.	0.	1.550865E+28	3.66125E-01
12	3.515E+27	5.45766E-02	1.902340E+28	3.66043E-01
13	0.	0.	1.902340E+28	3.65962E-01
14	2.848E+27	4.42233E-02	2.187140E+28	3.65880E-01
15	0.	0.	2.187140E+28	3.65797E-01
16	2.135E+27	3.31577E-02	2.406676E+28	3.65714E-01
17	0.	0.	2.406676E+28	3.65631E-01
18	1.490E+27	2.31306E-02	2.549632E+28	3.65547E-01
19	0.	0.	2.549632E+28	3.65463E-01
20	9.704E+26	1.50682E-02	2.646678E+28	3.65379E-01
21	0.	0.	2.646678E+28	3.65294E-01
22	5.919E+26	9.19037E-03	2.705805E+28	3.65209E-01
23	0.	0.	2.705805E+28	3.65124E-01
24	3.386E+26	5.25806E-03	2.739727E+28	3.65038E-01
25	0.	0.	2.739727E+28	3.64951E-01
26	1.820E+26	2.82593E-03	2.757920E+28	3.64865E-01
27	0.	0.	2.757920E+28	3.64778E-01
28	0.198E+25	1.42830E-03	2.767124E+28	3.64690E-01
29	0.	0.	2.767124E+28	3.64602E-01
30	4.376E+25	6.79462E-04	2.771500E+28	3.64514E-01
31	0.	0.	2.771500E+28	3.64426E-01
32	1.961E+25	3.04407E-04	2.773461E+28	3.64337E-01
33	0.	0.	2.773461E+28	3.64247E-01
34	0.280E+24	1.28574E-04	2.774209E+28	3.64158E-01
35	0.	0.	2.774209E+28	3.64068E-01
36	3.297E+24	5.11946E-05	2.774618E+28	3.63977E-01
37	0.	0.	2.774618E+28	3.63886E-01
38	1.238E+24	1.92274E-05	2.774742E+28	3.63795E-01
39	0.	0.	2.774742E+28	3.63704E-01
40	4.388E+23	6.81375E-06	2.774786E+28	3.63612E-01
41	0.	0.	2.774786E+28	3.63519E-01
42	1.468E+23	2.27900E-06	2.774801E+28	3.63427E-01
43	0.	0.	2.774801E+28	3.63334E-01
44	4.634E+22	7.19615E-07	2.774805E+28	3.63240E-01
45	0.	0.	2.774805E+28	3.63147E-01
46	1.382E+22	2.14558E-07	2.774807E+28	3.63052E-01
47	0.	0.	2.774807E+28	3.62958E-01
48	3.891E+21	6.04166E-08	2.774807E+28	3.62863E-01
49	0.	0.	2.774807E+28	3.62768E-01
50	1.035E+21	1.60696E-08	2.774807E+28	3.62672E-01
51	0.	0.	2.774807E+28	3.62576E-01
52	2.600E+20	4.03788E-09	2.774807E+28	3.62480E-01

TABLE E6.- (Cont'd)

J	Relative cross section $\Delta J = -2$	Normalized cross section	Running sum of normalized cross section	$\lambda, (\mu)$
53	0.	0.	2.774807E+28	3.62383E-01
54	6.174E+19	9.58635E-10	2.774807E+28	3.62286E-01
55	0.	0.	2.774807E+28	3.62189E-01
56	1.385E+19	2.15057E-10	2.774807E+28	3.62091E-01
57	0.	0.	2.774807E+28	3.61993E-01
58	2.936E+18	4.55930E-11	2.774807E+28	3.61894E-01
59	0.	0.	2.774807E+28	3.61795E-01
60	5.883E+17	9.13533E-12	2.774807E+28	3.61696E-01
61	0.	0.	2.774807E+28	3.61597E-01
62	1.114E+17	1.73009E-12	2.774807E+28	3.61497E-01
63	0.	0.	2.774807E+28	3.61398E-01
64	1.995E+16	3.09713E-13	2.774807E+28	3.61298E-01
65	0.	0.	2.774807E+28	3.61195E-01
66	3.375E+15	5.24118E-14	2.774807E+28	3.61093E-01
67	0.	0.	2.774807E+28	3.60992E-01
68	5.400E+14	8.38496E-15	2.774807E+28	3.60890E-01
69	0.	0.	2.774807E+28	3.60787E-01
70	8.167E+13	1.26823E-15	2.774807E+28	3.60684E-01
71	0.	0.	2.774807E+28	3.60581E-01
72	1.168E+13	1.81362E-16	2.774807E+28	3.60478E-01
73	0.	0.	2.774807E+28	3.60374E-01
74	1.579E+12	2.45223E-17	2.774807E+28	3.60270E-01
75	0.	0.	2.774807E+28	3.60165E-01
76	2.019E+11	3.13518E-18	2.774807E+28	3.60060E-01
77	0.	0.	2.774807E+28	3.59955E-01
78	2.441E+10	3.79024E-19	2.774807E+28	3.59849E-01
79	0.	0.	2.774807E+28	3.59743E-01
80	2.790E+09	4.33301E-20	2.774807E+28	3.59637E-01
81	0.	0.	2.774807E+28	3.59531E-01
82	3.017E+08	4.66431E-21	2.774807E+28	3.59424E-01
83	0.	0.	2.774807E+28	3.59316E-01
84	3.084E+07	4.78904E-22	2.774807E+28	3.59209E-01
85	0.	0.	2.774807E+28	3.59101E-01
86	2.982E+06	4.63031E-23	2.774807E+28	3.58992E-01
87	0.	0.	2.774807E+28	3.58884E-01
88	2.727E+05	4.23391E-24	2.774807E+28	3.58775E-01
89	0.	0.	2.774807E+28	3.58665E-01
90	2.358E+04	3.60146E-25	2.774807E+28	3.58556E-01
91	0.	0.	2.774807E+28	3.58446E-01
92	1.929E+03	2.99473E-26	2.774807E+28	3.58335E-01
93	0.	0.	2.774807E+28	3.58224E-01
94	1.492E+02	2.31666E-27	2.774807E+28	3.58113E-01
95	0.	0.	2.774807E+28	3.58002E-01
96	1.092E+01	1.69502E-28	2.774807E+28	3.57890E-01
97	0.	0.	2.774807E+28	3.57778E-01
98	7.554E-01	1.17302E-29	2.774807E+28	3.57666E-01
99	0.	0.	2.774807E+28	3.57553E-01
100	4.945E-02	7.67825E-31	2.774807E+28	3.57440E-01
101	0.	0.	2.774807E+28	3.57327E-01
102	3.062E-03	4.75391E-32	2.774807E+28	3.57213E-01

TABLE E7.- NORMALIZED BACKSCATTER CROSS SECTIONS FOR ROTATIONAL FINE STRUCTURE

ON THE $v = 0 \rightarrow 1$ RAMAN VIBRATIONAL TRANSITION OF N_2 . $\Delta J = +2$

J	Relative cross section $\Delta J = +2$	Normalized cross section	Running sum of normalized cross section	$\lambda, (\mu)$
0	9.796E+26	1.71574E-02	9.795945E+26	3.77880E-01
1	8.638E+26	1.51296E-02	1.843412E+27	3.77993E-01
2	2.372E+27	4.15475E-02	4.215555E+27	3.78105E-01
3	1.450E+27	2.53898E-02	5.665180E+27	3.78217E-01
4	3.291E+27	5.76401E-02	8.956125E+27	3.78328E-01
5	1.769E+27	3.09756E-02	1.072467E+28	3.78439E-01
6	3.638E+27	6.37150E-02	1.436246E+28	3.78550E-01
7	1.802E+27	3.15539E-02	1.616402E+28	3.78659E-01
8	3.451E+27	6.04501E-02	1.961540E+28	3.78769E-01
9	1.603E+27	2.80811E-02	2.121868E+28	3.78878E-01
10	2.896E+27	5.07144E-02	2.411421E+28	3.78986E-01
11	1.273E+27	2.22900E-02	2.538885E+28	3.79094E-01
12	2.181E+27	3.81931E-02	2.756747E+28	3.79202E-01
13	9.113E+26	1.59005E-02	2.847873E+28	3.79309E-01
14	1.487E+27	2.60455E-02	2.996579E+28	3.79415E-01
15	5.920E+26	1.03798E-02	3.055843E+28	3.79521E-01
16	9.233E+26	1.61718E-02	3.144175E+28	3.79627E-01
17	3.510E+26	6.15871E-03	3.183338E+28	3.79732E-01
18	5.238E+26	9.17611E-03	3.235729E+28	3.79837E-01
19	1.900E+26	3.34405E-03	3.254822E+28	3.79941E-01
20	2.724E+26	4.77049E-03	3.282059E+28	3.80045E-01
21	9.508E+25	1.60534E-03	3.291567E+28	3.80148E-01
22	1.360E+26	2.27664E-03	3.304565E+28	3.80251E-01
23	4.350E+25	7.61889E-04	3.308915E+28	3.80353E-01
24	5.703E+25	9.98793E-04	3.314618E+28	3.80454E-01
25	1.831E+25	3.20615E-04	3.316449E+28	3.80556E-01
26	2.362E+25	1.03266E-04	3.318751E+28	3.80658E-01
27	7.093E+24	1.24224E-04	3.319460E+28	3.80757E-01
28	8.562E+24	1.49969E-04	3.320310E+28	3.80857E-01
29	2.532E+24	4.43497E-05	3.320570E+28	3.80956E-01
30	2.935E+24	5.14075E-05	3.320830E+28	3.81055E-01
31	8.335E+23	1.45988E-05	3.320940E+28	3.81153E-01
32	9.279E+23	1.62521E-05	3.321039E+28	3.81251E-01
33	2.531E+23	4.43312E-06	3.321065E+28	3.81348E-01
34	2.707E+23	4.74085E-06	3.321092E+28	3.81445E-01
35	7.093E+22	1.24237E-06	3.321099E+28	3.81541E-01
36	7.288E+22	1.27654E-06	3.321106E+28	3.81637E-01
37	1.855E+22	3.21441E-07	3.321108E+28	3.81732E-01
38	1.812E+22	3.17386E-07	3.321110E+28	3.81827E-01
39	4.385E+21	7.66051E-08	3.321110E+28	3.81922E-01
40	4.101E+21	7.28854E-08	3.321113E+28	3.82015E-01
41	9.679E+20	1.69525E-08	3.321113E+28	3.82109E-01
42	8.829E+20	1.54631E-08	3.321113E+28	3.82202E-01
43	1.974E+20	3.45721E-09	3.321113E+28	3.82294E-01
44	1.731E+20	3.03144E-09	3.321113E+28	3.82386E-01
45	5.720E+19	6.51562E-10	3.321113E+28	3.82477E-01
46	3.150E+19	5.49250E-10	3.321113E+28	3.82568E-01
47	6.480E+18	1.13500E-10	3.321113E+28	3.82658E-01
48	5.252E+18	9.19907E-11	3.321113E+28	3.82748E-01
49	1.000E+18	1.82772E-11	3.321113E+28	3.82837E-01
50	8.130E+17	1.42435E-11	3.321113E+28	3.82927E-01

TABLE E7.- (Cont'd)

J	Relative cross section $\Delta J = +2$	Normalized cross section	Running sum of normalized cross section	$\lambda, (\mu)$
51	1.554E+17	2.72117E-12	3.321111F+28	3.83014E-01
52	1.164E+17	2.03916E-12	3.321111F+28	3.83102E-01
53	2.139E+16	3.74617E-13	3.321111F+28	3.83190F-01
54	1.541E+16	2.69954E-13	3.321111F+28	3.83276F-01
55	2.723E+15	4.76923E-14	3.321111F+28	3.83363F-01
56	1.887E+15	3.30507E-14	3.321111F+28	3.83448F-01
57	3.206E+14	5.61535E-15	3.321111F+28	3.83534F-01
58	2.137E+14	3.74248E-15	3.321111F+28	3.83618F-01
59	3.491E+13	6.11523E-16	3.321111F+28	3.83703F-01
60	2.238E+13	3.91978E-16	3.321111F+28	3.83786F-01
61	3.517E+12	6.16012E-17	3.321111F+28	3.83869F-01
62	2.168E+12	3.79768E-17	3.321111F+28	3.83952F-01
63	3.277E+11	5.74030E-18	3.321111F+28	3.84034F-01
64	1.943E+11	3.40377E-18	3.321111F+28	3.84116F-01
65	2.825E+10	4.94854E-19	3.321111F+28	3.84197E-01
66	1.611E+10	2.82235E-19	3.321111F+28	3.84278F-01
67	2.253E+09	3.94677E-20	3.321111F+28	3.84358F-01
68	1.236E+09	2.16518E-20	3.321111F+28	3.84437F-01
69	1.663E+08	2.91239E-21	3.321111F+28	3.84516F-01
70	8.775E+07	1.53685E-21	3.321111F+28	3.84595F-01
71	1.135E+07	1.98849E-22	3.321111F+28	3.84673F-01
72	5.763E+06	1.00936E-22	3.321111F+28	3.84750F-01
73	7.173E+05	1.25627E-23	3.321111F+28	3.84827F-01
74	3.502E+05	6.13412E-24	3.321111F+28	3.84904E-01
75	4.193E+04	7.34414E-25	3.321111F+28	3.84980F-01
76	1.970E+04	3.44960E-25	3.321111F+28	3.85055E-01
77	2.268E+03	3.97300E-26	3.321111F+28	3.85130E-01
78	1.025E+03	1.79519E-26	3.321111F+28	3.85204E-01
79	1.136E+02	1.98897E-27	3.321111F+28	3.85278F-01
80	4.936E+01	8.64554E-28	3.321111F+28	3.85351F-01
81	5.261E+00	9.21478E-29	3.321111F+28	3.85424F-01
82	2.206E+00	3.85325E-29	3.321111F+28	3.85496E-01
83	2.256E-01	3.95095E-30	3.321111F+28	3.85568F-01
84	9.075E-02	1.58938E-30	3.321111F+28	3.85639E-01
85	8.951E-03	1.56779E-31	3.321111F+28	3.85710E-01
86	3.464E-03	6.06744E-32	3.321111F+28	3.85780E-01
87	3.287E-04	5.75784E-33	3.321111F+28	3.85849E-01
88	1.224E-04	2.14374E-33	3.321111F+28	3.85918F-01
89	1.117E-05	1.95714E-34	3.321111F+28	3.85987E-01
90	4.002E-06	7.01027E-35	3.321111F+28	3.86055E-01
91	3.515E-07	6.15728E-36	3.321111F+28	3.86122F-01
92	1.211E-07	2.12181E-36	3.321111F+28	3.86189E-01
93	1.024E-08	1.79294E-37	3.321111F+28	3.86256E-01
94	3.394E-09	5.94419E-38	3.321111F+28	3.86321E-01
95	2.759E-10	4.83242E-39	3.321111F+28	3.86387E-01
96	8.800E-11	1.54136E-39	3.321111F+28	3.86452F-01
97	6.883E-12	1.20557E-40	3.321111F+28	3.86516E-01
98	2.112E-12	3.69954E-41	3.321111F+28	3.86579E-01
99	1.589E-13	2.78390E-42	3.321111F+28	3.86643E-01
00	4.693E-14	8.21923E-43	3.321111F+28	3.86705E-01

TABLE E8.- NORMALIZED BACKSCATTER CROSS SECTIONS FOR ROTATIONAL FINE STRUCTURE

ON THE $v = 0 \rightarrow 1$ RAMAN VIBRATIONAL TRANSITION OF N_2 . $\Delta J = -2$

J	Relative cross section $\Delta J = -2$	Normalized cross section	Running sum of normalized cross section	$\lambda, (\mu)$
2	9.280E+26	1.62544E-02	9.280430E+26	3.77539E-01
3	7.894E+26	1.38266E-02	1.717433E+27	3.77425E-01
4	2.091E+27	3.60237E-02	3.808454E+27	3.77310E-01
5	1.233E+27	2.15886E-02	5.041050E+27	3.77194E-01
6	2.699E+27	4.72757E-02	7.740241E+27	3.77078E-01
7	1.393E+27	2.45064E-02	9.139430E+27	3.76962E-01
8	2.776E+27	4.86239E-02	1.191560E+28	3.76845E-01
9	1.320E+27	2.32279E-02	1.324179E+28	3.76728E-01
10	2.451E+27	4.29201E-02	1.569253E+28	3.76610E-01
11	1.098E+27	1.92333E-02	1.679067E+28	3.76492E-01
12	1.913E+27	3.35066E-02	1.670372E+28	3.76373E-01
13	9.111E+26	1.42055E-02	1.951478E+28	3.76254E-01
14	1.341E+27	2.34790E-02	2.085551E+28	3.76134E-01
15	5.404E+26	0.40420E-03	2.135567E+28	3.76014E-01
16	6.506E+26	1.48970E-02	2.224623E+28	3.75894E-01
17	3.270E+26	5.72702E-03	2.257324E+28	3.75773E-01
18	4.914E+26	8.50670E-03	2.306484E+28	3.75651E-01
19	1.805E+26	3.16170E-03	2.324515E+28	3.75530E-01
20	2.594E+26	4.54398E-03	2.350459E+28	3.75407E-01
21	9.120E+25	1.59734E-03	2.359579E+28	3.75284E-01
22	1.255E+26	2.19803E-03	2.372129E+28	3.75161E-01
23	4.226E+25	2.40152E-04	2.370355E+28	3.75038E-01
24	5.573E+25	9.76023E-04	2.361927E+28	3.74914E-01
25	1.799E+25	3.15067E-04	2.363726E+28	3.74789E-01
26	2.775E+25	3.98413E-04	2.366001E+28	3.74664E-01
27	7.043E+24	1.23364E-04	2.366705E+28	3.74539E-01
28	8.545E+24	1.49670E-04	2.367560E+28	3.74413E-01
29	2.539E+24	4.44734E-05	2.367614E+28	3.74286E-01
30	2.957E+24	5.17897E-05	2.368100E+28	3.74160E-01
31	8.435E+23	1.47734E-05	2.368194E+28	3.74033E-01
32	9.431E+23	2.65182E-05	2.368280E+28	3.73905E-01
33	2.583E+23	4.52479E-06	2.368314E+28	3.73777E-01
34	2.774E+23	4.85888E-06	2.368341E+28	3.73648E-01
35	7.299E+22	1.27844E-06	2.368349E+28	3.73520E-01
36	7.530E+22	1.31878E-06	2.368356E+28	3.73390E-01
37	1.903E+22	3.33360E-07	2.368358E+28	3.73260E-01
38	1.886E+22	3.30400E-07	2.368360E+28	3.73130E-01
39	4.582E+21	8.02513E-08	2.368361E+28	3.73000E-01
40	4.364E+21	7.04335E-08	2.368361E+28	3.72868E-01
41	1.019E+21	1.78415E-08	2.368361E+28	3.72737E-01
42	9.324E+20	1.63315E-08	2.368361E+28	3.72605E-01
43	2.092E+20	3.60405E-09	2.368361E+28	3.72473E-01
44	1.841E+20	3.22382E-09	2.368361E+28	3.72340E-01
45	3.970E+19	6.95253E-10	2.368361E+28	3.72207E-01
46	3.357E+19	5.88043E-10	2.368361E+28	3.72073E-01
47	6.961E+18	1.21910E-10	2.368361E+28	3.71939E-01
48	5.660E+18	9.91337E-11	2.368361E+28	3.71805E-01
49	1.128E+18	1.97599E-11	2.368361E+28	3.71670E-01
50	8.820E+17	1.54481E-11	2.368361E+28	3.71534E-01
51	1.690E+17	2.96063E-12	2.368361E+28	3.71399E-01
52	1.271E+17	2.22554E-12	2.368361E+28	3.71263E-01

TABLE E8.- (Cont'd)

J	Relative cross section $\Delta J = -2$	Normalized cross section	Running sum of normalized cross section	$\lambda, (\mu)$
53	2.342E+16	4.10124E-13	2.388361E+28	3.71126E-01
54	1.693E+16	2.96450E-13	2.388361E+28	3.70989E-01
55	2.999E+15	5.25327E-14	2.388361E+28	3.70852E-01
56	2.085E+15	3.65153E-14	2.388361E+28	3.70714E-01
57	3.553E+14	6.22260E-15	2.388361E+28	3.70576E-01
58	2.375E+14	4.15956E-15	2.388361E+28	3.70437E-01
59	3.892E+13	6.81685E-16	2.388361E+28	3.70298E-01
60	2.502E+13	4.38235E-16	2.388361E+28	3.70159E-01
61	3.944E+12	6.90718E-17	2.388361E+28	3.70019E-01
62	2.438E+12	4.27060E-17	2.388361E+28	3.69879E-01
63	3.696E+11	6.47376E-18	2.388361E+28	3.69738E-01
64	2.198E+11	3.84969E-18	2.388361E+28	3.69597E-01
65	3.205E+10	5.61282E-19	2.388361E+28	3.69456E-01
66	1.833E+10	3.21029E-19	2.388361E+28	3.69314E-01
67	2.570E+09	4.50195E-20	2.388361E+28	3.69171E-01
68	1.414E+09	2.47669E-20	2.388361E+28	3.69029E-01
69	1.907E+08	3.34073E-21	2.388361E+28	3.68886E-01
70	1.009E+08	1.76780E-21	2.388361E+28	3.68742E-01
71	1.310E+07	2.20364E-22	2.388361E+28	3.68598E-01
72	6.666E+06	1.16747E-22	2.388361E+28	3.68454E-01
73	8.319E+05	1.45705E-23	2.388361E+28	3.68310E-01
74	4.073E+05	7.13398E-24	2.388361E+28	3.68165E-01
75	4.890E+04	8.50454E-25	2.388361E+28	3.68019E-01
76	2.303E+04	4.03377E-25	2.388361E+28	3.67873E-01
77	2.660E+03	4.65838E-26	2.388361E+28	3.67727E-01
78	1.205E+03	2.11056E-26	2.388361E+28	3.67580E-01
79	1.339E+02	2.34467E-27	2.388361E+28	3.67434E-01
80	5.835E+01	1.02190E-27	2.388361E+28	3.67286E-01
81	6.235E+00	1.09210E-28	2.388361E+28	3.67138E-01
82	2.614E+00	4.57889E-29	2.388361E+28	3.66990E-01
83	2.688E-01	4.70745E-30	2.388361E+28	3.66842E-01
84	1.084E-01	1.89872E-30	2.388361E+28	3.66693E-01
85	1.072E-02	1.87788E-31	2.388361E+28	3.66544E-01
86	4.160E-03	7.28665E-32	2.388361E+28	3.66394E-01
87	3.958E-04	6.93300E-33	2.388361E+28	3.66244E-01
88	1.478E-04	2.58803E-33	2.388361E+28	3.66093E-01
89	1.353E-05	2.36895E-34	2.388361E+28	3.65943E-01
90	4.857E-06	8.50743E-35	2.388361E+28	3.65791E-01
91	4.277E-07	7.49170E-36	2.388361E+28	3.65640E-01
92	1.478E-07	2.58835E-36	2.388361E+28	3.65488E-01
93	1.252E-08	2.19284E-37	2.388361E+28	3.65336E-01
94	4.161E-09	7.28870E-38	2.388361E+28	3.65183E-01
95	3.392E-10	5.94079E-39	2.388361E+28	3.65030E-01
96	1.085E-10	1.89976E-39	2.388361E+28	3.64877E-01
97	8.505E-12	1.48970E-40	2.388361E+28	3.64723E-01
98	2.617E-12	4.58318E-41	2.388361E+28	3.64569E-01
99	1.974E-13	5.45766E-42	2.388361E+28	3.64414E-01
100	5.843E-14	1.02345E-42	2.388361E+28	3.64259E-01
101	4.241E-15	7.42846E-44	2.388361E+28	3.64104E-01
102	1.208E-15	2.11545E-44	2.388361E+28	3.63948E-01

TABLE E9.- DIFFERENTIAL BACKSCATTER CROSS SECTIONS FOR PURE ROTATIONAL RAMAN

FINE STRUCTURE OF O₂. $\Delta J = +2$

J	$\lambda, (\mu)$	Normalized cross section $\Delta J = +2$	$\frac{d\sigma}{d\Omega}(\omega)_I$	$\frac{d\sigma}{d\Omega}(\omega)_{II}$
0	3.47254E-01	1.84216E-02	9.48712E-31	1.89742E-30
1	3.47323E-01	0.	0.	0.
2	3.47393E-01	4.53741E-02	2.33677E-30	4.67353E-30
3	3.47462E-01	0.	0.	0.
4	3.47532E-01	6.54275E-02	3.36952E-30	6.73904E-30
5	3.47601E-01	0.	0.	0.
6	3.47671E-01	7.68133E-02	3.95589E-30	7.91177E-30
7	3.47740E-01	0.	0.	0.
8	3.47810E-01	7.90928E-02	4.07328E-30	8.14656E-30
9	3.47879E-01	0.	0.	0.
10	3.47949E-01	7.35873E-02	3.78974E-30	7.57949E-30
11	3.48019E-01	0.	0.	0.
12	3.48088E-01	6.28020E-02	3.23430E-30	6.46661E-30
13	3.48158E-01	0.	0.	0.
14	3.48228E-01	4.95935E-02	2.55407E-30	5.10814E-30
15	3.48297E-01	0.	0.	0.
16	3.48367E-01	3.64367E-02	1.87645E-30	3.75298E-30
17	3.48437E-01	0.	0.	0.
18	3.48507E-01	2.49986E-02	1.28743E-30	2.57486E-30
19	3.48577E-01	0.	0.	0.
20	3.48647E-01	1.60576E-02	8.26968E-31	1.65394E-30
21	3.48716E-01	0.	0.	0.
22	3.48786E-01	9.67523E-03	4.98274E-31	9.96549E-31
23	3.48856E-01	0.	0.	0.
24	3.48926E-01	5.47615E-03	2.82022E-31	5.64044E-31
25	3.48996E-01	0.	0.	0.
26	3.49066E-01	2.91477E-03	1.50111E-31	3.00221E-31
27	3.49137E-01	0.	0.	0.
28	3.49207E-01	1.46025E-03	7.52027E-32	1.50405E-31
29	3.49277E-01	0.	0.	0.
30	3.49347E-01	6.89039E-04	3.54855E-32	7.09710E-32
31	3.49417E-01	0.	0.	0.
32	3.49487E-01	3.06412E-04	1.57802E-32	3.15604E-32
33	3.49558E-01	0.	0.	0.
34	3.49628E-01	1.28474E-04	6.61640E-33	1.32328E-32
35	3.49698E-01	0.	0.	0.
36	3.49769E-01	5.08092E-05	2.61667E-33	5.23334E-33
37	3.49839E-01	0.	0.	0.
38	3.49909E-01	1.89597E-05	9.76425E-34	1.95285E-33
39	3.49980E-01	0.	0.	0.
40	3.50050E-01	6.67738E-06	3.43885E-34	6.87770E-34
41	3.50121E-01	0.	0.	0.
42	3.50191E-01	2.22099E-06	1.14334E-34	2.28669E-34
43	3.50262E-01	0.	0.	0.
44	3.50332E-01	6.96971E-07	3.58940E-35	7.17880E-35
45	3.50403E-01	0.	0.	0.
46	3.50474E-01	2.06642E-07	1.06421E-35	2.12842E-35
47	3.50544E-01	0.	0.	0.
48	3.50615E-01	5.78700E-08	2.98030E-36	5.96061E-36
49	3.50686E-01	0.	0.	0.
50	3.50756E-01	1.53101E-08	7.88470E-37	1.57694E-36

TABLE E9.- (Cont'd)

J	$\lambda, (\mu)$	Normalized cross section $\Delta J = +2$	$\frac{d\sigma}{d\Omega}(\omega)_{\perp}$	$\frac{d\sigma}{d\Omega}(\omega)_{\parallel}$
51	3.50827E-01	0.	0.	0.
52	3.50898E-01	3.82690E-C9	1.97085E-37	3.94171E-37
53	3.50969E-01	0.	0.	0.
54	3.51040E-01	9.03877E-10	4.65497E-38	9.30994E-38
55	3.51111E-01	0.	0.	0.
56	3.51181E-01	2.01747E-10	1.03900E-38	2.07800E-38
57	3.51252E-01	0.	0.	0.
58	3.51323E-01	4.25579E-11	2.19173E-39	4.38346E-39
59	3.51394E-01	0.	0.	0.
60	3.51465E-01	8.48520E-12	4.36988E-40	8.73976E-40
61	3.51536E-01	0.	0.	0.
62	3.51608E-01	1.59913E-12	8.23554E-41	1.64711E-40
63	3.51679E-01	0.	0.	0.
64	3.51750E-01	2.84890E-13	1.46718E-41	2.93437E-41
65	3.51821E-01	0.	0.	0.
66	3.51892E-01	4.79805E-14	2.47095E-42	4.94199E-42
67	3.51963E-01	0.	0.	0.
68	3.52035E-01	7.63960E-15	3.93440E-43	7.86879E-43
69	3.52106E-01	0.	0.	0.
70	3.52177E-01	1.15005E-15	5.92277E-44	1.18455E-43
71	3.52249E-01	0.	0.	0.
72	3.52320E-01	1.63691E-16	8.43009E-45	1.68602E-44
73	3.52391E-01	0.	0.	0.
74	3.52463E-01	2.20298E-17	1.13454E-45	2.26907E-45
75	3.52534E-01	0.	0.	0.
76	3.52606E-01	2.80345E-18	1.44378E-46	2.88756E-46
77	3.52677E-01	0.	0.	0.
78	3.52749E-01	3.37354E-19	1.73737E-47	3.47475E-47
79	3.52820E-01	0.	0.	0.
80	3.52892E-01	3.83888E-20	1.97702E-48	3.95405E-48
81	3.52964E-01	0.	0.	0.
82	3.53035E-01	4.13106E-21	2.12750E-49	4.25499E-49
83	3.53107E-01	0.	0.	0.
84	3.53179E-01	4.20407E-22	2.16510E-50	4.33019E-50
85	3.53250E-01	0.	0.	0.
86	3.53322E-01	4.04614E-23	2.08376E-51	4.16753E-51
87	3.53394E-01	0.	0.	0.
88	3.53466E-01	3.68287E-24	1.89668E-52	3.79335E-52
89	3.53538E-01	0.	0.	0.
90	3.53610E-01	3.17040E-25	1.63276E-53	3.26552E-53
91	3.53682E-01	0.	0.	0.
92	3.53754E-01	2.58128E-26	1.32936E-54	2.65872E-54
93	3.53826E-01	0.	0.	0.
94	3.53898E-01	1.98774E-27	1.02368E-55	2.04737E-55
95	3.53970E-01	0.	0.	0.
96	3.54042E-01	1.44774E-28	7.45588E-57	1.49118E-56
97	3.54114E-01	0.	0.	0.
98	3.54186E-01	9.97338E-30	5.13629E-58	1.02726E-57
99	3.54258E-01	0.	0.	0.
100	3.54330E-01	6.49857E-31	3.34677E-59	6.69353E-59

TABLE ELO.- DIFFERENTIAL BACKSCATTER CROSS SECTIONS FOR PURE ROTATIONAL RAMAN

FINE STRUCTURE OF O₂. $\Delta J = -2$

J	$\lambda, (\mu)$	Normalized cross section $\Delta J = -2$	$\frac{d\sigma}{d\Omega}(\omega)_\perp$	$\frac{d\sigma}{d\Omega}(\omega)_\parallel$
2	3.47046E-01	1.77161E-02	9.12379E-31	1.82476E-30
3	3.46977E-01	0.	0.	0.
4	3.46908E-01	4.14226E-02	2.13326E-30	4.26653E-30
5	3.46838E-01	0.	0.	0.
6	3.46769E-01	5.66993E-02	2.92001E-30	5.84003E-30
7	3.46700E-01	0.	0.	0.
8	3.46631E-01	6.31890E-02	3.25424E-30	6.50847E-30
9	3.46562E-01	0.	0.	0.
10	3.46493E-01	6.17633E-02	3.18081E-30	6.36162E-30
11	3.46424E-01	0.	0.	0.
12	3.46355E-01	5.45487E-02	2.80926E-30	5.61851E-30
13	3.46286E-01	0.	0.	0.
14	3.46217E-01	4.41920E-02	2.27589E-30	4.55177E-30
15	3.46148E-01	0.	0.	0.
16	3.46079E-01	3.31271E-02	1.70604E-30	3.41209E-30
17	3.46010E-01	0.	0.	0.
18	3.45941E-01	2.31039E-02	1.18985E-30	2.37970E-30
19	3.45873E-01	0.	0.	0.
20	3.45804E-01	1.50470E-02	7.74920E-31	1.54984E-30
21	3.45735E-01	0.	0.	0.
22	3.45666E-01	9.17495E-03	4.72510E-31	9.45020E-31
23	3.45598E-01	0.	0.	0.
24	3.45529E-01	5.24773E-03	2.70258E-31	5.40516E-31
25	3.45460E-01	0.	0.	0.
26	3.45392E-01	2.81951E-03	1.45205E-31	2.90410E-31
27	3.45323E-01	0.	0.	0.
28	3.45254E-01	1.42459E-03	7.33666E-32	1.46733E-31
29	3.45186E-01	0.	0.	0.
30	3.45117E-01	6.77487E-04	3.48906E-32	6.97811E-32
31	3.45049E-01	0.	0.	0.
32	3.44980E-01	3.03464E-04	1.56284E-32	3.12568E-32
33	3.44912E-01	0.	0.	0.
34	3.44844E-01	1.28102E-04	6.59726E-33	1.31945E-32
35	3.44775E-01	0.	0.	0.
36	3.44707E-01	5.09863E-05	2.62580E-33	5.25159E-33
37	3.44639E-01	0.	0.	0.
38	3.44570E-01	1.91412E-05	9.85773E-34	1.97155E-33
39	3.44502E-01	0.	0.	0.
40	3.44434E-01	6.78027E-06	3.49184E-34	6.98368E-34
41	3.44366E-01	0.	0.	0.
42	3.44297E-01	2.26678E-06	1.16739E-34	2.33478E-34
43	3.44229E-01	0.	0.	0.
44	3.44161E-01	7.15421E-07	3.68442E-35	7.36884E-35
45	3.44093E-01	0.	0.	0.
46	3.44025E-01	2.13204E-07	1.09800E-35	2.19600E-35
47	3.43957E-01	0.	0.	0.
48	3.43889E-01	6.00050E-08	3.09026E-36	6.18052E-36
49	3.43821E-01	0.	0.	0.
50	3.43753E-01	1.59518E-08	8.21518E-37	1.64304E-36
51	3.43685E-01	0.	0.	0.
52	3.43617E-01	4.00611E-09	2.06315E-37	4.12629E-37

TABLE ELO.- (Cont'd)

J	$\lambda, (\mu)$	Normalized cross section $\Delta J = -2$	$\frac{d\sigma}{d\Omega}(\omega)_I$	$\frac{d\sigma}{d\Omega}(\omega)_{II}$
53	3.43549E-01	0.	0.	0.
54	3.43481E-01	9.50562E-10	4.89540E-38	9.79079E-38
55	3.43413E-01	0.	0.	0.
56	3.43346E-01	2.13123E-10	1.09759E-38	2.19517E-38
57	3.43278E-01	0.	0.	0.
58	3.43210E-01	4.51562E-11	2.32554E-39	4.65109E-39
59	3.43142E-01	0.	0.	0.
60	3.43075E-01	9.04229E-12	4.65678E-40	9.31356E-40
61	3.43007E-01	0.	0.	0.
62	3.42939E-01	1.71139E-12	8.81365E-41	1.76273E-40
63	3.42872E-01	0.	0.	0.
64	3.42804E-01	3.06168E-13	1.57676E-41	3.15353E-41
65	3.42736E-01	0.	0.	0.
66	3.42669E-01	5.17774E-14	2.66654E-42	5.33307E-42
67	3.42601E-01	0.	0.	0.
68	3.42534E-01	8.27782E-15	4.26308E-43	8.52615E-43
69	3.42466E-01	0.	0.	0.
70	3.42399E-01	1.25115E-15	6.44344E-44	1.28869E-43
71	3.42332E-01	0.	0.	0.
72	3.42264E-01	1.78791E-16	9.20774E-45	1.84155E-44
73	3.42197E-01	0.	0.	0.
74	3.42130E-01	2.41569E-17	1.24408E-45	2.48816E-45
75	3.42062E-01	0.	0.	0.
76	3.41995E-01	3.08614E-18	1.58936E-46	3.17873E-46
77	3.41928E-01	0.	0.	0.
78	3.41860E-01	3.72809E-19	1.91997E-47	3.83993E-47
79	3.41793E-01	0.	0.	0.
80	3.41726E-01	4.25861E-20	2.19318E-48	4.38637E-48
81	3.41659E-01	0.	0.	0.
82	3.41592E-01	4.60018E-21	2.36909E-49	4.73818E-49
83	3.41525E-01	0.	0.	0.
84	3.41458E-01	4.69916E-22	2.42007E-50	4.84014E-50
85	3.41391E-01	0.	0.	0.
86	3.41324E-01	4.53960E-23	2.33789E-51	4.67579E-51
87	3.41257E-01	0.	0.	0.
88	3.41190E-01	4.14741E-24	2.13592E-52	4.27183E-52
89	3.41123E-01	0.	0.	0.
90	3.41056E-01	3.58352E-25	1.84552E-53	3.69103E-53
91	3.40989E-01	0.	0.	0.
92	3.40922E-01	2.92838E-26	1.50812E-54	3.01623E-54
93	3.40855E-01	0.	0.	0.
94	3.40788E-01	2.26327E-27	1.16559E-55	2.33117E-55
95	3.40722E-01	0.	0.	0.
96	3.40655E-01	1.65443E-28	8.52032E-57	1.70406E-56
97	3.40588E-01	0.	0.	0.
98	3.40522E-01	1.14385E-29	5.89084E-58	1.17817E-57
99	3.40455E-01	0.	0.	0.
100	3.40388E-01	7.48014E-31	3.85227E-59	7.70454E-59
101	3.40322E-01	0.	0.	0.
102	3.40255E-01	4.62673E-32	2.38276E-60	4.76553E-60

TABLE E11.- DIFFERENTIAL BACKSCATTER CROSS SECTIONS FOR PURE ROTATIONAL RAMAN

FINE STRUCTURE OF N_2 . $\Delta J = +2$

J	$\lambda, (\mu)$	Normalized cross section $\Delta J = +2$	$\frac{d\sigma}{d\Omega}(\omega)_\perp$	$\frac{d\sigma}{d\Omega}(\omega)_\parallel$
0	3.47295E-01	1.71618E-02	5.53982E-31	1.10796E-30
1	3.47391E-01	1.51347E-02	4.88548E-31	9.77095E-31
2	3.47488E-01	4.15647E-02	1.34171E-30	2.68342E-30
3	3.47585E-01	2.54021E-02	8.19980E-31	1.63996E-30
4	3.47681E-01	5.76717E-02	1.86164E-30	3.72328E-30
5	3.47778E-01	3.09944E-02	1.0005CE-30	2.00100E-30
6	3.47875E-01	6.37570E-02	2.05808E-30	4.11615E-30
7	3.47972E-01	3.15762E-02	1.01928E-30	2.03856E-30
8	3.48069E-01	6.04953E-02	1.95279E-30	3.90558E-30
9	3.48166E-01	2.81031E-02	9.07167E-31	1.81433E-30
10	3.48263E-01	5.07558E-02	1.63840E-30	3.27679E-30
11	3.48360E-01	2.23087E-02	7.20124E-31	1.44025E-30
12	3.48457E-01	3.82259E-02	1.23393E-30	2.46786E-30
13	3.48554E-01	1.59744E-02	5.15652E-31	1.03130E-30
14	3.48651E-01	2.60684E-02	8.41489E-31	1.68298E-30
15	3.48749E-01	1.03890E-02	3.35358E-31	6.70716E-31
16	3.48846E-01	1.61860E-02	5.22483E-31	1.04497E-30
17	3.48943E-01	6.16406E-03	1.98976E-31	3.97952E-31
18	3.49041E-01	9.18394E-03	2.96458E-31	5.92915E-31
19	3.49138E-01	3.34684E-03	1.08036E-31	2.16072E-31
20	3.49236E-01	4.77434E-03	1.54116E-31	3.08231E-31
21	3.49334E-01	1.66663E-03	5.37588E-32	1.07558E-31
22	3.49431E-01	2.27832E-03	7.35441E-32	1.47088E-31
23	3.49529E-01	7.62416E-04	2.46108E-32	4.92216E-32
24	3.49627E-01	9.99436E-04	3.22618E-32	6.45236E-32
25	3.49725E-01	3.20803E-04	1.03555E-32	2.07111E-32
26	3.49823E-01	4.03472E-04	1.30241E-32	2.60482E-32
27	3.49921E-01	1.24281E-04	4.01178E-33	8.02357E-33
28	3.50019E-01	1.50027E-04	4.84287E-33	9.68574E-33
29	3.50117E-01	4.43635E-05	1.43205E-33	2.86411E-33
30	3.50215E-01	5.14192E-05	1.65981E-33	3.31962E-33
31	3.50313E-01	1.46008E-05	4.71315E-34	9.42629E-34
32	3.50411E-01	1.62528E-05	5.24641E-34	1.04928E-33
33	3.50509E-01	4.43286E-06	1.43093E-34	2.86185E-34
34	3.50608E-01	4.74006E-06	1.53009E-34	3.06019E-34
35	3.50706E-01	1.24203E-06	4.00926E-35	8.01852E-35
36	3.50805E-01	1.27603E-06	4.11903E-35	8.23807E-35
37	3.50903E-01	3.21274E-07	1.03707E-35	2.07414E-35
38	3.51002E-01	3.17180E-07	1.02386E-35	2.04771E-35
39	3.51100E-01	7.67448E-08	2.47732E-36	4.95464E-36
40	3.51199E-01	7.28179E-08	2.35056E-36	4.70113E-36
41	3.51298E-01	1.69343E-08	5.46638E-37	1.09328E-36
42	3.51397E-01	1.54442E-08	4.98538E-37	9.97076E-37
43	3.51495E-01	3.45243E-09	1.11444E-37	2.22889E-37
44	3.51594E-01	3.02675E-09	9.77033E-38	1.95407E-37
45	3.51693E-01	6.50442E-10	2.09963E-38	4.19925E-38
46	3.51792E-01	5.48215E-10	1.76964E-38	3.53928E-38
47	3.51891E-01	1.13264E-10	3.65616E-39	7.31233E-39
48	3.51990E-01	9.17825E-11	2.96274E-39	5.92548E-39
49	3.52090E-01	1.82323E-11	5.88538E-40	1.17708E-39
50	3.52189E-01	1.42057E-11	4.5856CE-40	9.17121E-40

TABLE Ell.- (Cont'd)

J	$\lambda, (\mu)$	Normalized cross section $\Delta J = +2$	$\frac{d\sigma}{d\Omega}(\omega)_{\perp}$	$\frac{d\sigma}{d\Omega}(\omega)_{\parallel}$
51	3.52288E-01	2.71339E-12	8.75882E-41	1.75176E-40
52	3.52387E-01	2.03289E-12	6.56218E-41	1.31244E-40
53	3.52487E-01	3.73385E-13	1.20529E-41	2.41057E-41
54	3.52586E-01	2.69007E-13	8.68355E-42	1.73671E-41
55	3.52686E-01	4.75139E-14	1.53375E-42	3.06750E-42
56	3.52785E-01	3.29195E-14	1.06264E-42	2.12528E-42
57	3.52885E-01	5.59170E-15	1.80500E-43	3.61000E-43
58	3.52985E-01	3.72580E-15	1.20269E-43	2.40538E-43
59	3.53084E-01	6.08645E-16	1.96471E-44	3.92941E-44
60	3.53184E-01	3.90032E-16	1.25902E-44	2.51805E-44
61	3.53284E-01	6.12793E-17	1.97810E-45	3.95619E-45
62	3.53384E-01	3.77682E-17	1.21916E-45	2.43832E-45
63	3.53484E-01	5.70719E-18	1.84228E-46	3.68456E-46
64	3.53584E-01	3.38318E-18	1.09209E-46	2.18418E-46
65	3.53684E-01	4.91720E-19	1.58727E-47	3.17455E-47
66	3.53784E-01	2.80365E-19	9.05018E-48	1.81004E-47
67	3.53884E-01	3.91945E-20	1.26520E-48	2.53040E-48
68	3.53985E-01	2.14954E-20	6.93871E-49	1.38774E-48
69	3.54085E-01	2.89045E-21	9.33039E-50	1.86608E-49
70	3.54185E-01	1.52479E-21	4.92203E-50	9.84407E-50
71	3.54286E-01	1.97225E-22	6.36642E-51	1.27328E-50
72	3.54386E-01	1.00079E-22	3.23054E-51	6.46108E-51
73	3.54487E-01	1.24518E-23	4.01944E-52	8.03887E-52
74	3.54587E-01	6.07792E-24	1.96195E-52	3.92390E-52
75	3.54688E-01	7.27433E-25	2.34815E-53	4.69631E-53
76	3.54789E-01	3.41561E-25	1.10256E-53	2.20512E-53
77	3.54889E-01	3.93243E-26	1.26939E-54	2.53878E-54
78	3.54990E-01	1.77622E-26	5.73363E-55	1.14673E-54
79	3.55091E-01	1.96722E-27	6.35018E-56	1.27004E-55
80	3.55192E-01	8.54778E-28	2.75922E-56	5.51845E-56
81	3.55293E-01	9.10710E-29	2.93977E-57	5.87954E-57
82	3.55394E-01	3.80675E-29	1.22882E-57	2.45764E-57
83	3.55495E-01	3.90173E-30	1.25946E-58	2.51895E-58
84	3.55596E-01	1.56895E-30	5.06458E-59	1.01292E-58
85	3.55698E-01	1.54701E-31	4.99376E-60	9.98753E-60
86	3.55799E-01	5.98456E-32	1.93182E-60	3.86363E-60
87	3.55900E-01	5.67681E-33	1.83248E-61	3.66495E-61
88	3.56002E-01	2.11267E-33	6.81971E-62	1.36394E-61
89	3.56103E-01	1.92796E-34	6.22345E-63	1.24469E-62
90	3.56205E-01	6.90272E-35	2.22820E-63	4.45640E-63
91	3.56306E-01	6.06014E-36	1.95621E-64	3.91242E-64
92	3.56408E-01	2.08740E-36	6.73812E-65	1.34762E-64
93	3.56509E-01	1.76307E-37	5.69118E-66	1.13824E-65
94	3.56611E-01	5.84246E-38	1.88595E-66	3.77189E-66
95	3.56713E-01	4.74751E-39	1.53249E-67	3.06499E-67
96	3.56815E-01	1.51356E-39	4.88578E-68	9.77155E-68
97	3.56917E-01	1.18326E-40	3.81956E-69	7.63912E-69
98	3.57019E-01	3.62933E-41	1.17155E-69	2.34309E-69
99	3.57121E-01	2.72973E-42	8.81157E-71	1.76231E-70
100	3.57223E-01	8.05530E-43	2.60025E-71	5.20050E-71

TABLE E12.- DIFFERENTIAL BACKSCATTER CROSS SECTIONS FOR PURE ROTATIONAL RAMAN

FINE STRUCTURE OF N₂. $\Delta J = -2$

J	$\lambda, (\mu)$	Normalized cross section $\Delta J = -2$	$\frac{d\sigma}{d\Omega}(\omega)_{\perp}$	$\frac{d\sigma}{d\Omega}(\omega)_{\parallel}$
2	3.47005E-01	1.62541E-02	5.24684E-31	1.04937E-30
3	3.46909E-01	1.38243E-02	4.46248E-31	8.92496E-31
4	3.46813E-01	3.66152E-02	1.18194E-30	2.36388E-30
5	3.46717E-01	2.15812E-02	6.96640E-31	1.39328E-30
6	3.46620E-01	4.72537E-02	1.52535E-30	3.05070E-30
7	3.46524E-01	2.44920E-02	7.90601E-31	1.58120E-30
8	3.46428E-01	4.85888E-02	1.56845E-30	3.13689E-30
9	3.46332E-01	2.32079E-02	7.49152E-31	1.49830E-30
10	3.46236E-01	4.28811E-02	1.38420E-30	2.76840E-30
11	3.46140E-01	1.92117E-02	6.20153E-31	1.24031E-30
12	3.46044E-01	3.34630E-02	1.08019E-30	2.16037E-30
13	3.45949E-01	1.41847E-02	4.57883E-31	9.15766E-31
14	3.45853E-01	2.34408E-02	7.56670E-31	1.51334E-30
15	3.45757E-01	9.44727E-03	3.04958E-31	6.09916E-31
16	3.45662E-01	1.48685E-02	4.79954E-31	9.59907E-31
17	3.45566E-01	5.71470E-03	1.84470E-31	3.68941E-31
18	3.45470E-01	8.58668E-03	2.77178E-31	5.54356E-31
19	3.45375E-01	3.15370E-03	1.01802E-31	2.03603E-31
20	3.45280E-01	4.53159E-03	1.46280E-31	2.92560E-31
21	3.45184E-01	1.59266E-03	5.14112E-32	1.02822E-31
22	3.45089E-01	2.19114E-03	7.07300E-32	1.41460E-31
23	3.44994E-01	7.37673E-04	2.38121E-32	4.76242E-32
24	3.44898E-01	9.72540E-04	3.13936E-32	6.27872E-32
25	3.44803E-01	3.13872E-04	1.01318E-32	2.02636E-32
26	3.44708E-01	3.96811E-04	1.28090E-32	2.56181E-32
27	3.44613E-01	1.22839E-04	3.96523E-33	7.93047E-33
28	3.44518E-01	1.48997E-04	4.80963E-33	9.61925E-33
29	3.44423E-01	4.42625E-05	1.42879E-33	2.85759E-33
30	3.44328E-01	5.15311E-05	1.66342E-33	3.32685E-33
31	3.44233E-01	1.46958E-05	4.74381E-34	9.48761E-34
32	3.44138E-01	1.64271E-05	5.30267E-34	1.06053E-33
33	3.44044E-01	4.49864E-06	1.45216E-34	2.90432E-34
34	3.43949E-01	4.82948E-06	1.55896E-34	3.11791E-34
35	3.43854E-01	1.27035E-06	4.10069E-35	8.20137E-35
36	3.43760E-01	1.31006E-06	4.22887E-35	8.45775E-35
37	3.43665E-01	3.31059E-07	1.06866E-35	2.13732E-35
38	3.43571E-01	3.28023E-07	1.05886E-35	2.11772E-35
39	3.43476E-01	7.96500E-08	2.57110E-36	5.14220E-36
40	3.43382E-01	7.58376E-08	2.44804E-36	4.89607E-36
41	3.43288E-01	1.76968E-08	5.71254E-37	1.14251E-36
42	3.43193E-01	1.61939E-08	5.22741E-37	1.04548E-36
43	3.43099E-01	3.63202E-09	1.17242E-37	2.34483E-37
44	3.43005E-01	3.19459E-09	1.03121E-37	2.06243E-37
45	3.42911E-01	6.88720E-10	2.22319E-38	4.44637E-38
46	3.42817E-01	5.82320E-10	1.87973E-38	3.75946E-38
47	3.42723E-01	1.20688E-10	3.89579E-39	7.79159E-39
48	3.42629E-01	9.81009E-11	3.16670E-39	6.33339E-39
49	3.42535E-01	1.95471E-11	6.30980E-40	1.26196E-39
50	3.42441E-01	1.52763E-11	4.93118E-40	9.86236E-40
51	3.42347E-01	2.92662E-12	9.44714E-41	1.88943E-40
52	3.42253E-01	2.19916E-12	7.09889E-41	1.41978E-40

TABLE E12.-- (Cont'd)

J	$\lambda, (\mu)$	Normalized cross section $\Delta J = -2$	$\frac{d\sigma}{d\Omega}(\omega)_I$	$\frac{d\sigma}{d\Omega}(\omega)_{II}$
53	3.42160E-01	4.05111E-13	1.30770E-41	2.61540E-41
54	3.42066E-01	2.92715E-13	9.44883E-42	1.88977E-41
55	3.41972E-01	5.18507E-14	1.67374E-42	3.34748E-42
56	3.41879E-01	3.60271E-14	1.16296E-42	2.32591E-42
57	3.41785E-01	6.13697E-15	1.98102E-43	3.96203E-43
58	3.41692E-01	4.10066E-15	1.32369E-43	2.64739E-43
59	3.41598E-01	6.71760E-16	2.16844E-44	4.33688E-44
60	3.41505E-01	4.31676E-16	1.39345E-44	2.78690E-44
61	3.41412E-01	6.80096E-17	2.19535E-45	4.39070E-45
62	3.41318E-01	4.20315E-17	1.35678E-45	2.71355E-45
63	3.41225E-01	6.36877E-18	2.05584E-46	4.11168E-46
64	3.41132E-01	3.78561E-18	1.22200E-46	2.44399E-46
65	3.41039E-01	5.51697E-19	1.78088E-47	3.56176E-47
66	3.40946E-01	3.15407E-19	1.01813E-47	2.03627E-47
67	3.40853E-01	4.42112E-20	1.42714E-48	2.85428E-48
68	3.40760E-01	2.43112E-20	7.84765E-49	1.56953E-48
69	3.40667E-01	3.27775E-21	1.05806E-49	2.11611E-49
70	3.40574E-01	1.73366E-21	5.59625E-50	1.11925E-49
71	3.40481E-01	2.24829E-22	7.25749E-51	1.45150E-50
72	3.40389E-01	1.14384E-22	3.69232E-51	7.38464E-51
73	3.40296E-01	1.42687E-23	4.60594E-52	9.21189E-52
74	3.40203E-01	6.98285E-24	2.25406E-52	4.50813E-52
75	3.40111E-01	8.37898E-25	2.70473E-53	5.40947E-53
76	3.40018E-01	3.94441E-25	1.27326E-53	2.54651E-53
77	3.39926E-01	4.55290E-25	1.46968E-54	2.93936E-54
78	3.39833E-01	2.06173E-26	6.65526E-55	1.33105E-54
79	3.39741E-01	2.28925E-27	7.38971E-56	1.47794E-55
80	3.39649E-01	9.97232E-28	3.21907E-56	6.43813E-56
81	3.39556E-01	1.06518E-28	3.43839E-57	6.87677E-57
82	3.39464E-01	4.46365E-29	1.44087E-57	2.88173E-57
83	3.39372E-01	4.58654E-30	1.48054E-58	2.96107E-58
84	3.39280E-01	1.84896E-30	5.96844E-59	1.19369E-58
85	3.39188E-01	1.82767E-31	5.89573E-60	1.17995E-59
86	3.39096E-01	7.08794E-32	2.28799E-60	4.57597E-60
87	3.39004E-01	6.74020E-33	2.17574E-61	4.35147E-61
88	3.38912E-01	2.51466E-33	8.11732E-62	1.62346E-61
89	3.38820E-01	2.30049E-34	7.42597E-63	1.48519E-62
90	3.38728E-01	8.25688E-35	2.66532E-63	5.33064E-63
91	3.38636E-01	7.26690E-36	2.34576E-64	4.69151E-64
92	3.38544E-01	2.50923E-36	8.09980E-65	1.61996E-64
93	3.38453E-01	2.12457E-37	6.85811E-66	1.37162E-65
94	3.38361E-01	7.05768E-38	2.27822E-66	4.55644E-66
95	3.38269E-01	5.74903E-39	1.85579E-67	3.71157E-67
96	3.38178E-01	1.83734E-39	5.93093E-68	1.18619E-67
97	3.38086E-01	1.43989E-40	4.64795E-69	9.29590E-69
98	3.37995E-01	4.42722E-41	1.42911E-69	2.85821E-69
99	3.37904E-01	3.33795E-42	1.07749E-70	2.15498E-70
100	3.37812E-01	9.87402E-43	3.18733E-71	6.37467E-71
101	3.37721E-01	7.16236E-44	2.31201E-72	4.62402E-72
102	3.37630E-01	2.03839E-44	6.57991E-73	1.31598E-72

TABLE E13.- DIFFERENTIAL BACKSCATTER CROSS SECTIONS FOR ROTATIONAL FINE STRUCTURE

ON THE $v = 0 \rightarrow 1$ RAMAN VIBRATIONAL TRANSITION OF O_2 . $\Delta J = +2$

J	$\lambda, (\mu)$	Normalized cross section $\Delta J = +2$	$\frac{d\sigma}{d\Omega}(\omega)_\perp$	$\frac{d\sigma}{d\Omega}(\omega)_\parallel$
0	3.67070E-01	1.84157E-02	3.76785E-33	7.53570E-33
1	3.67146E-01	0.	0.	0.
2	3.67222E-01	4.53569E-02	9.28003E-33	1.85601E-32
3	3.67298E-01	0.	0.	0.
4	3.67373E-01	6.54001E-02	1.33809E-32	2.67617E-32
5	3.67447E-01	0.	0.	0.
6	3.67521E-01	7.67795E-02	1.57091E-32	3.14182E-32
7	3.67595E-01	0.	0.	0.
8	3.67669E-01	7.90577E-02	1.61752E-32	3.23504E-32
9	3.67742E-01	0.	0.	0.
10	3.67814E-01	7.35558E-02	1.50495E-32	3.00990E-32
11	3.67887E-01	0.	0.	0.
12	3.67959E-01	6.27772E-02	1.28442E-32	2.56885E-32
13	3.68030E-01	0.	0.	0.
14	3.68101E-01	4.95766E-02	1.01434E-32	2.02868E-32
15	3.68172E-01	0.	0.	0.
16	3.68242E-01	3.64269E-02	7.45294E-33	1.49059E-32
17	3.68312E-01	0.	0.	0.
18	3.68381E-01	2.49941E-02	5.11379E-33	1.02276E-32
19	3.68450E-01	0.	0.	0.
20	3.68519E-01	1.60565E-02	3.28516E-33	6.57032E-33
21	3.68587E-01	0.	0.	0.
22	3.68655E-01	9.67577E-03	1.97966E-33	3.95933E-33
23	3.68723E-01	0.	0.	0.
24	3.68790E-01	5.47726E-03	1.12065E-33	2.24130E-33
25	3.68856E-01	0.	0.	0.
26	3.68923E-01	2.91584E-03	5.96581E-34	1.19316E-33
27	3.68988E-01	0.	0.	0.
28	3.69054E-01	1.46105E-03	2.98931E-34	5.97862E-34
29	3.69119E-01	0.	0.	0.
30	3.69183E-01	6.89558E-04	1.41084E-34	2.82167E-34
31	3.69248E-01	0.	0.	0.
32	3.69311E-01	3.06710E-04	5.27530E-35	1.25506E-34
33	3.69375E-01	0.	0.	0.
34	3.69438E-01	1.28630E-04	2.63177E-35	5.26354E-35
35	3.69500E-01	0.	0.	0.
36	3.69562E-01	5.08841E-05	1.04109E-35	2.08218E-35
37	3.69624E-01	0.	0.	0.
38	3.69685E-01	1.89929E-05	3.88596E-36	7.77191E-36
39	3.69746E-01	0.	0.	0.
40	3.69807E-01	6.69106E-06	1.36899E-36	2.73798E-36
41	3.69867E-01	0.	0.	0.
42	3.69927E-01	2.22534E-06	4.55304E-37	9.10609E-37
43	3.69986E-01	0.	0.	0.
44	3.70045E-01	6.98354E-07	1.42985E-37	2.85971E-37
45	3.70103E-01	0.	0.	0.
46	3.70161E-01	2.07274E-07	4.24082E-38	8.48165E-38
47	3.70219E-01	0.	0.	0.
48	3.70276E-01	5.87585E-08	1.18808E-38	2.37616E-38
49	3.70333E-01	0.	0.	0.
50	3.70390E-01	1.53566E-08	3.14442E-39	6.28884E-39

TABLE E13.- (Cont'd)

J	$\lambda, (\mu)$	Normalized cross section $\Delta J = +2$	$\frac{d\sigma}{d\Omega}(\omega)_\perp$	$\frac{d\sigma}{d\Omega}(\omega)_\parallel$
51	3.70445E-01	0.	0.	0.
52	3.70501E-01	3.84311E-09	7.86300E-40	1.57260E-39
53	3.70556E-01	0.	0.	0.
54	3.70610E-01	9.08095E-10	1.85796E-40	3.71593E-40
55	3.70665E-01	0.	0.	0.
56	3.70719E-01	2.02780E-10	4.14887E-41	8.29774E-41
57	3.70772E-01	0.	0.	0.
58	3.70825E-01	4.27957E-11	8.75600E-42	1.75120E-41
59	3.70878E-01	0.	0.	0.
60	3.70930E-01	8.53676E-12	1.74662E-42	3.49324E-42
61	3.70982E-01	0.	0.	0.
62	3.71033E-01	1.60967E-12	3.29338E-43	6.58675E-43
63	3.71084E-01	0.	0.	0.
64	3.71134E-01	2.86917E-13	5.87031E-44	1.17406E-43
65	3.71184E-01	0.	0.	0.
66	3.71234E-01	4.83481E-14	9.89202E-45	1.97840E-44
67	3.71283E-01	0.	0.	0.
68	3.71332E-01	7.70247E-15	1.57593E-45	3.15185E-45
69	3.71381E-01	0.	0.	0.
70	3.71428E-01	1.16019E-15	2.37375E-46	4.74751E-46
71	3.71476E-01	0.	0.	0.
72	3.71523E-01	1.65234E-16	3.38068E-47	6.76136E-47
73	3.71570E-01	0.	0.	0.
74	3.71616E-01	2.22512E-17	4.55260E-48	9.10521E-48
75	3.71662E-01	0.	0.	0.
76	3.71707E-01	2.83344E-18	5.79721E-49	1.15944E-48
77	3.71752E-01	0.	0.	0.
78	3.71797E-01	3.41187E-19	6.98069E-50	1.39614E-49
79	3.71841E-01	0.	0.	0.
80	3.71885E-01	3.88513E-20	7.94898E-51	1.58980E-50
81	3.71928E-01	0.	0.	0.
82	3.71971E-01	4.18375E-21	8.55995E-52	1.71199E-51
83	3.72013E-01	0.	0.	0.
84	3.72055E-01	4.26074E-22	8.71748E-53	1.74350E-52
85	3.72097E-01	0.	0.	0.
86	3.72138E-01	4.10371E-23	3.39618E-54	1.67924E-53
87	3.72179E-01	0.	0.	0.
88	3.72219E-01	3.73808E-24	7.64812E-55	1.52962E-54
89	3.72259E-01	0.	0.	0.
90	3.72298E-01	3.22043E-25	5.58900E-56	1.31780E-55
91	3.72337E-01	0.	0.	0.
92	3.72376E-01	2.62410E-26	5.36890E-57	1.07378E-56
93	3.72414E-01	0.	0.	0.
94	3.72452E-01	2.02235E-27	4.13772E-58	8.27544E-58
95	3.72489E-01	0.	0.	0.
96	3.72526E-01	1.47418E-28	3.01617E-59	6.03234E-59
97	3.72563E-01	0.	0.	0.
98	3.72599E-01	1.01641E-29	2.07958E-60	4.15917E-60
99	3.72634E-01	0.	0.	0.
100	3.72669E-01	6.62864E-31	1.35622E-61	2.71244E-61

TABLE E14.- DIFFERENTIAL BACKSCATTER CROSS SECTIONS FOR ROTATIONAL FINE STRUCTURE

ON THE $v = 0 \rightarrow 1$ RAMAN VIBRATIONAL TRANSITION OF O_2 . $\Delta J = -2$

J	$\lambda, (\mu)$	Normalized cross section $\Delta J = -2$	$\frac{d\sigma}{d\Omega}(\omega)_\perp$	$\frac{d\sigma}{d\Omega}(\omega)_\parallel$
2	3.66839E-01	1.77126E-02	3.62400E-33	7.24800E-33
3	3.66761E-01	0.	0.	0.
4	3.66683E-01	4.14188E-02	8.47428E-33	1.69486E-32
5	3.66604E-01	0.	0.	0.
6	3.66525E-01	5.67011E-02	1.16010E-32	2.32021E-32
7	3.66446E-01	0.	0.	0.
8	3.66366E-01	6.32000E-02	1.29307E-32	2.58614E-32
9	3.66286E-01	0.	0.	0.
10	3.66206E-01	6.17838E-02	1.26410E-32	2.52819E-32
11	3.66125E-01	0.	0.	0.
12	3.66043E-01	5.45766E-02	1.11664E-32	2.23327E-32
13	3.65962E-01	0.	0.	0.
14	3.65880E-01	4.42233E-02	9.04808E-33	1.80962E-32
15	3.65797E-01	0.	0.	0.
16	3.65714E-01	3.31577E-02	6.78406E-33	1.35681E-32
17	3.65631E-01	0.	0.	0.
18	3.65547E-01	2.31306E-02	4.73253E-33	9.46506E-33
19	3.65463E-01	0.	0.	0.
20	3.65379E-01	1.50682E-02	3.08296E-33	6.16591E-33
21	3.65294E-01	0.	0.	0.
22	3.65209E-01	9.19037E-03	1.88035E-33	3.76070E-33
23	3.65124E-01	0.	0.	0.
24	3.65038E-01	5.25806E-03	1.07580E-33	2.15160E-33
25	3.64951E-01	0.	0.	0.
26	3.64865E-01	2.82593E-03	5.78185E-34	1.15637E-33
27	3.64778E-01	0.	0.	0.
28	3.64690E-01	1.42830E-03	2.92230E-34	5.84460E-34
29	3.64602E-01	0.	0.	0.
30	3.64514E-01	6.79482E-04	1.39022E-34	2.78044E-34
31	3.64426E-01	0.	0.	0.
32	3.64337E-01	3.04467E-04	6.22940E-35	1.24588E-34
33	3.64247E-01	0.	0.	0.
34	3.64158E-01	1.28574E-04	2.63063E-35	5.26127E-35
35	3.64068E-01	0.	0.	0.
36	3.63977E-01	5.11946E-05	1.04744E-35	2.09488E-35
37	3.63886E-01	0.	0.	0.
38	3.63795E-01	1.92274E-05	3.93392E-36	7.86785E-36
39	3.63704E-01	0.	0.	0.
40	3.63612E-01	6.81375E-06	1.39409E-36	2.78819E-36
41	3.63519E-01	0.	0.	0.
42	3.63427E-01	2.27900E-06	4.66283E-37	9.32566E-37
43	3.63334E-01	0.	0.	0.
44	3.63240E-01	7.19615E-07	1.47233E-37	2.94466E-37
45	3.63147E-01	0.	0.	0.
46	3.63052E-01	2.14558E-07	4.38985E-38	8.77971E-38
47	3.62958E-01	0.	0.	0.
48	3.62863E-01	6.04166E-08	1.23612E-38	2.47225E-38
49	3.62768E-01	0.	0.	0.
50	3.62672E-01	1.60696E-08	3.28784E-39	6.57569E-39
51	3.62576E-01	0.	0.	0.
52	3.62480E-01	4.03788E-09	8.26150E-40	1.65230E-39

TABLE E14.- (Cont'd)

J	$\lambda, (\mu)$	Normalized cross section $\Delta J = -2$	$\frac{d\sigma}{d\Omega}(\omega)_\perp$	$\frac{d\sigma}{d\Omega}(\omega)_\parallel$
53	3.62383E-01	0.	0.	0.
54	3.62286E-01	9.58635E-10	1.96137E-40	3.92273E-40
55	3.62189E-01	0.	0.	0.
56	3.62091E-01	2.15057E-10	4.40007E-41	8.80014E-41
57	3.61993E-01	0.	0.	0.
58	3.61894E-01	4.55930E-11	9.32832E-42	1.86566E-41
59	3.61795E-01	0.	0.	0.
60	3.61696E-01	9.13533E-12	1.86909E-42	3.73818E-42
61	3.61597E-01	0.	0.	0.
62	3.61497E-01	1.73009E-12	3.53976E-43	7.07952E-43
63	3.61396E-01	0.	0.	0.
64	3.61296E-01	3.09713E-13	6.33674E-44	1.26735E-43
65	3.61195E-01	0.	0.	0.
66	3.61093E-01	5.24118E-14	1.07234E-44	2.14469E-44
67	3.60992E-01	0.	0.	0.
68	3.60890E-01	8.38496E-15	1.71556E-45	3.43112E-45
69	3.60787E-01	0.	0.	0.
70	3.60684E-01	1.26823E-15	2.59481E-46	5.18961E-46
71	3.60581E-01	0.	0.	0.
72	3.60478E-01	1.81362E-16	3.71066E-47	7.42133E-47
73	3.60374E-01	0.	0.	0.
74	3.60270E-01	2.45223E-17	5.01726E-48	1.00345E-47
75	3.60165E-01	0.	0.	0.
76	3.60060E-01	3.13518E-18	6.41457E-49	1.28291E-48
77	3.59955E-01	0.	0.	0.
78	3.59849E-01	3.79024E-19	7.75483E-50	1.55097E-49
79	3.59743E-01	0.	0.	0.
80	3.59637E-01	4.33301E-20	8.86534E-51	1.77307E-50
81	3.59531E-01	0.	0.	0.
82	3.59424E-01	4.68431E-21	9.58410E-52	1.91682E-51
83	3.59316E-01	0.	0.	0.
84	3.59209E-01	4.78904E-22	9.79837E-53	1.95967E-52
85	3.59101E-01	0.	0.	0.
86	3.58992E-01	4.63031E-23	9.47361E-54	1.89472E-53
87	3.58884E-01	0.	0.	0.
88	3.58775E-01	4.23391E-24	8.66258E-55	1.73252E-54
89	3.58665E-01	0.	0.	0.
90	3.58556E-01	3.66146E-25	7.49134E-56	1.49827E-55
91	3.58446E-01	0.	0.	0.
92	3.58335E-01	2.99473E-26	6.12722E-57	1.22544E-56
93	3.58224E-01	0.	0.	0.
94	3.58113E-01	2.31666E-27	4.73988E-58	9.47977E-58
95	3.58002E-01	0.	0.	0.
96	3.57890E-01	1.69502E-28	3.46802E-59	6.93603E-59
97	3.57778E-01	0.	0.	0.
98	3.57666E-01	1.17302E-29	2.40000E-60	4.80001E-60
99	3.57553E-01	0.	0.	0.
100	3.57440E-01	7.67825E-31	1.57097E-61	3.14194E-61
101	3.57327E-01	0.	0.	0.
102	3.57213E-01	4.75391E-32	9.72649E-63	1.94530E-62

TABLE E15.- DIFFERENTIAL BACKSCATTER CROSS SECTIONS FOR ROTATIONAL FINE STRUCTURE

ON THE $v = 0 \rightarrow 1$ RAMAN VIBRATIONAL TRANSITION OF N_2 . $\Delta J = +2$

J	$\lambda, (\mu)$	Normalized cross section $\Delta J = +2$	$\frac{d\sigma}{d\Omega}(\omega)_\perp$	$\frac{d\sigma}{d\Omega}(\omega)_\parallel$
0	3.77880E-01	1.71574E-02	2.18070E-33	4.36140E-33
1	3.77993E-01	1.51296E-02	1.92297E-33	3.84593E-33
2	3.78105E-01	4.15475E-02	5.28069E-33	1.05614E-32
3	3.78217E-01	2.53898E-02	3.22705E-33	6.45409E-33
4	3.78328E-01	5.76401E-02	7.32606E-33	1.46521E-32
5	3.78439E-01	3.09756E-02	3.93700E-33	7.87400E-33
6	3.78550E-01	6.37150E-02	8.09818E-33	1.61964E-32
7	3.78659E-01	3.15539E-02	4.01050E-33	8.02101E-33
8	3.78769E-01	6.04501E-02	7.68321E-33	1.53664E-32
9	3.78878E-01	2.80811E-02	3.56910E-33	7.13820E-33
10	3.78986E-01	5.07144E-02	6.44581E-33	1.28916E-32
11	3.79094E-01	2.22900E-02	2.83305E-33	5.66611E-33
12	3.79202E-01	3.81931E-02	4.85435E-33	9.70869E-33
13	3.79309E-01	1.59605E-02	2.02857E-33	4.05715E-33
14	3.79415E-01	2.60455E-02	3.31039E-33	6.62078E-33
15	3.79521E-01	1.03799E-02	1.31928E-33	2.63857E-33
16	3.79627E-01	1.61718E-02	2.05543E-33	4.11087E-33
17	3.79732E-01	6.15871E-03	7.82772E-34	1.56554E-33
18	3.79837E-01	9.17611E-03	1.16628E-33	2.33257E-33
19	3.79941E-01	3.34405E-03	4.25029E-34	8.50059E-34
20	3.80045E-01	4.77049E-03	6.06329E-34	1.21266E-33
21	3.80148E-01	1.66534E-03	2.11665E-34	4.23329E-34
22	3.80251E-01	2.27664E-03	2.89361E-34	5.78723E-34
23	3.80353E-01	7.61889E-04	9.68360E-35	1.93672E-34
24	3.80454E-01	9.98793E-04	1.26947E-34	2.53893E-34
25	3.80556E-01	3.20615E-04	4.07501E-35	8.15003E-35
26	3.80656E-01	4.03260E-04	5.12543E-35	1.02509E-34
27	3.80757E-01	1.24224E-04	1.57388E-35	3.15776E-35
28	3.80857E-01	1.49969E-04	1.90410E-35	3.81220E-35
29	3.80956E-01	4.43497E-05	5.63585E-36	1.12737E-35
30	3.81055E-01	5.14075E-05	6.53390E-36	1.30678E-35
31	3.81153E-01	1.45988E-05	1.85551E-36	3.71102E-36
32	3.81251E-01	1.62521E-05	2.06565E-36	4.13129E-36
33	3.81348E-01	4.43312E-05	5.63449E-37	1.12690E-36
34	3.81445E-01	4.74085E-05	5.02562E-37	1.20512E-36
35	3.81541E-01	1.24237E-05	1.57905E-37	3.15811E-37
36	3.81637E-01	1.27654E-06	1.62248E-37	3.24496E-37
37	3.81732E-01	3.21441E-07	4.09551E-38	8.17102E-38
38	3.81827E-01	3.17386E-07	4.03398E-38	8.06796E-38
39	3.81922E-01	7.68051E-08	9.76193E-39	1.95239E-38
40	3.82015E-01	7.28854E-08	9.26374E-39	1.85275E-38
41	3.82109E-01	1.69525E-08	2.15466E-39	4.30931E-39
42	3.82202E-01	1.54631E-08	1.96536E-39	3.93073E-39
43	3.82294E-01	3.45721E-09	4.39412E-40	8.78824E-40
44	3.82386E-01	3.03144E-09	3.85296E-40	7.70592E-40
45	3.82477E-01	6.51562E-10	8.28135E-41	1.65627E-40
46	3.82568E-01	5.49256E-10	5.98104E-41	1.39621E-40
47	3.82658E-01	1.13500E-10	1.44258E-41	2.88516E-41
48	3.82748E-01	9.19907E-11	1.16920E-41	2.33840E-41
49	3.82837E-01	1.82772E-11	2.32303E-42	4.64606E-42
50	3.82926E-01	1.42435E-11	1.81035E-42	3.62071E-42

TABLE E15.- (Cont'd)

J	$\lambda, (\mu)$	Normalized cross section $\Delta J = +2$	$\frac{d\sigma}{d\Omega}(\omega)_{\perp}$	$\frac{d\sigma}{d\Omega}(\omega)_{\parallel}$
51	3.83014E-01	2.72117E-12	3.45861E-43	6.91722E-43
52	3.83102E-01	2.03916E-12	2.59177E-43	5.18354E-43
53	3.83190E-01	3.74617E-13	4.76138E-44	9.52275E-44
54	3.83276E-01	2.69954E-13	3.43112E-44	6.86224E-44
55	3.83363E-01	4.76921E-14	6.06167E-45	1.21233E-44
56	3.83448E-01	3.30507E-14	4.20074E-45	8.40148E-45
57	3.83534E-01	5.61535E-15	7.13710E-46	1.42742E-45
58	3.83618E-01	3.74248E-15	4.75669E-46	9.51338E-46
59	3.83703E-01	6.11523E-16	7.77246E-47	1.55449E-46
60	3.83786E-01	3.91978E-16	4.98204E-47	9.96408E-47
61	3.83869E-01	6.16012E-17	7.82951E-48	1.56590E-47
62	3.83952E-01	3.79768E-17	4.82686E-48	9.65371E-48
63	3.84034E-01	5.74030E-18	7.29592E-49	1.45918E-48
64	3.84116E-01	3.40377E-18	4.32619E-49	8.65237E-49
65	3.84197E-01	4.94854E-19	6.28960E-50	1.25792E-49
66	3.84278E-01	2.82235E-19	3.58720E-50	7.17440E-50
67	3.84358E-01	3.94677E-20	5.01634E-51	1.00327E-50
68	3.84437E-01	2.16518E-20	2.75194E-51	5.50389E-51
69	3.84516E-01	2.91239E-21	3.70165E-52	7.40330E-52
70	3.84595E-01	1.53685E-21	1.95334E-52	3.90668E-52
71	3.84673E-01	1.98849E-22	2.52737E-53	5.05475E-53
72	3.84750E-01	1.00936E-22	1.28290E-53	2.56579E-53
73	3.84827E-01	1.25627E-23	1.59671E-54	3.19343E-54
74	3.84904E-01	6.13412E-24	7.79647E-55	1.55929E-54
75	3.84980E-01	7.34414E-25	9.33440E-56	1.86688E-55
76	3.85055E-01	3.44960E-25	4.38444E-56	8.76888E-56
77	3.85130E-01	3.97300E-25	5.04968E-57	1.00994E-56
78	3.85204E-01	1.79519E-25	2.28169E-57	4.56338E-57
79	3.85278E-01	1.98897E-27	2.52798E-58	5.05596E-58
80	3.85351E-01	8.64554E-28	1.09885E-58	2.19770E-58
81	3.85424E-01	9.21478E-29	1.17120E-59	2.34240E-59
82	3.85496E-01	3.85325E-29	4.89748E-60	9.79496E-60
83	3.85568E-01	3.95095E-30	5.02165E-61	1.00433E-60
84	3.85639E-01	1.58938E-30	2.02010E-61	4.04020E-61
85	3.85710E-01	1.56779E-31	1.99267E-62	3.98533E-62
86	3.85780E-01	6.06744E-32	7.71172E-63	1.54234E-62
87	3.85849E-01	5.75784E-33	7.31821E-64	1.46364E-63
88	3.85918E-01	2.14374E-33	2.72469E-64	5.44938E-64
89	3.85987E-01	1.95714E-34	2.48753E-65	4.97506E-65
90	3.86055E-01	7.01027E-35	8.91005E-66	1.78201E-65
91	3.86122E-01	6.15728E-36	7.82590E-67	1.56518E-66
92	3.86189E-01	2.12181E-36	2.69682E-67	5.39363E-67
93	3.86256E-01	1.79294E-37	2.27883E-68	4.55766E-68
94	3.86321E-01	5.94419E-38	7.55507E-69	1.51101E-68
95	3.86387E-01	4.83242E-39	6.14201E-70	1.22840E-69
96	3.86452E-01	1.54136E-39	1.95907E-70	3.91814E-70
97	3.86516E-01	1.20557E-40	1.53228E-71	3.06455E-71
98	3.86579E-01	3.89954E-41	4.70212E-72	9.40424E-72
99	3.86643E-01	2.78390E-42	3.53834E-73	7.07668E-73
100	3.86705E-01	8.21923E-43	1.04466E-73	2.08933E-73

TABLE E16.- DIFFERENTIAL BACKSCATTER CROSS SECTIONS FOR ROTATIONAL FINE STRUCTURE

ON THE $v = 0 \rightarrow 1$ RAMAN VIBRATIONAL TRANSITION OF N_2 . $\Delta J = -2$

J	$\lambda, (\mu)$	Normalized cross section $\Delta J = -2$	$\frac{d\sigma}{d\Omega}(\omega)_I$	$\frac{d\sigma}{d\Omega}(\omega)_II$
2	3.77539E-01	1.62544E-02	2.06594E-33	4.13188E-33
3	3.77425E-01	1.38260E-02	1.75728E-33	3.51456E-33
4	3.77310E-01	3.66237E-02	4.65487E-33	9.30975E-33
5	3.77194E-01	2.15886E-02	2.74391E-33	5.48783E-33
6	3.77078E-01	4.72757E-02	6.00874E-33	1.20175E-32
7	3.76962E-01	2.45064E-02	3.11477E-33	6.22954E-33
8	3.76845E-01	4.86239E-02	6.18010E-33	1.23602E-32
9	3.76728E-01	2.32279E-02	2.95226E-33	5.90452E-33
10	3.76610E-01	4.29241E-02	5.45565E-33	1.09113E-32
11	3.76492E-01	1.92338E-02	2.44461E-33	4.88923E-33
12	3.76373E-01	3.35066E-02	4.25869E-33	8.51738E-33
13	3.76254E-01	1.42055E-02	1.80552E-33	3.61103E-33
14	3.76134E-01	2.34790E-02	2.98418E-33	5.96836E-33
15	3.76014E-01	9.46426E-03	1.20291E-33	2.40581E-33
16	3.75894E-01	1.48978E-02	1.89351E-33	3.78702E-33
17	3.75773E-01	5.72702E-03	7.27904E-34	1.45581E-33
18	3.75651E-01	8.60679E-03	1.09392E-33	2.18785E-33
19	3.75530E-01	3.16170E-03	4.01852E-34	8.03703E-34
20	3.75407E-01	4.54398E-03	5.77540E-34	1.15508E-33
21	3.75284E-01	1.59734E-03	2.03022E-34	4.06044E-34
22	3.75161E-01	2.19803E-03	2.79370E-34	5.58740E-34
23	3.75038E-01	7.40152E-04	9.40734E-35	1.88147E-34
24	3.74914E-01	9.76023E-04	1.24052E-34	2.48105E-34
25	3.74789E-01	3.15067E-04	4.00450E-35	8.00900E-35
26	3.74664E-01	3.98413E-04	5.06383E-35	1.01277E-34
27	3.74539E-01	1.23364E-04	1.56795E-35	3.13591E-35
28	3.74413E-01	1.49670E-04	1.90231E-35	3.80462E-35
29	3.74286E-01	4.44734E-05	5.65258E-36	1.13052E-35
30	3.74160E-01	5.17897E-05	6.58247E-36	1.31649E-35
31	3.74033E-01	1.47734E-05	1.87770E-36	3.75539E-36
32	3.73905E-01	1.65182E-05	2.09946E-36	4.19891E-36
33	3.73777E-01	4.52479E-06	5.75100E-37	1.15020E-36
34	3.73648E-01	4.85888E-06	6.17564E-37	1.23513E-36
35	3.73520E-01	1.27844E-06	1.62490E-37	3.24980E-37
36	3.73390E-01	1.31878E-06	1.67617E-37	3.35234E-37
37	3.73260E-01	3.33360E-07	4.23700E-38	8.47400E-38
38	3.73130E-01	3.30400E-07	4.19939E-38	8.39878E-38
39	3.73000E-01	8.02513E-08	1.01999E-38	2.03999E-38
40	3.72868E-01	7.64335E-08	9.71470E-39	1.94294E-38
41	3.72737E-01	1.78415E-08	2.26765E-39	4.53530E-39
42	3.72605E-01	1.63315E-08	2.07573E-39	4.15146E-39
43	3.72473E-01	3.66405E-09	4.65701E-40	9.31402E-40
44	3.72340E-01	3.22382E-09	4.09747E-40	8.19494E-40
45	3.72207E-01	6.95253E-10	8.83666E-41	1.76733E-40
46	3.72073E-01	5.88043E-10	7.47403E-41	1.49481E-40
47	3.71939E-01	1.21916E-10	1.54955E-41	3.09909E-41
48	3.71805E-01	9.91337E-11	1.25999E-41	2.51998E-41
49	3.71670E-01	1.97599E-11	2.51148E-42	5.02296E-42
50	3.71534E-01	1.54481E-11	1.96346E-42	3.92692E-42
51	3.71399E-01	2.96063E-12	3.76296E-43	7.52592E-43
52	3.71263E-01	2.22554E-12	2.82866E-43	5.65732E-43

TABLE E16.- (Cont'd)

J	$\lambda, (\mu)$	Normalized cross section $\Delta J = -2$	$\frac{d\sigma}{d\Omega}(\omega)_I$	$\frac{d\sigma}{d\Omega}(\omega)_II$
53	3.71126E-01	4.10124E-13	5.21268E-44	1.04254E-43
54	3.70989E-01	2.96450E-13	3.76788E-44	7.53577E-44
55	3.70852E-01	5.25327E-14	6.67691E-45	1.33538E-44
56	3.70714E-01	3.65153E-14	4.64109E-45	9.28219E-45
57	3.70576E-01	6.22260E-15	7.90893E-46	1.58179E-45
58	3.70437E-01	4.15956E-15	5.28680E-46	1.05736E-45
59	3.70298E-01	6.81685E-16	8.66421E-47	1.73284E-46
60	3.70159E-01	4.38235E-16	5.56996E-47	1.11399E-46
61	3.70019E-01	6.90718E-17	8.77903E-48	1.75581E-47
62	3.69879E-01	4.27060E-17	5.42794E-48	1.08559E-47
63	3.69738E-01	6.47376E-18	8.22815E-49	1.64563E-48
64	3.69597E-01	3.84969E-18	4.89296E-49	9.78591E-49
65	3.69456E-01	5.61282E-19	7.13389E-50	1.42678E-49
66	3.69314E-01	3.21029E-19	4.08028E-50	8.16057E-50
67	3.69171E-01	4.50195E-20	5.72198E-51	1.14440E-50
68	3.69029E-01	2.47669E-20	3.14788E-51	6.29576E-51
69	3.68886E-01	3.34073E-21	4.24607E-52	8.49214E-52
70	3.68742E-01	1.76780E-21	2.24687E-52	4.49373E-52
71	3.68598E-01	2.29364E-22	2.91522E-53	5.83044E-53
72	3.68454E-01	1.16747E-22	1.48385E-53	2.96771E-53
73	3.68310E-01	1.45705E-23	1.85191E-54	3.70381E-54
74	3.68165E-01	7.13398E-24	9.06729E-55	1.81346E-54
75	3.68019E-01	8.56454E-25	1.08855E-55	2.17711E-55
76	3.67873E-01	4.03377E-25	5.12692E-56	1.02538E-55
77	3.67727E-01	4.65838E-26	5.92080E-57	1.18416E-56
78	3.67580E-01	2.11056E-26	2.68253E-57	5.36505E-57
79	3.67434E-01	2.34467E-27	2.98008E-58	5.96016E-58
80	3.67286E-01	1.02190E-27	1.29884E-58	2.59768E-58
81	3.67138E-01	1.09210E-28	1.38806E-59	2.77611E-59
82	3.66990E-01	4.57889E-29	5.81977E-60	1.16395E-59
83	3.66842E-01	4.70745E-30	5.98317E-61	1.19663E-60
84	3.66693E-01	1.89872E-30	2.41328E-61	4.82656E-61
85	3.66544E-01	1.87788E-31	2.38679E-62	4.77358E-62
86	3.66394E-01	7.28665E-32	9.26133E-63	1.85227E-62
87	3.66244E-01	6.93300E-33	8.81185E-64	1.76237E-63
88	3.66093E-01	2.58803E-33	3.28939E-64	6.57878E-64
89	3.65943E-01	2.36895E-34	3.01093E-65	6.02186E-65
90	3.65791E-01	8.50743E-35	1.08129E-65	2.16259E-65
91	3.65640E-01	7.49170E-36	9.52195E-67	1.90439E-66
92	3.65488E-01	2.58835E-36	3.28979E-67	6.57959E-67
93	3.65336E-01	2.19284E-37	2.78710E-68	5.57420E-68
94	3.65183E-01	7.28876E-38	9.26402E-69	1.85280E-68
95	3.65030E-01	5.94079E-39	7.55074E-70	1.51015E-69
96	3.64877E-01	1.89976E-39	2.41460E-70	4.82919E-70
97	3.64723E-01	1.48970E-40	1.89341E-71	3.78683E-71
98	3.64569E-01	4.58318E-41	5.82523E-72	1.16505E-71
99	3.64414E-01	3.45766E-42	4.39469E-73	8.78937E-73
100	3.64259E-01	1.02345E-42	1.30080E-73	2.60161E-73
101	3.64104E-01	7.42846E-44	9.44157E-75	1.88831E-74
102	3.63948E-01	2.11545E-44	2.68873E-75	5.37747E-75

APPENDIX F

AN ESTIMATE OF THE QUANTITY $(i_D + i_B)$

The manufacturer's measurements of the particular Amperex 56DUVP phototube used in these experiments indicated that

$$i_D \simeq 2.4 \times 10^{-16} \text{ amperes}$$

The value of i_B is calculated from the relationship

$$i_B = \eta \gamma \Omega A \Delta \lambda R_\lambda$$

where

Ω is the solid angle of the receiver $\simeq 3.1 \times 10^{-5}$ steradians

$\Delta \lambda$ is the passband of the interference filters $\simeq 35 \text{ \AA}$

R_λ is the night sky radiance $\simeq 10^{-9} \text{ watts m}^{-2} \text{ster}^{-1} \text{A}^{-1}$ (34,35)

η is the cathode sensitivity $\simeq 0.04 \text{ ampere watt}^{-1}$

γ is the optical efficiency $\simeq 0.3$

and

A is the area of the receiver = 0.13 meter^2

Using these values,

$$i_B \simeq 1.7 \times 10^{-15} \text{ amperes}$$

Therefore, a reasonable estimate is

$$(i_D + i_B) \simeq 2 \times 10^{-15} \text{ amperes}$$

REFERENCES

1. Synge, E. H.
"A Method of Investigating the Higher Atmosphere."
Phil. Mag. 9, 1014 (1930)
2. Hulburt, E. O.
Observations of a Searchlight Beam to an Altitude of 28 km.
J. Opt. Soc. Amer. 27, 377 (1937)
3. Elterman, L.
The Measurement of Stratospheric Density Distribution with the
Searchlight Technique.
Geophys. Res. Papers No. 10 (1951), AFCL
4. Friedland, S.; Katzenstein, J.; Zatzick, M.
Pulsed Searchlighting the Atmosphere.
J. Geophys. Res. 61, 415 (1956)
5. Rosenberg, G. V.
Light Scattering in the Earth's Atmosphere.
Soviet Physics Uspekhi 3, 346 (1960)
6. Fiocco, G.; Smullin, L. D.
Detection of Scattering Layers in the Upper Atmosphere (60-140 km)
by Optical Radar.
Nature 199, 1275 (1963)
7. Bain, W. C.; Sanford, M. C. W.
Light Scatter from a Laser Beam at Heights above 40 km.
J. Atmos. Terr. Phys., 21, 323 (1964)
8. Collis, R. T. H.; Ligda, M. G. H.
Laser Radar Echoes from the Stratified Clear Atmosphere.
Nature 203, 508 (1964)
9. Kent, G. S.; Clemesha, B. R.; Wright, R. W.
High Altitude Atmospheric Scattering of Light from a Laser Beam.
J. Atmos. Terr. Phys. 29, 169 (1967)
10. Schotland, R. M.; Bradley, James; Nathan, Allen
Optical Sounding III.
Technical report ECOM-02207-F, June 1967, N.Y.U.
11. Bowman, M. R.; Gibson, A. J.; Sandford, M. C. W.
Nature, 221, 456 (1969)

12. Leonard, D. A.
"Observation of Raman Scattering from the Atmosphere Using a Pulsed Nitrogen Ultraviolet Laser."
Nature, 216, 142 (1967)
13. Cooney, J. A.
"Measurements on the Raman Component of Laser Atmospheric Backscatter."
App. Phys. Letters, 12, 40 (1968)
14. Melfi, S. H.; Lawrence, J. D., Jr.; McCormick, M. P.
"Observation of Raman Scattering by Water Vapor in the Atmosphere."
App. Phys. Letters, 15, 295 (1969)
15. Cooney, J. A.
"Remote Measurements of Atmospheric Water Vapor Profiles Using the Raman Component of Laser Backscatter."
J. Applied Met. 9, 182 (1970)
16. Kobayasi, T.; Inaba, H.
To be published in
Proceeding of the IEEE 58, September 1970
17. Raman, C. V.
Indian J. Phys. 2, 387 (1928)
18. Smekal, A.
Naturwiss 11, 873 (1923)
19. Kramers, H. A.; Heisenberg, W.
Z. Phys. 31, 681 (1925)
20. Dirac, P. A. M.
Proc. Roy. Soc. A114, 710 (1927)
21. Heitler, W.
The Quantum Theory of Radiation.
3rd edition, Cambridge Press, London, 1953, Chap. 5
22. Placzek, G.
"The Rayleigh and Raman Scattering."
Handbuch der Radiologie, edited by Erich Marx,
Leipzig, Akademische Verlagsgesellschaft VI,
2, 209-374 (1934)
UCRL translation No. 526(L)

23. Ory, H. A.; Yura, H. T.
"Rayleigh and Raman Scattering in Molecular Nitrogen."
Rand Corporation Memorandum No. RM-4664-ARPA
August 1965
24. Pauling L.; Wilson, E. B., Jr.
Introduction to Quantum Mechanics.
McGraw-Hill Book Company, New York, 1935
25. Stansbury, E. J.; Crawford, M. F.; Welsh, H. L.
"Determination of Rates of Change of Polarizability from Raman
and Rayleigh Intensities."
Can. J. Phys. 31, 954 (1953)
26. Herzberg, G.
Spectra of Diatomic Molecules, 2nd edition
Van Nostrand Reinhold Co., New York, 1950, Chap. 3
27. Elterman, L.
"Altitude Variation of Rayleigh, Aerosol, and Ozone Attenuating
Components in the Ultraviolet Region."
AFCRL Environmental Research Paper No. 20, 1964.
28. U.S. Standard Atmosphere, 1962
U.S. Government Printing Office, Washington, D.C.
December 1962
29. Prandtl, L.
"Bericht über Untersuchungen zur ausgebildeten turbulenz."
Z. Angew. Math Mech. 5, 136 (1925)
30. Taylor, G. I.
"Eddy Motion in the Atmosphere."
Philos. Trans. 215, 1 (1915)
31. Fleagle, R. G.; Businger, J. A.
An Introduction to Atmospheric Physics.
Academic Press, New York, 1963, Chap. 5
32. Ross, M.
Laser Receivers.
John Wiley and Sons, Inc., New York, 1966.
33. Porto, S. P. S.
"Angular Dependence and Depolarization Ratio of the Raman Effect."
J. Opt. Soc. Am. 56, 1585 (1966)

34. van de Hulst, H. C.
Light Scattering by Small Particles.
John Wiley and Sons, Inc., New York, 1957
35. Pavlova, E. N.; Rodinov, S. F.; Sholovkhova, E. D.
"Energy Distribution in the Spectrum of the Luminosity of the
Night Sky."
Doklady Ak. Nauk, 98 (1954)
36. Broadfoot, A. L.; Kendall, K. R.
"The Airglow Spectrum 3100 - 10,000 Å."
J. Geophys. Res. 73, 426 (1968)

VITA

The author, Samuel Harvey Melfi, [REDACTED]

[REDACTED] [REDACTED] [REDACTED] He completed his elementary and secondary education in Charleston. He received a bachelor of science degree in Electrical Engineering from The Citadel, Charleston, South Carolina, in 1963, and was elected to The Citadel Honorary Society for high scholastic achievement. After graduation from The Citadel, the author accepted a research position with the National Aeronautics and Space Administration at Langley Research Center. While at Langley, he has performed research on laser light scattering by gas molecules, both in laboratory test chambers and in the atmosphere. During this time he has been enrolled in the graduate program of the Department of Physics at the College of William and Mary and received a master of science degree in 1967. Since receiving this degree the author has been performing research related to this dissertation.